Antagonism of Host Interferon Response by Emerging Positive-Strand RNA Viruses

by

Ray Ishida

A thesis submitted in partial fulfillment of the requirements of the degree of

Master of Science

in

Virology

Department of Medical Microbiology and Immunology
University of Alberta

Abstract

Positive strand RNA ((+)ssRNA) viruses are some of the most important pathogens that impact the public health, economy, and quality of life. The interferon (IFN) response plays a critical role in innate immune response targeting (+)ssRNA viruses, which in turn have evolved various strategies to circumvent this response in order to establish infection. In this thesis, I investigated how two emerging (+)ssRNA viruses, Mayaro virus (MAYV) and severe acute respiratory syndrome coronavirus 2 (SARS-CoV-2), affect the host IFN response and determined the mechanisms by which specific viral proteins antagonize this pathway.

MAYV infection was found to significantly impair the induction phase of the IFN response and mapping studies revealed that non-structural protein 2 (NSP2) was responsible for this effect. Expression of MAYV NSP2 depleted DNA-directed RNA polymerase II subunit A (Rpb1) and transcription initiation factor II E subunit 2 (TFIIE2) which are indispensable for host mRNA synthesis. This indicated that NSP2-mediated transcriptional shutoff was the primary mechanism by which MAYV blocks IFN induction.

Induction of IFNs and IFN-stimulated genes (ISGs) were also blocked during SARS-CoV-2 infection. The viral proteins NSP1 and nucleocapsid (N) both blocked the IFN response indicating that SARS-CoV-2 employs multiple mechanisms to subvert the host antiviral defenses. Translational shutoff by NSP1 resulted in depletion of key IFN signaling proteins, such as tyrosine kinase 2 (Tyk2) and signal transducer and activator of transcription 2 (STAT2).

Together, this research provides new insights into the mechanisms by which two recently emerged (+)ssRNA viruses antagonize the host IFN response. Current findings should be taken into account when developing and administering antiviral therapeutics.

Preface

Many findings presented in this thesis are the result of collaborative works.

Chapter 3 of this thesis is published as Ishida, R., Cole, J., Lopez-Orozco, J., Fayad, N., Felix-Lopez, A., Elaish, M., Luo, S.Y., Julien, O., Kumar, A., and Hobman, T.C. 2021. Mayaro Virus Non-Structural Protein 2 Circumvents the Induction of Interferon in Part by Depleting Host Transcription Initiation Factor IIE Subunit 2. Cells 10 (12). doi: doi.org/10.3390/cells10123510. Project was conceived by T.C. Hobman and A. Kumar. J. Moore performed mass spectrometry analyses. A. Felix-Lopez performed the Molecular Interaction Search Tool (MiST) analysis, while N. Fayed performed the Gene Ontology (GO) enrichment analysis. I was responsible for experimental design and performance, data collection and analysis, and composition and revision of manuscript. T. C. Hobman was supervisory author and contributed to concept formation and manuscript composition.

Chapter 4 of the thesis is published as Kumar, A., Ishida, R., Strilets, T., Cole, J., Lopez-Orozco, J., Fayad, N., Felix-Lopez, A., Elaish, M., Evseev, D., Magor, K.E., Mahal, L.K., Nagata, L.P., Evans, D.H., and Hobman, T.C. 2021. SARS-CoV-2 Nonstructural Protein 1 Inhibits the Interferon Response by Causing Depletion of Key Host Signaling Factors. J Virol 95 (13): doi: 10.1128/JVI.00266-21. Project was conceived by T.C. Hobman and A. Kumar. A. Kumar, T. Strilets, and I contributed equally to experimental design and performance, data collection and analysis, and composition and revision of manuscript. T. C. Hobman was supervisory author and contributed to concept formation and manuscript composition.

Acknowledgements

To my supervisor Dr. Tom Hobman, for welcoming me to his team and for providing guidance and support throughout my MSc studies. I am truly grateful for the opportunity for carrying out my research in virology and growing in the field of scientific research.

To my supervisory committee members Dr. Jim Smiley and Dr. Amit Bhavsar, for their constructive criticism and insights which helped shape my research. I would also like to thank Dr. Paul LaPointe for serving as a defense examiner and reading my thesis.

To my wonderful colleagues Dr. Anil Kumar, Dr. Joaquin Lopez-Orozco, Dr. Zaikun Xu, Dr. Daniel Limonta, Dr. Mohamed Elaish, Dr. Adriana Airo, Valeria Mancinelli, Eileen Reklow, Alberto Felix-Lopez, Nawell Fayad, Cheung Pang Wong, for creating such a positive work environment. Thank all of you for your technical support and insights which were indispensable for my thesis work. I truly enjoyed all the conversations and discussions we have shared.

To my parents for being loving and supportive throughout my life. You have taught me to be curious, adventurous, hardworking, and most importantly encouraged to pursue my passion. Thank you to the rest of my family members for their love and support as well.

Last but not least, to my wife Sarah, for supporting me in countless ways over the years. It is your love and companionship which made my everyday more enjoyable. Thank you for always being loving, kind, hardworking, and supportive throughout this journey.

Table of Contents

List of Tables

List of Figures

Abbreviations

°C	Degree Celsius
A549	Human alveolar basal epithelial 549 cells
ACE2	Angiotensin converting enzyme 2
APS	Ammonium persulphate
ATP	Adenosine triphosphate
BSA	Bovine serum albumin
C protein	Capsid protein
C6/36	Aedes albopictus clone C6/36 cells
CARD	Caspase recruitment domain
cDNA	Complementary deoxyribonucleic acid
CHIKV	Chikungunya virus
CIP	Calf intestinal alkaline phosphatase
CMV	Cytomegalovirus
CoV	Coronavirus
COVID-19	Coronavirus infectious disease 2019
DENV	Dengue virus
DMEM	Dulbecco's Modified Eagle Medium
DMSO	Dimethyl sulfoxide
DNA	Deoxyribonucleic acid
dsRNA	Double-stranded ribonucleic acid
DTT	Dithiothreitol
E protein	Envelope protein
EDTA	Ethylenediaminetetraacetic acid
EGTA	Ethylene glycol-bis (β-aminoethyl ether)-N, N, N', N'-tetraacetic acid
eIF	Eukaryotic translation initiation factor
ELISA	Enzyme-linked immunosorbent assay
FBS	Fetal bovine serum
GAF	Interferon-ɣ (gamma) activated factor
GAS	Interferon-ɣ (gamma) activated site

GFP	Green fluorescent protein
GO	Gene ontology
HAU	Hemagglutinating unit
HEK 293T	Human embryo kidney 293T cells
HEPES	N-2-hydroxyethylpiperazine-N-2-ethane sulfonic acid
Hpi	Hour post-infection
Huh7	Human hepatoma 7 cells
IAV	Influenza A virus
IF	Immunofluorescence
IFITM	Interferon-inducible transmembrane
IFN	Interferon
IFNAR	Interferon-α/β receptor
IFNGR	Interferon-ɣ receptor
IFNLR	Interferon-λ receptor
IKK	IκB kinase
IP	Immunoprecipitation
IRES	Internal ribosome entry site
IRF	Interferon regulatory factor
ISG	Interferon stimulated gene
ISGF	ISG factor
ISRE	Interferon-stimulated response element
IκB	Inhibitor of NFκB
Jak	Janus kinase
kb	Kilo base
kDa	Kilo Daltons
L	Liter
m	Mili (10^{-3})
M protein	Membrane protein
M	Moles per liter
MAVS	Mitochondrial antiviral signaling protein
MAYV	Mayaro virus

MDA5	Melanoma differentiation associated gene 5
MEM	Minimal Essential Media
MERS	Middle East respiratory syndrome
MiST	Molecular Interaction Search Tool
MOI	Multiplicity of infection
mRNA	Messenger ribonucleic acid
Mxra	Matrix remodeling-associated protein
MyD88	Myeloid differentiation primary response gene 88
n	Nano (10^{-9})
N protein	Nucleocapsid protein
NEAA	Non-essential Amino Acids
NEMO	NFκB essential modulator
NFκB	Nuclear factor κ B
NLS	Nuclear localization signal
NS	Non-structural
NSP	Non-structural protein
OAS	Oligoadenylate synthetase
ONNV	O'nyong nyong virus
ORF	Open reading frame
PAMP	Pathogen-associated molecular pattern
PBS	Phosphate buffered saline
PCR	Polymerase chain reaction
PFA	Paraformaldehyde
PFU	Plaque forming unit
pH	Power hydrogenii
PKR	Protein kinase R
Poly(I:C)	Polyinosinic-polycytidylic acid
PP1	Protein phosphatase 1
PRR	Pattern recognition receptor
PVDF	Polyvinylidene difluoride
qRT-PCR	Quantitative real-time polymerase chain reaction

RdRp	RNA-dependent RNA polymerase
RIG-I	Retinoic acid inducible gene I
RLR	RIG-I-like receptor
RNA	Ribonucleic acid
RNase	Ribonuclease
Rpb1	DNA-directed RNA polymerase II subunit A
RRV	Ross River virus
RTC	Replication and transcription complex
S protein	Spike protein
SARS	Severe acute respiratory syndrome
SDS	Sodium dodecyl sulphate
SDS-PAGE	Sodium dodecyl sulphate-polyacrylamide gel electrophoresis
SeV	Sendai virus
SFV	Semliki Forest virus
SINV	Sindbis virus
SOC medium	Super Optimal broth with Catabolite repression medium
SOCS	Suppressor of cytokine signaling
ssRNA	Single-stranded ribonucleic acid
STAT	Signal transducer and activator of transcription
TAE	Tris-acetate-EDTA
TBK1	TANK-binding kinase 1
TEMED	N, N, N', N'-tetramethylethylenediamine
Th1	T helper type 1
TLR	Toll-like receptor
TMPRSS2	Transmembrane serine protease 2
TF	Transframe
TFIIE2	Transcription initiation factor II E subunit 2
TRAF	Tumor necrosis factor receptor-associated factor
TRIF	TIR domain-containing adaptor-inducing IFN
TRIM25	Tripartite motif-containing protein 25
Tyk	Tyrosine kinase

U	Unit
USP18	Ubiquitin specific peptidase 18
V	Volt
v/v	Volume per volume
VERO	African green monkey kidney cells
VOC	Variant of concern
WB	Western blot
w/v	Weight per volume
ZIKV	Zika virus
µ	Micro (10^{-6})

Chapter 1

Introduction

1.1 The Interferon Response

The interferon (IFN) response is one of the most important arms of innate immunity for controlling viral infection. This response entails two signaling pathways: 1) the IFN induction pathway which involves the sensing of pathogen-associated molecular patterns (PAMPs) and the production and secretion of IFN molecules, and 2) the IFN signaling pathway, initiated by binding of IFNs on to cell surface receptors, resulting in the expression of IFN-stimulated genes (ISGs) which collectively restrict viral infection (Reviewed in (Fensterl 2015)). Furthermore, IFNs play an important role in activating and shaping the adaptive immune response, which is required for the clearance of viral infections (McNab et al., 2015).

1.1.1 Types of IFNs

Interferons are small peptides that can be divided into three classes: type I, II and III IFNs, according to the cell surface receptors they bind to. Type I IFNs comprise IFN-α, -β, -κ, -ω, -ε, -τ, -δ, and -ζ, and they bind to IFN-α/β receptors (IFNAR), which consist of IFNAR1 and IFNAR2. The only known member of type II IFNs is IFN-ɣ, which binds to tetrameric IFN-ɣ receptors (IFNGR), consisting of two subunits of each of IFNGR1 and IFNGR2. Type III IFNs include IFN-λ1, -λ2, -λ3, and -λ4, and they signal through IFN-λ receptors (IFNLR), consisting of IFNLR1 and interleukin 10 receptor B (de Weerd and Nguyen 2012; O'Brien et al., 2014). As secreted IFNs bind to receptors in an autocrine and/or paracrine manner, the effects of IFNs are usually limited to the site where IFN-inducing stimuli are present (Mesev et al., 2019).

In addition to the difference in the cell surface receptors that each class of IFNs binds, cells that produce and respond to a given class of IFN vary widely. Given that all nucleated cells have

the capacity to produce type I IFNs and almost all cell types express IFNARs (McNab et al., 2015; Mesev et al., 2019), type I IFNs provide a first line of protection against microbes at the site of infection. Type II IFNs are mainly produced by leukocytes (de Weerd and Nguyen 2012) and their expression is induced by type I IFNs, a subset of interleukins, and pattern recognition receptor (PRR)-mediated PAMP recognition (Bogdan and Schleicher 2006; Lee and Ashkar 2018). IFN-ɣ plays an important role in the activation of the adaptive immune response against intracellular pathogens as it activates antigen presenting cells and promotes T cells to differentiate into the T helper type 1 (Th1) lineage (Kak et al., 2018). Similar to type I IFNs, type III IFNs are produced by various cell types (Witte et al., 2010). However, IFNLR expression is limited to a small subset of cell types, such as epithelial cells, which allows them to respond to these IFNs (Mesev et al., 2019). Overall, cell type-specific expression of IFNs and IFN-receptors results in a targeted and complex IFN response *in vivo* in concert with the rest of the immune response.

1.1.2 IFN induction during positive-strand RNA virus infection

All classes of IFNs are induced by PRR-mediated detection of microbial PAMPs (Figure 1.1) although type II IFNs are mainly upregulated by cytokines (Bogdan and Schleicher 2006; Lee and Ashkar 2018)). In mammals, these PRRs include Toll-like receptors (TLRs) and retinoic acid-inducible gene 1 (RIG-I)-like receptors (RLRs), which sense common structures of pathogens (Fensterl 2015). Certain endosomal TLRs and cytosolic RLRs are particularly important for detecting infection by positive-strand RNA ((+)ssRNA) viruses and the subsequent upregulation of IFNs. For example, TLR3 senses double-stranded RNA (dsRNAs) intermediates that are produced by (+)ssRNA viruses during replication, and TLR7/8 recognizes single-stranded RNA (ssRNA). While TLRs are expressed in different cell types, they are highly expressed in innate

immune cells and play significant roles in their cell signaling (Kawai and Akira 2009). Converesly, RLRs, such as RIG-I and melanoma differentiation-associated gene 5 (MDA5) are ubiquitously expressed and are predominantly involved in the detection of infection by (+)ssRNA viruses. While both RIG-I and MDA5 sense cytosolic dsRNA, they bind to different RNA structures. RIG-I preferentially binds to dsRNA with 5'-triphosphate or 5'-diphosphate structures instead of the 5'-7-methylguanosine cap found on cellular messenger RNA (mRNA) (Hornung et al., 2006; Pichlmair et al., 2006). MDA5 has greater affinity for dsRNAs that are relatively long compared to RIG-I substrates (Kato et al., 2008).

The recognition of PAMPs by the aforementioned PRRs leads to downstream signaling that culminates in the upregulation of IFNs. Ligand binding of TLR3 and TLR7/8 leads to the recruitment of TIR domain-containing adaptor-inducing IFN (TRIF) and myeloid differentiation primary response gene 88 (MyD88) adaptor proteins, respectively (Kawasaki and Kawai 2014). These adaptor proteins recruit tumor necrosis factor receptor-associated protein (TRAF) family members, which then recruit kinases such as the inhibitor of NFκB kinase (IKK) family and TANK-binding kinase 1 (TBK1). TRAF3 mediates the recruitment of IKKε and TBK1 together with nuclear factor κB (NFκB) essential modulator (NEMO; also known as IKKɣ) which phosphorylate interferon regulatory factor 3 and/or 7 (IRF3/7) (Kawai and Akira 2009). Upon phosphorylation, the antiviral transcription factors IRF3 and IRF7 form homodimers or heterodimers which then translocate to the nucleus where they upregulate IFN expression (Honda et al., 2006). Of note, IRF7 is particularly important for MyD88-dependent type I IFN induction by plasmacytoid dendritic cells (Honda et al., 2005). Another signaling cascade involves TRAF6 which recruits IKKα, IKKβ, and NEMO that phosphorylate inhibitor of NFκB (IκB) (Kawai and Akira 2009). IκB normally retains NFκB in cytoplasm, thereby preventing the transcription factor

function of NFκB. However, phosphorylation of IκB results in its subsequent polyubiquitination and proteasomal degradation, thereby releasing NFκB, which translocates to the nucleus and mediates the expression of proinflammatory cytokines including IFNs (Liu et al., 2017).

RLRs such as RIG-I and MDA5 have caspase activation domains (CARD) that are exposed once they bind their dsRNA substrates (Brisse and Ly 2019). In addition to binding dsRNA, RIG-I activation requires dephosphorylation by protein phosphatase 1 (PP1) and ubiquitination by tripartite motif-containing protein 25 (TRIM25) (Gack et al., 2007; Wies et al., 2013). Once these RLRs are in their active conformations, they oligomerize and interact with mitochondrial antiviral signaling protein (MAVS) through CARD-CARD interactions (Brisse and Ly 2019). MAVS is an adaptor protein that is present on mitochondria and peroxisomes (Seth et al., 2005; Dixit et al., 2010) and recruits TRAF3 and TRAF6 following interaction with RLRs. TRAF3 and TRAF6 then recruit TBK1/IKKε/NEMO and IKKα/IKKβ/NEMO, respectively, resulting in activation of IRF3/7 and NFκB that facilitate the transcription of IFN genes. IFNs are secreted from infected cells, after which they bind to IFN-receptors in an autocrine and/or paracrine manner.

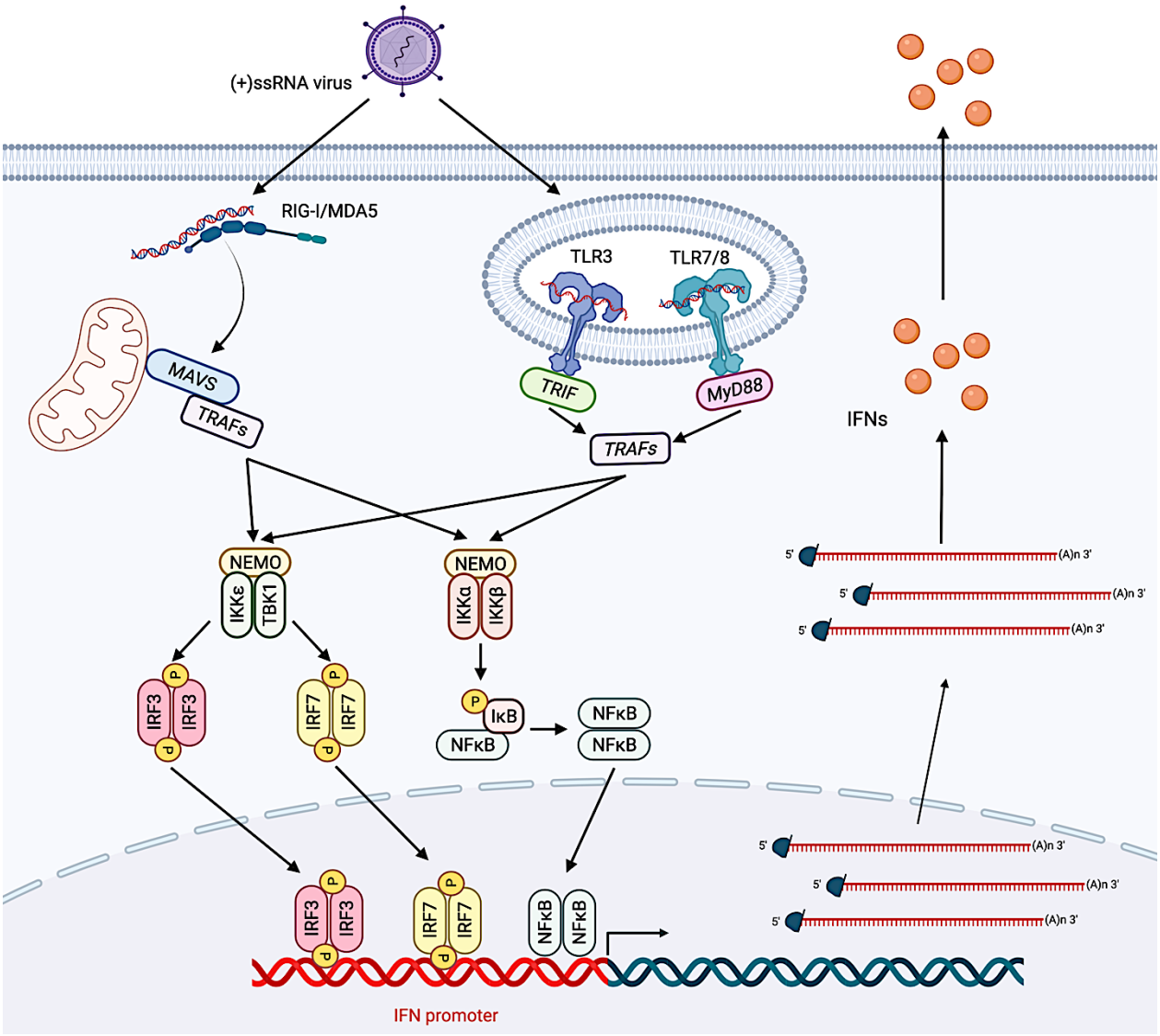

Figure 1.1 The IFN induction pathway induced by (+)ssRNA viruses. During infection by (+)ssRNA virus, genomic RNA and/or its dsRNA replication products are sensed by PRRs such as RIG-I, MDA5, TLR3, TLR7, and TLR8. RIG-I and MDA5 are cytoplasmic RLRs with affinity towards dsRNA. Upon binding dsRNAs and subsequent activation, these RLRs expose their CARD domains, which associate with CARD domains on MAVS adaptor protein. MAVS recruits TRAF3 and TFAF6 which further recruit kinase complexes: IKKα/IKKβ/NEMO that phosphorylate IκB and activate NFκB, and TBK1/IKKε/NEMO which phosphorylate and activate IRF3/7. TLR3 and TLR7/8 recognize endosomal ssRNA and dsRNA, and recruits TRIF and MyD88 adaptor proteins, respectively. These adaptor proteins further recruit TRAF3 and TRAF6, thereby mediate activation of NFκB and IRF3/7. These transcription factors bind to promoters of IFNs and facilitate their transcription. IFN-transcripts are subsequently translated and secreted outside of the cell where they can bind to IFN receptors in autocrine and/or paracrine manner. (Figure created with Biorender.com)

1.1.3 IFN signaling and ISGs

Secreted IFNs bind to their respective cell surface receptors and initiate IFN signaling, which results in the upregulation of ISGs (Figure 1.2). Although type I and III IFNs bind to different IFN receptors, IFNARs and IFNLRs, respectively, they activate the same IFN signaling pathway and thus induce a similar set of ISGs (Bolen et al., 2014). Ligand binding by IFNAR and IFNLR leads to autophosphorylation of IFN-receptor-associated kinases Janus kinase 1 (Jak1) and tyrosine kinase 2 (Tyk2) which phosphorylate tyrosine residues on IFN receptors. Signal transducer and activator of transcription 1 (STAT1) and 2 (STAT2) associate with phosphotyrosines on IFN receptors where they are then phosphorylated by Jak1 and Tyk2, respectively (Heim et al., 1995). Phosphorylation of STAT1 and STAT2 leads to the formation of a complex called ISG factor 3 (ISGF3), which consists of STAT1, STAT2, and IRF9 (Fu et al., 1990). ISGF3 translocates to the nucleus and facilitates transcription of ISGs using an IFN-stimulated response element (ISRE) promoter (Levy et al., 1988). Of note, while type I and III IFNs induce a similar group of ISGs, type I IFN-mediated signaling leads to a higher expression of ISGs due to their higher receptor binding affinity (Bolen et al., 2014; Mesev et al., 2019). The binding of type II IFNs to IFNGRs leads to autophosphorylation of Jak1 and Jak2 which together phosphorylate STAT1. STAT1 subsequently homodimerizes, forming IFN-ɣ-activated factor (GAF), and induces expression of ISGs with an IFN-ɣ-activated sequence (GAS) in their promoter (Decker et al., 1991). Of note, in addition to ISGF3, GAF can also form during type I and III IFN signaling after STAT1 phosphorylation by Jak1. However, during type I and III IFN signaling, IKKε-dependent phosphorylation of serine residues on STAT1 prevents GAF formation but not ISGF3 formation (Ng et al., 2011).

ISGF3- and GAF-induced ISGs have three main functions: antagonism of viral infection, increased sensitivity to viral infection, and regulation of IFN signaling (Reviewed in (Schneider et al., 2014)). Many ISGs inhibit multiple steps in the virus lifecycle such as cell entry, transcription, translation, and viral egress. For instance, IFN-inducible transmembrane (IFITM) proteins prevent membrane fusion, thereby blocking the entry of various enveloped viruses (Li et al., 2013). Viperin and tetherin block viral egress respectively by altering cell membrane composition and by anchoring enveloped viruses to the plasma membrane (Wang et al., 2007; Sauter et al., 2010). Oligoadenylate synthase (OAS) is an ISG that produces 2',5'-oligoadenylates that activate ribonuclease L (RNaseL) after recognition of dsRNA. Active RNaseL indiscriminately degrades viral and cellular transcripts, thereby halting protein synthesis as well as degrading the genomes of RNA viruses (Floyd-Smith et al., 1981; Chakrabarti et al., 2011). The ISG protein kinase R (PKR) also senses dsRNA but its antiviral effect involves phosphorylation of the translation initiation factor eIF2α, thereby impeding translation of cellular and viral transcripts (Dar et al., 2005).

The expression of various PRRs and their signaling components are also induced by IFNs, thus enhancing viral recognition and IFN production. These ISGs include RIG-I, MDA5, TRIM25, and IRF7, all of which augment the PRR-mediated induction of IFNs (Schoggins and Rice 2011). Thus sustained PAMP-recognition can lead to a positive feedback loop resulting in robust production of IFNs. However, since the induction of IFNs still requires the presence of PAMPs, the production of IFNs is proportional to the viral load.

Lastly, a subset of ISGs is involved in downregulating IFN signaling to avoid further ISG induction in cells that have already undergone IFN signaling. Notably, cells lose their ability to respond to IFN for several days after treatment with IFNs (Larner et al., 1986). For example,

suppressor of cytokine signaling (SOCS) proteins inhibit Jak-STAT signaling by sequestering phosphotyrosine residues on IFN receptors and Jak proteins, thereby impeding STAT recruitment and phosphorylation (Krebs and Hilton 2001). Furthermore, ubiquitin specific peptidase 18 (USP18) binds to IFNAR2 and prevents Jak from binding the IFN receptor, thus disrupting Jak-STAT signaling (Malakhova et al., 2006). Evidence suggests that while an acute, robust IFN response is effective in clearing viral infection, a chronic IFN response can have pathogenic effects and is less productive in clearing viral infections (reviewed in (Teijaro 2016)). Therefore, ISG-mediated downregulation of IFN signaling is critical for controlling infection and resolving inflammation.

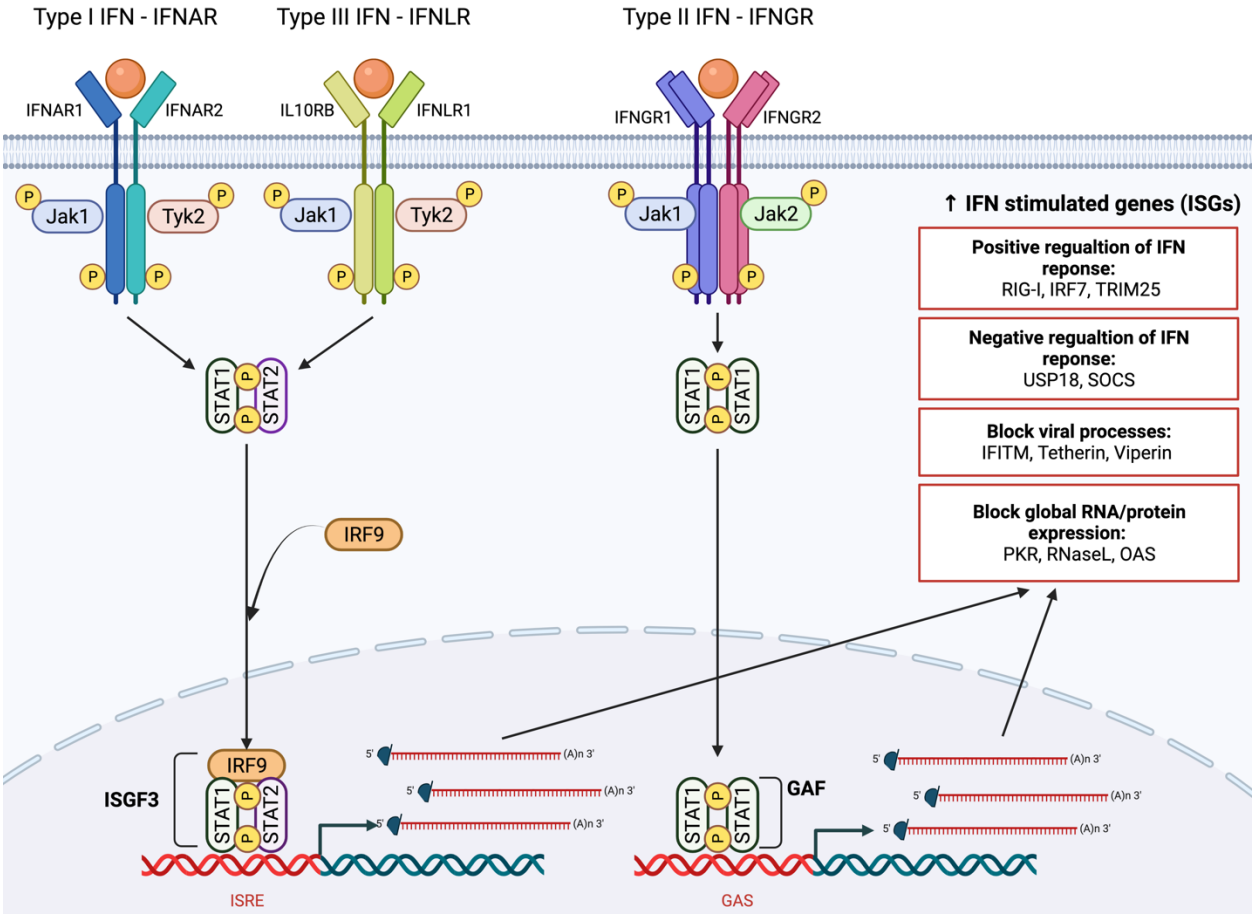

Figure 1.2 The IFN signaling pathway. Secreted IFNs bind to cell surface IFN receptors and activate the IFN signaling pathway. Type I IFNs bind to IFNARs, which are composed of IFNAR1 and IFNAR2, while type III IFNs bind to IFNLRs, which are composed of IL10RB and IFNLR1. Intracellular domains of both IFNAR and IFNLR are associated with Jak1 and Tyk2, and these are autophosphorylated upon binding of IFN to its receptor. Jak1 and Tyk2 further phosphorylate intracellular domains of IFN receptors, where STAT1 and STAT2 are recruited. Here, STAT1 and STAT2 are phosphorylated and forms STAT1/2 heterodimer, which further associates with IRF9 to form ISGF3. ISGF3 binds to ISRE, thus mediates transcription of ISGs with ISRE promoters. Type II IFNs bind to IFNGRs, which consist of two subunits of each IFNGR1 and IFNGR2. Receptor binding of type II IFNs result in autophosphorylation of Jak1 and Jak2 which further phosphorylate IFNGR and STAT1. Phosphorylated STAT1 forms a homodimer (GAF), which mediates transcription of ISGs with GAS-containing promoters. ISG-transcripts are subsequently translated and collectively antagonize viral infection, increase cell's sensitivity to viral infection, and desensitize cell to further stimulation by IFNs. (Figure created with Biorender.com)

1.1.4 Viral strategies of evading the IFN response

As the IFN response is integral for antiviral immunity, RNA viruses that infect mammals have evolved strategies to evade and hinder this response to effectively establish infection. Three common strategies which viruses use to circumvent the IFN response are: sequestration of the viral genome and replication complex, disruption of IFN induction and/or signaling, and interfering of host protein synthesis (reviewed in (Garcia-Sastre 2017)).

As viral RNA genomes and their dsRNA replication products are susceptible to detection by PRRs, RNA viruses in turn have evolved strategies to circumvent this detection. Some RNA viruses such as picornaviruses and flaviviruses carry out their genome replication in membranous organelles, thereby making their dsRNA intermediates inaccessible to cytoplasmic RLRs (Dorobantu et al., 2015; Paul and Bartenschlager 2015). Others, such as influenza virus and bornaviruses carry out replication in the nucleus where RLRs are absent (Schlee et al., 2009; Herrel et al., 2012). Some RNA viruses also modify or sequester the 5'-end of their genomes and transcripts (Habjan et al., 2008; Daffis et al., 2010; Goodfellow 2011) to evade detection by RIG-I that senses RNA with 5'-triphosphate.

Many RNA viruses also express viral proteins that directly interfere with IFN induction and/or signaling pathways, thereby preventing the secretion of IFNs and the induction of ISGs. To mount a robust IFN response, the functions of adaptors, kinases, phosphatases, ubiquitin ligases, and transcription factors involved in the pathways must be intact. Viruses can impede the IFN induction and/or signaling pathways by disrupting the functions of host proteins in these pathways. For instance, non-structural protein 5 (NS5) of yellow fever virus binds STAT2, thereby preventing ISGF3-dependent ISG transcription (Laurent-Rolle et al., 2014). Additionally, the nucleoprotein of arenaviruses prevents IRF3 phosphorylation by interacting with the kinase

domain of IKKε (Pythoud et al., 2012). Another example involves Influenza A virus (IAV) NS1, which sequesters TRIM25 from RIG-I, thus preventing the activation of RIG-I which relies on ubiquitination (Gack et al., 2007; Gack et al., 2009).

Viruses can also limit the expression of IFNs and ISGs by disrupting entire host transcription and/or translation machineries. For many viruses with their own RNA polymerases, transcriptional shutoff is beneficial for replication as it prioritizes translation of viral transcripts over host mRNA, including IFN and ISG transcripts. Poliovirus encoded protease 3C has been shown to proteolytically cleave TATA-binding protein, thereby suppressing RNA polymerase II-mediated transcription (Kundu et al., 2005). While both viral and host transcripts rely on ribosomes for their protein expression, many viral transcripts do not require certain host translation factors. Therefore, viruses exploit these differences to facilitate translation of viral transcripts and suppress host protein translation. For example, hepatitis C virus induces host translational shutoff through PKR dependent inactivation of eIF2α (Garaigorta and Chisari 2009). The transcripts of hepatitis C virus have internal ribosomal entry sites (IRES) that do not require eIF2α, thus their protein expression is not affected.

1.2 Alphavirus

Alphaviruses are enveloped, (+)ssRNA viruses that belong to the genus Alphavirus and family *Togaviridae*. Many alphaviruses are mosquito-transmitted arboviruses that infect different vertebrate hosts, including humans. Alphaviruses can be further classified as “New World” and “Old World” alphaviruses based on genetic similarities and the diseases they cause in humans. New World alphaviruses such as eastern, western, and Venezuelan equine encephalitis viruses often cause serious neurological diseases when they infect humans. Old World alphaviruses

include chikungunya virus (CHIKV), Ross River virus (RRV), Semliki Forest virus (SFV), O'nyong-nyong virus (ONNV), and Mayaro virus (MAYV). Most of these viruses cause rheumatic diseases and are also referred to as arthritogenic alphaviruses. Old World alphaviruses such as CHIKV, RRV, and ONNV have caused significant epidemics in the past, collectively infecting ~10 million people (Suhrbier et al., 2012).

Most alphaviruses are maintained in rural or isolated areas via the sylvatic cycle where they circulate between mosquito vectors and wild animals such as non-human primates. However, many of these viruses also have the potential to cause large outbreaks by spreading via the urban cycle where they circulate between mosquito species such as *Aedes* and *Anopheles* mosquitoes and humans. For instance, a single mutation in the envelope (E1) protein of CHIKV led to increased fitness and transmission in the *Aedes albopictus* vector (Tsetsarkin et al., 2007). In turn, this was associated with epidemics in peri-urban settings. Habitats of these alphavirus-transmitting mosquitos are expanding due to climate change (Cao-Lormeau and Musso 2014; Leal Filho et al., 2017), driving further spread of these viruses in new geographical regions. As such, there is concern that emerging alphaviruses may cause large epidemics similar to what was observed with arboviruses such as CHIKV, Zika virus (ZIKV), and Dengue virus (DENV) in the recent past.

1.2.1 Mayaro virus

Mayaro virus (MAYV) is an emerging Old World alphavirus that was first discovered in Trinidad in 1954 (Casals and Whitman 1957). Similar to CHIKV, SFV, and ONNV, MAYV is transmitted by mosquitos and causes debilitating rheumatic disease (Lavergne et al., 2006). There are three distinct MAYV genotypes: the most prevalent disseminated (D), limited (L), and new (N) genotypes (Auguste et al., 2015). MAYV is currently endemic in rural communities of Central

and South America, where it is maintained via the sylvatic cycle. However, recent human-driven phenomena such as climate change, international travel, deforestation, and land development is driving the spread of MAYV to new environments including urban settings. Indeed, data show that the prevalence of MAYV has increased in recent decades (Diagne et al., 2020), potentiating the risk of global spread and future outbreaks.

1.2.1.1 Epidemiology and clinical significance of MAYV

The main vectors for MAYV in Central and South America are *Haemagogus* mosquitos (Tasso de Oliveira Mota et al., 2015). Accurate tracing of human infections is hindered by the sporadic nature of the outbreaks and low level of diagnostic testing in endemic areas (Ganjian and Riviere-Cinnamond 2020). As such, the actual prevalence of MAYV may be significantly underestimated. Recent studies have shown that MAYV can be transmitted by *Aedes* and *Anopheles* mosquito species which have comparatively wide global distributions and can support an urban transmission cycle (Brustolin et al., 2018; Wiggins et al., 2018). Imported cases of MAYV infections have already been reported in Europe and North America (Taylor et al., 2005; Theilacker et al., 2013; Slegers et al., 2014; Llagonne-Barets et al., 2016) but the virus has not become endemic in these areas yet.

MAYV is the causative agent of Mayaro fever, which is characterized as a debilitating flu-like disease. After inoculation of MAYV through a mosquito bite, the incubation period is typically 7 to 12 days, followed by viremia, which coincides with acute symptoms such as fever, chills, skin rashes, arthralgia, and myalgia (Torres et al., 2004). These symptoms are very similar to the acute symptoms caused by CHIKV, ZIKV, and DENV, which are also prevalent where MAYV circulates, thus complicating the diagnosis of Mayaro fever. Additionally, approximately 50% of

MAYV infections are thought to be asymptomatic (Nakkhara et al., 2013), further contributing to the underestimation of MAYV infection in humans. Conversely, more than half of the patients with acute Mayaro fever experience long-term arthritis, which can persist for over a year (Halsey et al., 2013). MAYV-associated arthritis is due to persistent viral infection and/or a prolonged proinflammatory response initiated by the virus (Hoarau et al., 2010; Santiago et al., 2015; Uhrlaub et al., 2016; Figueiredo et al., 2019) but further studies are required to elucidate the mechanism of this chronic condition. There is considerable interest in developing therapeutics against MAYV (Langendries et al., 2021; Powers et al., 2021; Hoque et al., 2021; Rafael et al., 2020; Campos et al., 2020) but so far, no vaccines or specific antiviral treatments have been licensed.

1.2.1.2 Biology and replication cycle of MAYV

Similar to other arthritogenic alphaviruses, MAYV infects a wide range of cell types which include macrophages and monocytes, dendritic cells, synovial and dermal fibroblasts, endothelial cells, muscle cells, osteoblasts, chondrocytes, and keratinocytes (Suhrbier et al., 2012). A cellular receptor for MAYV entry was recently identified as matrix remodeling-associated protein 8 (Mxra8), which is highly expressed in dermal and synovial fibroblasts, osteoblasts, chondrocytes, and skeletal muscle cells (Zhang et al., 2018). MAYV is thought to have additional receptors since it can infect keratinocytes, which express little to no Mxra8 on their cell surface (Zhang et al., 2018).

MAYV is first introduced to the host through the bite of an infected mosquito. The virus initially infects local keratinocytes in the skin and further multiplies in dermal fibroblasts (Fong et al., 2018). Viral replication in these cells activates the innate immune response and results in recruitment of phagocytes such as dendritic cells and macrophages, which are also susceptible to

MAYV infection. Infected phagocytes travel to lymph nodes where the virus further multiplies and activates the innate and adaptive immune response. Thereon, MAYV spreads to other tissues, such as muscle and joints, through blood circulation or the lymphatic system. At this stage, viremia and symptoms of acute MAYV fever are observed. Viral RNA were found in joints, especially in synovial fibroblasts and macrophages, months after infection when no viremia is observed, causing long-term arthralgia (Suhrbier and Mahalingam 2009).

MAYV has a ~11.5 kb (+)ssRNA genome with two open reading frames (ORFs). The 5' ORF encodes four nonstructural proteins (NSP1, 2, 3, and 4), which together form the viral RNA-dependent RNA polymerase (RdRp) replication complex. The 3' ORF encodes the viral structural proteins: capsid (C), envelope (E1, 2, and 3), 6K, and transframe (TF) protein which are the building blocks of infectious virions. Mature virions contain a single RNA genome surrounded by nucleocapsid proteins, a host plasma membrane-derived envelope, and E1-E2 heterodimer surface glycoproteins. The nucleocapsid adopts an icosahedral symmetry and interacts with the intracellular domains of E1 and E2 proteins (Ribeiro-Filho et al., 2021).

MAYV entry is mediated by the interaction between MAYV E2 and Mxra8 at the cell surface. This protein interaction initiates clathrin-dependent endocytosis of the virion (Carvalho et al., 2017; Zhang et al., 2018). Upon exposure to the low pH of the endosome, the envelope of MAYV fuses with the endosomal membrane, releasing its (+)ssRNA genome into the cytoplasm (Figure 1.3). The viral genome contains a 5'cap and 3-poly(A) tail which allows immediate translation of 5'-end ORF to yield the nonstructural polyproteins, P123 and P1234. There is an opal stop codon at the 3'-end of the NSP3-encoding sequence which is occasionally readthrough (Strauss et al., 1983). As a result of this stop codon, only ~10% of nonstructural polyproteins are full length (P1234), while most nonstructural polyproteins do not contain NSP4 (P123) (Pietila et

al., 2017). The viral NSP2 protease is responsible for cleaving the non-structural polyproteins into individual NSPs (de Groot et al., 1990). However, since NSP2 cannot access adjacent cleavage sites within the same polyprotein, NSP2 only mediates *cis*-cleavage at the site between NSP3 and NSP4. Thus, NSP4 is promptly released from the nonstructural polyprotein during the early phase of the infection when the concentrations of both P123 and P1234 are low. NSP4 and P123 form the early RdRp complex, which is responsible for minus strand synthesis from genomic (+)ssRNA (Lemm et al., 1994). When P123 reaches a high enough concentration, NSP2 can mediate *trans*-cleavage of neighboring nonstructural polyproteins, now being able to release all the individual NSPs. A late replication complex, composed of fully processed NSP1, 2, 3, and 4, synthesizes 49S genomic and 26S subgenomic RNAs from the minus strand RNA template. Of note, the minus strand RNA and the dsRNA replication intermediates are encased in structures called spherules (Pietila et al., 2017), which are plasma or endosomal membrane protrusions created by the late replication complex and some host proteins. Spherules protect the viral RNA from degradation by host RNases and recognition by RLRs.

The viral structural polyprotein is translated from 26S subgenomic RNA. C is promptly released from the polyprotein by its C-terminal auto-protease activity (Hahn et al., 1985). With the release of C, a signal peptide is exposed at the N-terminus of the E3-E2-6K-E1polyprotein or the translational frameshift product E3-E2-TF and these proteins are translated on and inserted into membranes of the endoplasmic reticulum (ER) (Jose et al., 2009). The structural polyproteins are further processed by furins and glycosyltransferases as move through the *trans*-Golgi network to plasma membrane. At the plasma membrane, E1-E2 heterodimers and nucleocapsids assemble to form mature virions which bud out of the cell.

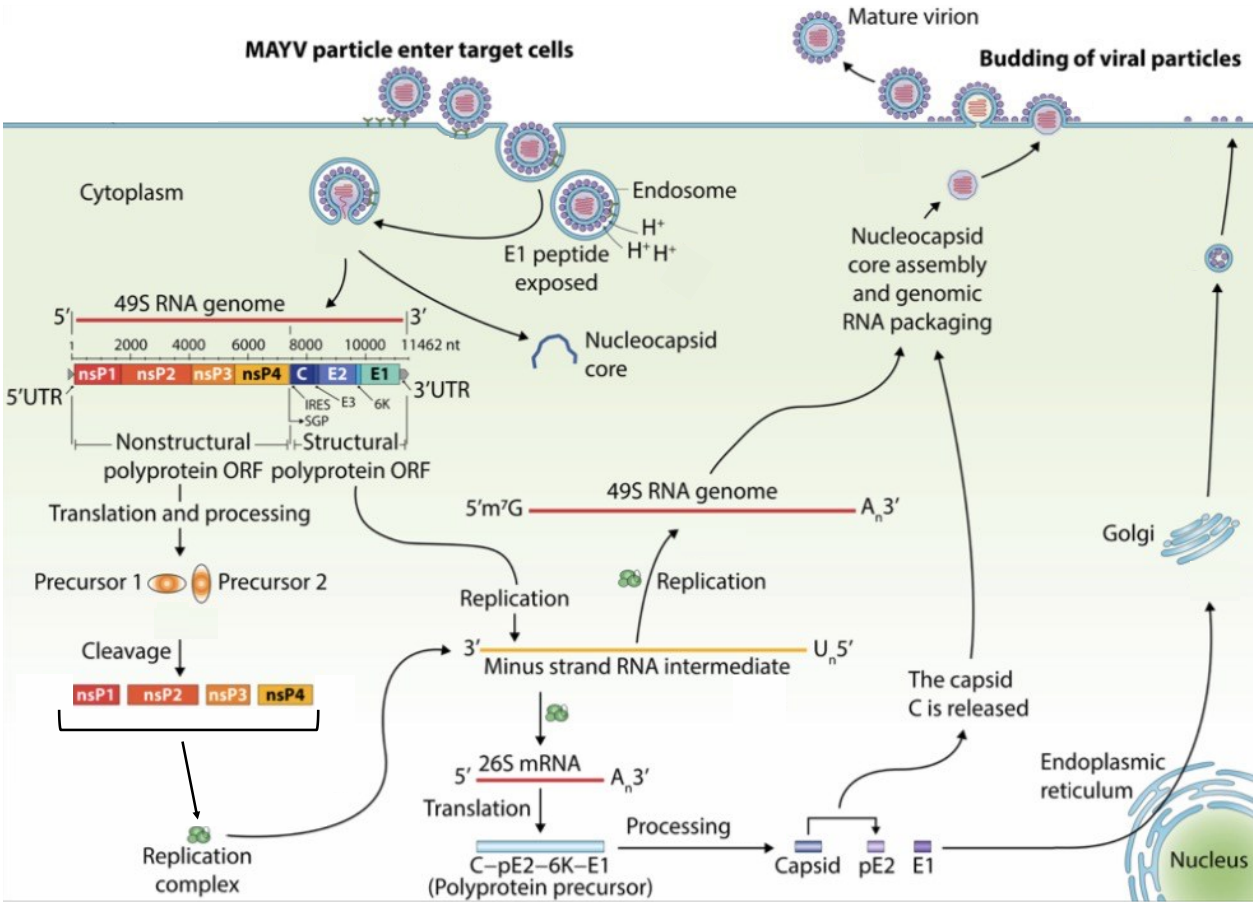

Figure 1.3 Replication cycle of MAYV. MAYV virion is internalized in the endosome after attachment to host target cell, mediated by interaction between E2 and Mxra8. As the endosome acidifies, the viral E1 proteins are exposed which mediate the fusion of viral envelope with endosomal membrane, releasing the viral (+)ssRNA genome into the cytoplasm. The 5'-proximal ORF encoding the viral non-structural proteins are promptly translated from the viral genome, yielding the non-structural polyproteins (P123 and P1234). NSP4 is immediately released from the polyprotein through the protease activity of NSP2 and associates with P123. The P123+NSP4 (early RdRp complex) is responsible for the synthesis of minus strand RNA, which serves as a template for genomic and subgenomic RNA synthesis. Once P123 are substantially abundant, all individual NSPs are released from polyproteins via proteolytic cleavage and forms the late RdRp complex, which synthesizes 49S genomic and 26S subgenomic RNAs. The latter RNAs are translated to yield the structural polyproteins (C-E3-E2-6K-E1 and C-E3-E2-TF). C is promptly released into the cytoplasm after translation due to its autoprotease activity, while the rest of the polyproteins are embedded into the ER membrane as translation proceeds. E1 and E2 are processed by furins and glycosyltransferases as they are traffic through the *trans*-Golgi network to the plasma membrane. Here, C-encapsidated genomic (+)ssRNA, E1, and E2 are assembled into infectious viral particle, which buds out to the extracellular environment. (Modified from Diagne et al., 2020)

1.2.1.3 Antagonism of IFN response by MAYV

Despite the clinical relevance of MAYV, how this pathogen affects the IFN response is not well understood. However, studies on how other arthritogenic alphaviruses interact with the IFN response may apply to MAYV in some respects. Alphavirus RNAs are sensed by both RIG-I and MDA5 during infection (Akhrymuk et al., 2016), however little to no IFN secretion occurs during infection of fibroblasts (Burke et al., 2009; Bhalla et al., 2019; Akhrymuk et al., 2018). Alphaviruses are sensitive to IFN pretreatment in which ISGs are upregulated prior to infection, but are resistant to IFN treatment once they have established infection (Fros et al., 2010; Reynaud et al., 2015; Lane et al., 2018). Indeed, several studies have revealed mechanisms used by alphaviruses to suppress IFN signaling. CHIKV and SFV NSP2 proteins dampen the IFN response by inducing degradation of host DNA-directed RNA polymerase II subunit A (Rpb1), thereby impeding host mRNA transcription (Akhrymuk et al., 2019; Fros et al., 2013; Frolova et al., 2002; Gorchakov et al., 2005; Breakwell et al., 2007). Moreover, CHIKV NSP2 stimulates nuclear export of STAT1 which in turn blocks IFN signalling (Goertz et al., 2018). However, very little is known regarding how alphaviruses block IFN induction.

1.3 Coronavirus

Coronaviruses are enveloped viruses with the largest genomes among (+)ssRNA viruses. They are members of the subfamily *Coronavirinae*, family *Coronaviridae,* and the order *Nidovirales*. The subfamily is composed of four genera: *Alphacoronavirus*, *Betacoronavirus*, *Gammacoronavirus*, and *Deltacoronavirus*. Alphacoronaviruses (α-CoV) and betacoronaviruses (β-CoV) exclusively infect mammals and they include pathogens that are of significance to humans and livestock. Human coronaviruses (HCoV), such as HCoV-NL63 (α-CoV), HCoV-229E (α-

CoV), HCoV-OC43 (β-CoV), and HCoV-HKU1 (β-CoV), infect the upper respiratory tracts of humans and are associated with the common seasonal cold (Forni et al., 2017). Porcine enteric diarrhoea virus (α-CoV), porcine transmissible gastroenteritis virus (α-CoV), and swine acute diarrhoea coronavirus (β-CoV) are all threats to the swine industry (Lin et al., 2016; Zhou et al., 2018; Chen et al., 2019). Since the beginning of the 21st century, there have been three spillover events of highly pathogenic β-CoVs from bats to humans that resulted in significant epidemics/pandemics. Severe acute respiratory syndrome coronavirus (SARS-CoV) emerged in 2002 in the Guangdong province of China and rapidly spread human-to-human via respiratory droplets, resulting in more than 8,000 human cases and 774 deaths (Zhong et al., 2003; Anderson et al., 2004). Middle East respiratory syndrome coronavirus (MERS-CoV) emerged in 2012 and is a highly pathogenic virus with a mortality rate of 35% (Zaki et al., 2012; Dighe et al., 2019). While MERS-CoV is inefficient at transmitting human-to-human, this virus continues to infect humans primarily due to close contacts to camels, which are reservoir hosts. SARS-CoV-2 emerged in 2019 in the Hubei province of China (Huang et al., 2020) and rapidly spread globally, resulting in the ongoing pandemic.

1.3.1 SARS-CoV-2

SARS-CoV-2 is a recently emerged betacoronavirus and the causative agent of the currently ongoing coronavirus infectious disease 2019 (COVID-19) pandemic. As the name suggests, SARS-CoV-2 is closely related to SARS-CoV and other bat SARS-like coronaviruses (Wu et al., 2020). Most SARS-CoV-2 infections result in asymptomatic or mild illness, however up to 20% of infections lead to a severe form of the disease, causing irreversible damage to lungs and other organs (Wu and McGoogan 2020; Tsai et al., 2021). While there are vaccines and

therapeutics available against SARS-CoV-2, it is important to understand the biology of the virus to guide the development of novel antivirals that may be used for future pandemics and vaccine-resistant variants.

1.3.1.1 Epidemiology and clinical significance of SARS-CoV-2

The SARS-CoV-2 outbreak was first detected in the city of Wuhan, within the Hubei province of China in December of 2019 (Huang et al., 2020). While its origins have been debated, SARS-CoV-2 was likely passed onto humans from bats with or without an intermediate animal host (Casadevall et al., 2021; Sallard et al., 2021). Since its emergence, human-to-human transmission was apparent as the virus spread exponentially across the globe, forcing the World Health Organization to declare a Public Health Emergency of International Concern on January 30th, 2020 and a global pandemic on March 11th of the same year. SARS-CoV-2 is primarily transmitted through respiratory droplets during periods of close contact with infected individuals. SARS-CoV-2 outbreaks are particularly difficult to contain since the virus can be transmitted from asymptomatic and pre-symptomatic individuals (Buitrago-Garcia et al., 2020), as opposed to SARS-CoV, which is primarily transmitted from symptomatic patients. As of this writing, SARS-CoV-2 is responsible for over 250 million infections and over 5 million deaths. Recently, several viral variants of concern (VOCs) have emerged and have completely replaced the contemporary SARS-CoV-2 strains (Khateeb et al., 2021; Bano et al., 2021; Kumar, Singh, et al., 2021). These VOCs are highly transmissible and some variants are less susceptible to neutralization by antibodies that target contemporary SARS-CoV-2 strains (Krause et al., 2021). Additionally, as more adults have gained vaccine-induced immunity against SARS-CoV-2, the latest VOCs are circulating and affecting younger children, particularly in developed countries.

The incubation period for COVID-19 is normally 2 to7 days, after which a myriad of symptoms is observed (reviewed in (Wiersinga et al., 2020)). About a third of infected individuals never develop symptoms, but can still transmit SARS-CoV-2 to others (Johansson et al., 2021). Approximately 80% of symptomatic people experience only mild symptoms such as fever, dry cough, shortness of breath, diarrhea, and loss of smell/taste, while others experience more severe symptoms that require hospitalization. Severe complications of COVID-19 include pneumonia and acute respiratory distress syndrome which cause patients to become hypoxic, thus requiring mechanical ventilation or oxygen supplementation (Wiersinga et al., 2020). Severe complications can also manifest in tissues outside the lungs, such as in the liver, kidney, heart, brain, and the vascular system which are associated with multi-organ failure, encephalitis, hypercoagulations, and septic shock (Mir et al., 2021). COVID-19 can also lead to what is known as "long COVID", where the individual is no longer infected with SARS-CoV-2 but continues to experience symptoms (Mahase 2020). Up to 90% of hospitalized patients experience long COVID, which manifests as fatigue, shortness of breath, arthralgia, and chest pain (Carfi et al., 2020), debilitating these individuals and worsening their quality of life.

Age and sex are important determinants of severe COVID-19 outcomes, where the highest hospitalization rates are observed in males that are > 65 years (Wiersinga et al., 2020). On the other hand, SARS-CoV-2 infections in younger age groups are often asymptomatic or very mild as the infection is usually limited to the upper respiratory tract. However, the latest VOCs are more likely to cause disease in these demographics since vaccinations have yet to be approved for younger individuals in many countries (Khateeb et al., 2021; Kumar, Singh, et al., 2021). Other risk factors for severe COVID-19 include diabetes, hypertension, cardiovascular disease, pulmonary disease, and malignancy (Wiersinga et al., 2020).

1.3.1.2 Biology and replication cycle of SARS-CoV-2

Similar to SARS-CoV and bat SARS-like coronaviruses, SARS-CoV-2 uses angiotensin converting enzyme 2 (ACE2) as a receptor for host cell entry (Figure 1.4) (Li et al., 2003; Menachery et al., 2015; Lan et al., 2020). Cell surface expression of type 2 transmembrane serine protease (TMPRSS2) can further promote entry of SARS-CoV-2 (Hoffmann et al., 2020). ACE2 and TMPRSS2 are expressed on the surface of many cell types, particularly on type II alveolar epithelial cells of the lungs (Wiersinga et al., 2020). ACE2 and TMPRSS2 are also expressed in cells of the liver, kidney, heart, and gastrointestinal tract (Sungnak et al., 2020; Zou et al., 2020). Expression of these proteins in multiple tissues broadens SARS-CoV-2 tropism and correlates with the various symptoms observed in individuals with COVID-19.

SARS-CoV-2 has a ~29.8 kb (+)ssRNA genome that encodes 15 non-structural proteins (NSP1-10 and NSP12-16), 4 structural proteins (spike (S); envelope (E); membrane (M); nucleocapsid (N)), and 9 accessory proteins (ORF10, ORF14, P6, NS3A, NS3B, NS7A, NS7B, ORF8, and NS9B) (Wu et al., 2020). Infectious virions contain a single (+)ssRNA genome encapsulated by N, M and E proteins that are embedded in the viral envelope, and S glycoprotein trimers which protrude out of the viral envelope and give the infectious particle a crown-like (corona) appearance (V'Kovski et al., 2021). Virion binding to target cells is mediated by the interaction between S and ACE2. SARS-CoV-2 S is cleaved by cell surface TMPRSS2 or endosomal proteases to allow for fusion of the viral envelope and host membrane at the cell surface or within endosomes, respectively (Hoffmann et al., 2020; Ou et al., 2020). SARS-CoV-2 S protein can be divided into domains S1 and S2: S1 contains the receptor-binding domain and is exposed on the surface of a virion, while S2 is mostly embedded in the viral envelope and mediates fusion of membranes (Letko et al., 2020). A polybasic cleavage site exists between the two S domains,

which is cleaved by the host protease furin (Walls et al., 2020). The pre-processing of SARS-CoV-2 S improves viral infection and is also associated with greater zoonosis potential (Letko et al., 2020; Walls et al., 2020).

Once the viral and host membranes fuse, the viral (+)ssRNA genome is released to the cytoplasm where the viral non-structural polyproteins (pp1a and pp1ab) are directly translated from the genome (V'Kovski et al., 2021). Pp1a contains NSP1-10, while pp1ab, which results from a programmed ribosomal frameshift product, contains all 15 NSPs. There are two viral proteases, NSP3 (papain-like protease; PLpro) and NSP5 (main protease; Mpro), that are responsible for releasing individual NSPs from polyproteins. The viral NSP1 is promptly released from pp1a/pp1ab through proteolytic cleavage by PLpro (Denison and Perlman 1986). PLpro releases NSP1-3, while Mpro releases the remaining non-structural proteins. NSP2-16 form the viral replication and transcription complex (RTC) which synthesizes the viral genomic and subgenomic RNAs. Notably, NSP14 of coronaviruses have 3'-5' exonuclease activity and mediate proofreading during RNA synthesis (Eckerle et al., 2007). Thus, unlike other RNA viruses, RNA synthesis by coronaviruses is less prone to errors, allowing for large RNA genomes. Negative-strand RNA synthesis is frequently disrupted following transcription regulatory sequences located 3' of each negative-sense ORF. These negative-strand RNAs are used as templates for subgenomic RNA synthesis. As a result, subgenomic RNAs have different ORFs on their 5'-ends, depending on where the negative-strand RNA synthesis was disrupted. Only the most 5' ORF will be translated from a given viral transcript, hence the viral protein expression profile is governed by this arbitrary transcription process (V'Kovski et al., 2021).

Viral structural proteins, except N, are translated and embedded at the ER membrane, and virion assembly occurs at the ER-Golgi intermediate compartment (ERGIC) where the

encapsulated genome is also incorporated (Klein et al., 2020). Once mature SARS-CoV-2 virions are assembled, they are released through exocytosis. Accessory proteins of coronaviruses are not required for viral replication or virion formation. However, their sequences are conserved among many coronavirus species which suggests that they are beneficial to these viruses (V'Kovski et al., 2021). Elucidating the functions of accessory proteins which may suppress the host immune response has been challenging (Li et al., 2020; Miorin et al., 2020; Xia et al., 2020; Yuen et al., 2020; Rashid et al., 2021; Shemesh et al., 2021). While their existence within SARS-CoV-2-infected cells is debated, there have been dozens of additional accessory proteins proposed to be expressed by the virus (Finkel et al., 2021), however further investigations are required to understand their roles during infection.

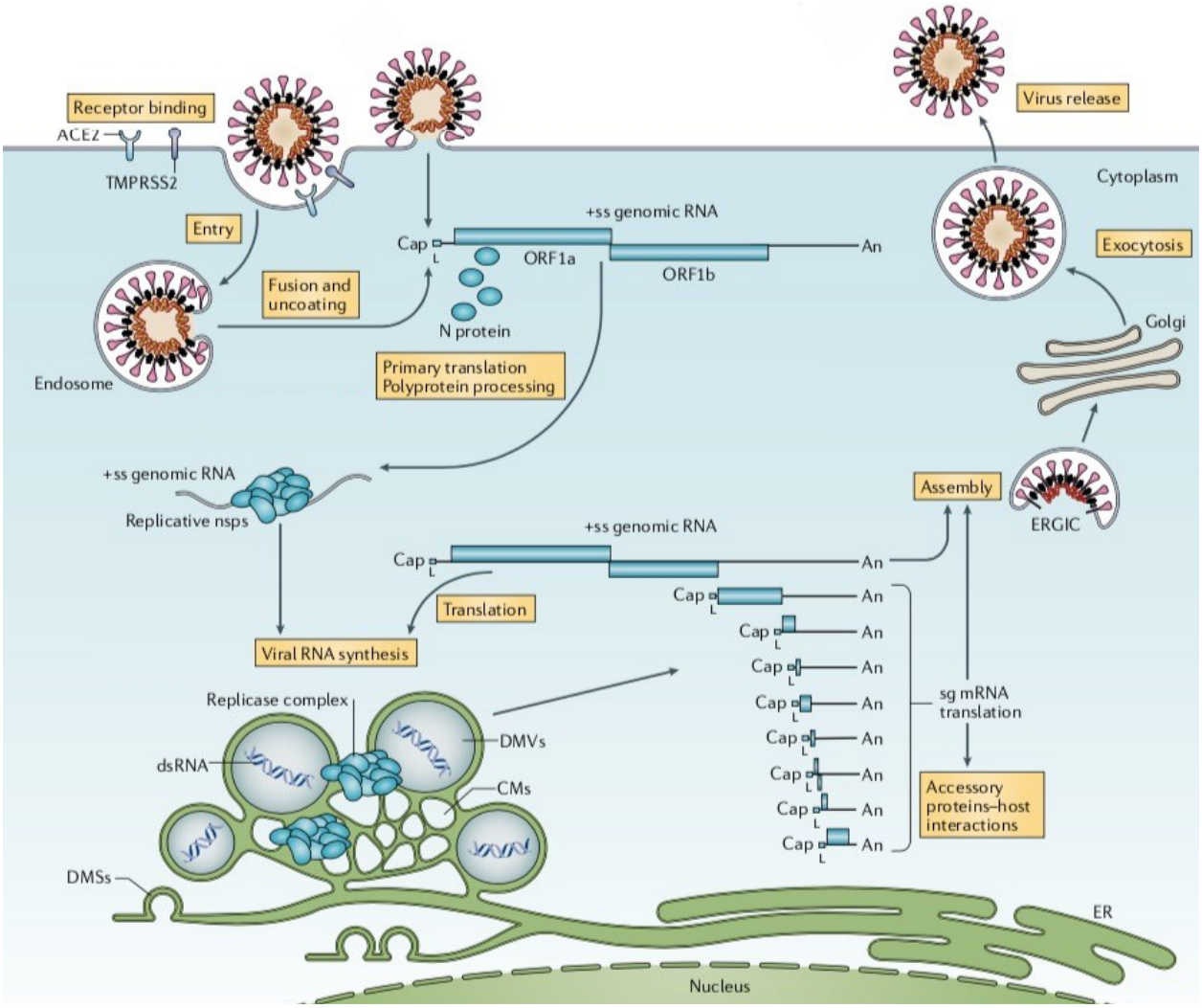

Figure 1.4 Replication cycle of SARS-CoV-2. The attachment of SARS-CoV-2 to target cell is mediated through the interaction between viral S and ACE2. Cell surface TMPRSS2 cleaves viral S and allows the viral envelope to fuse with plasma membrane and the subsequent release of encapsidated (+)ssRNA genome to the cytoplasm. Alternatively, the virion is endocytosed and S is cleaved by endosomal proteases and mediate fusion of viral envelope with endosomal membrane. The genome are immediately translated to yield non-structural polyproteins (pp1a and pp1ab). Pp1a and pp1ab are processed by viral NSP3 and NSP5 proteases, releasing individual NSPs. All NSPs except for NSP1 form the replicase complex, which synthesizes genomic and subgenomic RNAs. Structural proteins (S, M, E, N) and accessory proteins (NS3A, NS3B, P6, NS7A, NS7B, NS8B, NS9B, ORF10, and ORF14) are translated from subgenomic RNAs. The structural proteins and SARS-CoV-2 genome is assembled at the ER-Golgi intermediate compartment (ERGIC) to form infectious virion, which is trafficked across Golgi. Here the viral S proteins are processed by furins and glycosyltransferases, after which the virion is released to the extracellular environment via exocytosis. (Modified from V'Kovski et al., 2021)

1.3.1.3 Antagonism of IFN response by SARS-CoV-2

Since the emergence of SARS-CoV-2, extensive studies have focused on understanding how this virus affects the host IFN response. Mounting evidence suggests that SARS-CoV-2 is a poor inducer of IFNs and ISGs during infection (Neufeldt et al., 2020; Israelow et al., 2020; Hadjadj et al., 2020; Blanco-Melo et al., 2020; Vanderheiden et al., 2020b; Miorin et al., 2020). SARS-CoV-2 and other coronaviruses replicate their genomes in double-membrane vesicles, thereby protecting their dsRNA replication intermediates from recognition by RLRs (van Hemert et al., 2008; Knoops et al., 2008; Snijder et al., 2020). Thus far, more than half of SARS-CoV-2 proteins (NSP1, NSP3, NSP6, NSP7, NSP12, NSP13, NSP14, NSP15, N, M, S, NS3A, NS3B, P6, NS7A, NS7B, NS8B, and NS9B) have been implicated to suppress IFN induction and/or IFN signaling, however many studies report conflicting results (Li et al., 2020; Xia et al., 2020; Lei et al., 2020; Yuen et al., 2020; Shin et al., 2020; Jiang et al., 2020; Miorin et al., 2020; Zheng et al., 2020; Gori Savellini et al., 2021; Shemesh et al., 2021; Zhao et al., 2021; Oh and Shin 2021; Wang et al., 2021; Rashid et al., 2021; Mu et al., 2020a).

Notably, SARS-CoV-2 NSP1, N, and P6 are consistently reported as an antagonist of the IFN response. NSP1 has been shown to impede host translation, thereby limiting the expression of IFNs and ISGs (Banerjee et al., 2020; Thoms et al., 2020). N protein was recently reported to interfere with RIG-I activation by sequestering TRIM25, while high concentrations of N lead to upregulation of IFN signaling (Zhao et al., 2021). Lastly, P6 (also known as ORF6) disrupts bidirectional nuclear transport of proteins through its interaction with Nup98 and Rae1, thereby blocking the nuclear translocation of IRF3 and STAT1/2 (Miorin et al., 2020; Xia et al., 2020; Addetia et al., 2021).

1.4 Objectives of thesis

The IFN response is critical for controlling infections by (+)ssRNA viruses, which in turn have evolved multiple strategies to overcome this cellular antiviral response. Due to their broad spectrum antiviral activity, IFNs are often considered for treating viral infections, especially by emerging (+)ssRNA viruses. Therefore, understanding the relationships between (+)ssRNA viruses and the IFN response is important for determining the therapeutic options against these viruses. The objective of this thesis is to characterize how two emerging (+)ssRNA viruses, MAYV and SARS-CoV-2, interact with the host IFN response during infection.

Chapter 3 describes how MAYV antagonizes the IFN induction pathway through general transcriptional shutoff. The NSP2 of MAYV downregulated Rpb1 and transcription initiation factor II E subunit 2 (TFIIE2), both of which are required for host RNA polymerase II-mediated transcription. As a result, MAYV disrupts host mRNA synthesis, including that of IFNs during infection.

Chapter 4 describes how SARS-CoV-2 robustly subverts both induction and signaling arms of the IFN response. Mapping analysis revealed that the viral NSP1 and N block IFN induction, while only NSP1 antagonizes IFN signaling. Specifically, NSP1-mediated host translational shutoff limits the expression of key IFN response mediators such as Tyk2 and STAT2, in addition to IFNs and ISGs, aggravating the inhibition of the IFN response.

Chapter 2

Materials and Methods

2.1 Materials

2.1.1 Reagents

The reagents listed below were used according to the manufacturers' instructions unless specified otherwise.

Table 2.1 Sources of commercially prepared reagents

Reagent	Source
30% Acrylamide/Bis solution (29:1)	Bio-Rad
Adenosine triphosphate (ATP)	Boeheringer Mannheim
Agar	Sigma-Aldrich
Agarose, Ultrapure	Invitrogen
Ammonium persulphate (APS)	Invitrogen
Ampicillin	Sigma-Aldrich
Anti-Flag M2 Magnetic Beads	Millipore
Bafilomycin A1	Sigma-Aldrich
Bovine Serum Albumin (BSA)	Sigma-Aldrich
Bovine Serum Albumin (BSA) Endotoxin-free	Millipore
Bromophenol Blue	Sigma-Aldrich
Coelenterazine	Gold Biotechnology USA
cOmplete^{TM} EDTA-free Protease Inhibitor Cocktail	Roche
Crystal Violet	Sigma-Aldrich
Dimethyl sulfoxide (DMSO)	Sigma-Aldrich
Dithiothreitol (DTT)	Sigma-Aldrich
D-luciferin	Gold Biotechnology USA
DNA Gel Loading Dye (6X)	Thermo Fisher Scientific
Dulbecco's Modified Eagle Medium (DMEM)	Gibco
Ethanol	Commercial Alcohols
Ethidium bromide solution	Sigma-Aldrich
Ethylenediaminetetraacetic acid (EDTA)	EMD Chemicals

Reagent	Source
Ethylene glycol-bis (β-aminoethyl ether)-N, N, N‘, N‘-tetraacetic acid (EGTA)	Sigma-Aldrich
Epoxomicin	Sigma-Aldrich
Fetal Bovine Serum (FBS)	Invitrogen
40% Formaldehyde (v/v)	Sigma-Aldrich
Glycerol	Thermo Fisher Scientific
Glycine	EM Science
Glycylglycine	Sigma-Aldrich
Hydrochloric acid	Thermo Fisher Scientific
Isopropanol	Sigma-Aldrich
Immobulin®-P PVDF Membrane	EMD Millipore
Kanamycin	Sigma-Aldrich
LB agar	Invitrogen
L-glutamine	Invitrogen
Lipofectamine 2000	Invitrogen
Magnesium sulphate ($MgSO_4$)	BDH Inc.
Methanol	Sigma-Aldrich
Methylcellulose	Sigma-Aldrich
Minimal Essential Media (MEM)	Gibco
N-2-hydroxyethylpiperazine-N-2-ethane sulfonic acid (HEPES)	Gibco
N, N, N’, N’-tetramethylethylenediamine (TEMED)	Sigma-Aldrich
Non-essential Amino Acids (NEAA)	Gibco
OptiMEM	Gibco
16% Paraformaldehyde (PFA) EM Grade	Electron Microscopy Science
Penicillin-streptomycin solution (100X)	Invitrogen
Polyinosinic-polycytidylic acid (Poly(I:C))	Invivogen
Potassium chloride (KCl)	Becton Dickinson & Company
Potassium phosphate (K_2PO_4)	BDH Inc.

Reagent	Source
ProLong Gold Antifade Reagent without DAPI	Invitrogen
Random Oligonucleotide Primers	Invitrogen
Sodium azide	Sigma-Aldrich
Sodium chloride (NaCl)	Sigma-Aldrich
Sodium dodecyl sulphate (SDS)	Bio-Rad
Sodium fluoride (NaF)	Sigma-Aldrich
Sodium hydroxide (NaOH)	Sigma-Aldrich
Super Optimal broth with Catabolite repression (SOC) medium	Invitrogen
TransIT-LT1	Mirus Bio
Tris base	EMD Chemicals
Triton X-100	Thermo Fisher Scientific
0.25% Trypsin-EDTA	Invitrogen
Tween 20	Thermo Fisher Scientific

Table 2.2 Molecular markers

Molecular marker	Source
GeneRuler 1kb Plus DNA Ladder	Thermo Fisher Scientific
PageRuler™ Prestained Protein Ladder	Thermo Fisher Scientific

Table 2.3 Enzymes used for manipulation of nucleic acid

Enzyme	Source
Alkaline Phosphatase, Calf Intestinal (CIP)	New England Biolabs
Benzonase	Millipore
Improm-II Reverse Transcriptase System	Promega
PerfeCTa SYBR Green Super Mix, Low Rox	Quanta Biosciences
Platinum™ *Taq* DNA Polymerase High Fidelity	Invitrogen
Restriction Endonucleases	New England Biolabs and Thermo Fisher Scientific
T4 Ligase (EL0011)	Thermo Fisher Scientific
SuperScript™ III Reverse Transcriptase	Invitrogen

Table 2.4 Commercially available kits

Kit	Source
Human IFN-beta Quantikine ELISA Kit	R&D Systems
NucleoBond Xtra Maxi Kit for Plasmid DNA	Macherey-Nagel
NucleoSpin RNA, Mini Kit for RNA Purification	Macherey-Nagel
QIAEX II Gel Extraction Kit	QIAGEN
QIAprep Spin Miniprep Kit	QIAGEN
QIAquick PCR Purification Kit	QIAGEN

2.1.2 Commonly used buffers and solutions

Table 2.5 Buffers and solutions

Buffer/Solution	Ingredients
Blocking Buffer	5% (w/v) BSA, 137 mM NaCl, 2.7 mM KCl, 8 mM Na_2HPO_4 (pH 7.4), 0.05% (v/v) Tween-20
IP Buffer	150 mM NaCl, 50 mM Tris pH 7.5, 1% Triton X-100, 1 mM NaF, 1 mM DTT, and protease inhibitor cocktail
LB Growth Media	1% (w/v) Bacto Tryptone, 0.5% (w/v) Bacto-yeast Extract, 0.5% (w/v) NaCl, 1 mM NaOH
Luciferase Assay Buffer	25 mM Glycylglycine (pH 7.8), 15 mM K_2PO_4 (pH 7.8), 15 mM $MgSO_4$, 4 mM EGTA
Luciferase Lysis Buffer	0.1% (v/v) Triton X-100, 25 mM Glycylglycine (pH 7.8), 15 mM $MgSO_4$, 4 mM EGTA and fresh 1mM DTT
Phosphate buffered saline (PBS)	137 mM NaCl, 2.7 mM KCl, 8 mM Na_2HPO_4 (pH 7.4)
PBS-Tween	137 mM NaCl, 2.7 mM KCl, 8 mM Na_2HPO_4 (pH 7.4), 0.05% (v/v) Tween-20
SDS-PAGE Running Buffer	192 mM Glycine, 0.1% (w/v) SDS, 25 mM Tris Base (pH 8.3)
5X SDS Sample Buffer	62.5 mM Tris-HCl (pH 6.8), 50% (v/v) Glycerol, 2% (w/v) SDS, 0.01% (w/v) Bromophenol blue, 100mM DTT
Tris-acetate-EDTA (TAE) Buffer	40 mM Tris acetate, 1 mM EDTA (pH 8.0)
Transfer Buffer	200 mM Glycine, 25 mM Tris base (pH 8.3), 20% (v/v) Methanol, 0.1% (w/v) SDS

2.1.3 Antibodies

Table 2.6 Primary antibodies

Antibody	Catalog #	Dilution	Application	Source
Goat anti-ACE-2	AF933-SP	1:200	FC	R&D Systems
Goat anti-GFP	ab6673	1:1000	WB	Abcam
Mouse anti-CHIKV-E2		1:200	IF	Dr. M. Diamond, Washington University School of Medicine
Mouse anti-FLAG M2	F3165	1:2000, 1:500	WB, IF	Sigma Aldrich
Mouse anti-HA-HRP	A01244	1:2000	WB	GenScript
Mouse anti-Jak1	sc-1677	1:1000	WB	Santa Cruz
Mouse anti-Rpb1	GTX60342	1:1000, 1:250	WB, IF	GeneTex
Mouse anti-SARS-CoV/ SARS-CoV-2 Spike	GTX632604	1:2000, 1:250	WB, IF	GeneTex
Mouse anti-V5	R96025	1:2000	WB	Invitrogen
Mouse anti-β-Actin	A3853	1:5000	WB	Sigma Aldrich
Rabbit anti-CHIKV-Capsid		1:1000/10,000	IF/WB	Dr. A. Merit, University of Tartu
Rabbit anti-GST	G7781	1:2000	WB	Sigma Aldrich
Rabbit anti-GTF2E2	ab187143	1:500/2000	IF/WB	Abcam
Rabbit anti-IFNAR1	ab124764	1:1000	WB	Abcam
Rabbit anti-IRF3	#11904	1:250/1000	IF/WB	Cell Signaling
Rabbit anti-Phospho-IRF3	#4947	1:500	WB	Cell Signaling
Rabbit anti-SFV-Capsid		1:2000	WB	Dr. A. Merit, University of Tartu
Rabbit anti-STAT1	sc-346	1:500/2000	IF/WB	Santa Cruz
Rabbit anti-STAT2	sc-476	1:500/2000	IF/WB	Santa Cruz

Table 2.7 Secondary antibodies

Antibody	Catalog #	Dilution	Application	Source
Donkey anti-Goat Alexa680	A21084	1:10000	WB	Invitrogen
Donkey anti-Mouse Alexa488	A10038	1:1000	IF	Invitrogen
Donkey anti-Mouse Alexa546	A21202	1:1000	IF	Invitrogen
Donkey anti-Mouse Alexa680	A10038	1:10000	WB	Invitrogen
Donkey anti-Mouse IRDye800	926-32212	1:10000	WB	Li-COR
Donkey anti-Rabbit Alexa488	A21206	1:1000	IF	Invitrogen
Donkey anti-Rabbit Alexa546	A10040	1:1000	IF	Invitrogen
Donkey anti-Rabbit Alexa680	A21076	1:10000	WB	Invitrogen

2.1.4 Oligonucleotides

Table 2.8 Primers used for cloning reactions

Name	Sequence (5'→3')
MAYV NSP1 NheI Fwd	ATATATGCTAGCATGTCGAAAGTCTTTGTAGATATC
MAYV NSP1 FseI Rev	ATATATGGCCGGCCAAACTCCAACTCTTCCACATCCAC
MAYV NSP2 NheI Fwd	ATATATGCTAGCATGCGAGCGGGAGCCGGTGTTGTCGAGA
MAYV NSP2 FseI Rev	ATATATGGCCGGCCGCAACCAGCTGCCTGCAGCACTGT

Name	Sequence (5'→3')
MAYV NSP3 NheI Fwd	ATATATGCTAGCATGGCTCCAGTGTATGCCGTTAAAAGG
MAYV NSP3 FseI Rev	ATATATGGCCGGCCTCAAGATGAATTACTAATGGTTTC
MAYV NSP4 NheI Fwd	ATATATGCTAGCATGCTAGGCCGTGCGGGGGCCTATATT
MAYV NSP4 FseI Rev	ATATATGGCCGGCCTTTAGGACCGCCGTACAGATGTAT
MAYV C NheI 3xFLAG Fwd	GCTGGCTAGCATGGACTACAAAGACCATGACGGTGATTATA AAGATCATGACATCGACTACAAGGATGACGATGACAAGGGC GGGAGCGGCGGGATGGACTTCCTACCAACTCAAGTGTTATAT ATGCTAGCATGGCGGCCTCGACAGTGACAGCTATG
MAYV C BamHI Rev	GTTTAAACTTAAGCTTGGATCCTACCACTCCACAGTGCCT TCAGGTGT
MAYV E3-E2 NheI Fwd	ATATATGCTAGCATGGCGGCCTCGACAGTGACAGCTATG
MAYV E3-E2 FseI Rev	ATATATGGCCGGCCTGCATGTGCTTTCGGTGCGCAACA
MAYV 6K-E1 NheI Fwd	ATATATGCTAGCATGGCAACAAATGTCTGACACCATATG
MAYV 6K-E1 NheI Rev	ATATATGGCCGGCCCCTTCTCAAAGTTATGCAAGTAAC
MAYV NSP2$^{\Delta protease}$ NheI Fwd	CAAGCTGGCTAGCATGCGAGCGGG
MAYV NSP2$^{\Delta protease}$ FseI Rev	CCGCCGGGCCGGCCCACATCCAAAGGAGCTGCTTCCTG
MAYV NSP2$^{\Delta helicase}$ NheI Fwd	AGCTGGCTAGCATGTTCCAGAATAAAGCTAAAGTGTGC

Name	Sequence (5'→3')
MAYV NSP2$^{\Delta helicase}$ FseI Rev	CGCCGGGCCGGCCGCAACCAGCTG
MAYV NSP2^{K197N} NheI Fwd	CAAGCTGGCTAGCATGCGAGCGGG
MAYV NSP2^{K197N} KpnI Rev	TTCCAAAACGGGTACCAGGCATTT
MAYV NSP2^{K197N} Fusion Fwd	GTCTTGGGCGTGCCCGGATCTGGAAATTCAGGTATAATCAA GAGCCTGGTT
MAYV NSP2^{K197N} Fusion Rev	AACCAGGCTCTTGATTATACCTGAATTTCCAGATCCGGGCA CGCCCAAGAC
MAYV NSP2^{C478A} NheI Fwd	CAAGCTGGCTAGCATGCGAGCGGG
MAYV NSP2^{C478A} KpnI Rev	AAAACGGGTACCAGGCATTTGGCCCAGGCCACTTTAGCTTT ATTCTGGAAC
MAYV NSP2^{RK653AA} KpnI Fwd	AAATGCCTGGTACCCGTTTTGGAA
MAYV NSP2^{RK653AA} FseI Rev	CGCCGGGCCGGCCGCAACCAGCTG
MAYV NSP2^{RK653AA} Fusion Fwd	GAGTACAACCTCATCTTGCCGAGGGCAGCGGTGACGTGGAT TGCTCCGCCGACT
MAYV NSP2^{RK653AA} Fusion Rev	AGTCGGCGGAGCAATCCACGTCACCGCTGCCCTCGGCAAGA TGAGGTTGTACTC
MAYV NSP2^{P722S} KpnI Fwd	AAATGCCTGGTACCCGTTTTGGAA
MAYV NSP2^{P722S} FseI Rev	CGCCGGGCCGGCCGCAACCAGCTG
SARS-CoV-2 NSP1 NheI Fwd	AGCTGGCTAGCCCCAGGGGCCACCATGGAGAGCCTTGTCC CTGGTTTC

Name	Sequence (5'→3')
SARS-CoV-2 NSP1 FseI Rev	CGCCGGGCCGGCCCCCTCCGTTAAGCTCACGCATGAG
SARS-CoV-2 NSP2 PasI Fwd	TAGCCCCAGGGGCCACCATGGCATACACTCGCTATGTCGA TAAC
SARS-CoV-2 NSP2 FseI Rev	CGCCGGGCCGGCCACCGCCTTTGAGTGTGAAGGTATT
SARS-CoV-2 NSP3 PasI Fwd	CTAGCCCCAGGGGCCACCATGGCACCAACAAAGGTTA CTTTTGGT
SARS-CoV-2 NSP3 FseI Rev	CGCCGGGCCGGCCACCACCCTTAAGTGCTATCTTTGT
SARS-CoV-2 NSP4 NheI Fwd	AGCTGGCTAGCCCCAGGGGCCACCATGAAAATTGTTAAT AATTGGTTGAAG
SARS-CoV-2 NSP4 FseI Rev	CGCCGGGCCGGCCCTGCAAAACAGCTGAGGTGATAGA
SARS-CoV-2 NSP5 NheI Fwd	AGCTGGCTAGCCCCAGGGGCCACCATGAGTGGTTTTAG AAAAATGGCATTC
SARS-CoV-2 NSP5 FseI Rev	CGCCGGGCCGGCCTTGGAAAGTAACACCTGAGCATTG
SARS-CoV-2 NSP6 FseI Fwd	AGCTGGCTAGCCCCAGGGGCCACCATGAGTGCAGTGAAA AGAACAATCAAG
SARS-CoV-2 NSP6 FseI Rev	CGCCGGGCCGGCCCTGTACAGTGGCTACTTTGATACA
SARS-CoV-2 NSP7 NheI Fwd	AGCTGGCTAGCCCCAGGGGCCACCATGTCTAAAATGTCAG ATGTAAAGTGC
SARS-CoV-2 NSP7 FseI Rev	CGCCGGGCCGGCCTTGTAAGGTTGCCCTGTTGTCCAG
SARS-CoV-2 NSP8 NheI Fwd	AGCTGGCTAGCCCCAGGGGCCACCATGGCTATAGCCTCAG AGTTTAGTTCC

Name	Sequence (5'→3')
SARS-CoV-2 NSP8 FseI Rev	CGCCGGGCCGGCCCTGTAATTTGACAGCAGAATTGGC
SARS-CoV-2 NSP9 NheI Fwd	AGCTGGCTAGCCCCAGGGGCCACCATGAATAATGAGCTTA GTCCTGTTGCA
SARS-CoV-2 NSP9 FseI Rev	CGCCGGGCCGGCCTTGTAGACGTACTGTGGCAGCTAA
SARS-CoV-2 NSP10 NheI 3xFLAG Fwd	AAGCTGGCTAGCCCCAGGGGCCACCATGGACTACAAAGAC CATGACGGTGATTATAAAGATCATGACATCGACTACAAGG ATGACGAGACAAGGGCCGGCCCGGCGGGAGCGGCGGGGC TGGTAATGCAACAGAAGTGCCT
SARS-CoV-2 NSP10 FseI Rev	AAGCTTGGATCCTACTGAAGCATGGGTTCGCGGAGTTG
SARS-CoV-2 NSP12 PasI Fwd	CTAGCCCCAGGGGCCACCATGTCAGCTGATGCACAATCGT TCCTAAACCGGGTTTGCGGTGTAAGTGCAGCC
SARS-CoV-2 NSP12 FseI Rev	CGCCGGGCCGGCCCTGTAAGACTGTATGCGGTGTGTA
SARS-CoV-2 NSP13 NheI Fwd	AGCTGGCTAGCCCCAGGGGCCACCATGGCTGTTGGGGCTT GTGTTCTTTGC
SARS-CoV-2 NSP13 FseI Rev	CGCCGGGCCGGCCTTGTAAAGTTGCCACATTCCTACG
SARS-CoV-2 NSP14 NheI Fwd	AGCTGGCTAGCCCCAGGGGCCACCATGGCTGAAAATGTA ACAGGACTCTTT
SARS-CoV-2 NSP14 FseI Rev	CGCCGGGCCGGCCCTGAAGTCTTGTAAAAGTGTTCCA
SARS-CoV-2 NSP15 NheI Fwd	AGCTGGCTAGCCCCAGGGGCCACCATGAGTTTAGAAAAT GTGGCTTTTAAT
SARS-CoV-2 NSP15 FseI Rev	CGCCGGGCCGGCCTTGTAATTTTGGGTAAAATGTTTC

Name	Sequence (5'→3')
SARS-CoV-2 NSP16 PasI Fwd	CTAGCCCCAGGGGCCACCATGTCTAGTCAAGCGTGGCAA CCGGGT
SARS-CoV-2 NSP16 FseI Rev	CGCCGGGCCGGCCGTTGTTAACAAGAACATCACTAGA
SARS-CoV-2 N NheI Fwd	AGCTGGCTAGCCCCAGGGGCCACCATGTCTGATAACGGA CCCCAAAATCAGCGAAAT
SARS-CoV-2 N FseI Rev	CGCCGGGCCGGCCAGCCTGAGTTGAGTCAGCACTGCTC
SARS-CoV-2 ORF10 PasI Fwd	AGCTGGCTAGCCCCAGGGGCCACCATGGGCTATATAAAC GTTTTCGCT
SARS-CoV-2 ORF10 FseI Rev	CGCCGGGCCGGCCTGTGAGATTAAAGTTAACTACATC
SARS-CoV-2 ORF14 NheI Fwd	AGCTGGCTAGCCCCAGGGGCCACCATGCTGCAATCGTGC TACAACTTC
SARS-CoV-2 ORF14 FseI Rev	CGCCGGGCCGGCCATCTGTCAAGCAGCAGCAAAGCAA
SARS-CoV-2 P6 NheI Fwd	AGCTGGCTAGCCCCAGGGGCCACCATGTTTCATCTCGTTG ACTTTCAG
SARS-CoV-2 P6 FseI Rev	CGCCGGGCCGGCCATCAATCTCCATTGGTTGCTCTTC
SARS-CoV-2 S NheI Fwd	AGCTGGCTAGCCCCAGGGGCCACCATGTTTGTTTTTCTT GTTTTATTG
SARS-CoV-2 S FseI Rev	CGCCGGGCCGGCCTGTGTAATGTAATTTGACTCCTTT
SARS-CoV-2 E NheI Fwd	AGCTGGCTAGCCCCAGGGGCCACCATGTACTCATTCGT TTCGGAAGAG
SARS-CoV-2 E FseI Rev	CGCCGGGCCGGCCGACCAGAAGATCAGGAACTCTAGA

Name	Sequence (5'→3')
SARS-CoV-2 M PasI Fwd	AGCTGGCTAGCCCCAGGGGCCACCATGGCAGATTCCAACGGTACTATT
SARS-CoV-2 M FseI Rev	CGCCGGGCCGGCCCTGTACAAGCAAAGCAATATTGTC
SARS-CoV-2 NS3A NheI Fwd	AGCTGGCTAGCCCCAGGGGCCACCATGGATTTGTTTATGAGAATCTTC
SARS-CoV-2 NS3A FseI Rev	CGCCGGGCCGGCCCAAAGGCACGCTAGTAGTCGTCGT
SARS-CoV-2 NS3B PasI Fwd	AGCTGGCTAGCCCCAGGGGCCACCATGATGCCAACTATTTTCTTTGCT
SARS-CoV-2 NS3B FseI Rev	CGCCGGGCCGGCCCACTATTGTAAGGTATACAATAGT
SARS-CoV-2 NS7A NheI Fwd	AGCTGGCTAGCCCCAGGGGCCACCATGAAAATTATTCTTTTCTTGGCA
SARS-CoV-2 NS7A FseI Rev	CGCCGGGCCGGCCTTCTGTCTTTCTTTTGAGTGTGAA
SARS-CoV-2 NS7B NheI Fwd	AGCTGGCTAGCCCCAGGGGCCACCATGATTGAACTTTCATTAATTGAC
SARS-CoV-2 NS7B FseI Rev	CGCCGGGCCGGCCGGCGTGACAAGTTTCATTATGATC
SARS-CoV-2 NS8B NheI Fwd	AGCTGGCTAGCCCCAGGGGCCACCATGAAATTTCTTGTTTTCTTAGGA
SARS-CoV-2 NS8B FseI Rev	CGCCGGGCCGGCCGATGAAATCTAAAACAACACGAAC
SARS-CoV-2 NS9B NheI Fwd	AGCTGGCTAGCCCCAGGGGCCACCATGGACCCCAAAATCAGCGAAATG
SARS-CoV-2 NS9B FseI Rev	CGCCGGGCCGGCCTTTTACCGTCACCACCACGAATTC

Name	Sequence (5'→3')
SARS-CoV-2 NSP1-KH164AA Fusion Fwd	TTTCAAGAAAACTGGAACACTGCAGCAAGCAGTGGTGTTACCCGTGAA
SARS-CoV-2 NSP1-KH164AA Fusion Rev	TTCACGGGTAACACCACTGCTTGCTGCAGTGTTCCAGTTTTCTTGAAA

Table 2.9 Primers used for qRT-PCR

Target Gene	Sequence (5'→3')
MAYV NSP1 Fwd	TTCCGAACCAAGTGGGATTC
MAYV NSP1 Rev	CACTTTACGTAYGGKGATGG
Actb Fwd	CCTGGCACCCAGCACAAT
Actb Rev	GCCGATCCACACGGAGTACT
Ifnb Fwd	TAGCACTGGCTGGAATGAGA
Ifnb Rev	TCCTTGGCCTTCAGGTAATG
Ifnl2 Fwd	AGTTCCGGGCCTGTATCCAG
Ifnl2 Rev	GAGCCGGTACAGCCAATGGT
SeV HN Fwd	AAAATTACATGGCTAGGAGGGAAAC
SeV HN Rev	GTGAATGGAATGGTTGTGACTCTTA
GAPDH Fwd	ACAGTCAGCCGCATCTTCTT
GAPDH Rev	GTTAAAAGCAGCCCTGGTGA
Tuba1a Fwd	GCAACAACCTCTCCTCTTCG
Tuba1a Rev	GAATCATCTCCTCCCCCAAT
Ifit1 Fwd	AGAAGCAGGCAATCACAGAAAA
Ifit1 Rev	CTGAAACCGACCATAGTGGAAAT
SARS-CoV-2 Spike Fwd	CCTACTAAATTAAATGATCTCTGCTTTACT
SARS-CoV-2 Spike Rev	CAAGCTATAACGCAGCCTGTA
GFP Fwd	AAGCTGACCCTGAAGTTCATCTGC
GFP Rev	CTTGTAGTTGCCGTCGTCCTTGAA

2.1.5 Detection systems and software

Table 2.10 Detection system and analysis software

System/Software	Source
CFX96 Real-Time PCR Detection System	Bio-Rad
Image Studio™ Lite Version 5.2	LI-COR
IX-81 spinning-disk confocal microscope	Olympus
Moxi Z Mini Automated Cell Counter	ORFLO
NanoDrop ND-1000 Spectrophotometer	Thermo Scientific
Odyssey Infrared Imaging System	LI-COR
T100 Thermo Cycler	Bio-Rad
Synergy HTX Plate Reader	Biotek
Ultraviolet Transilluminator	Thermo Fisher Scientific
Volocity Acquisition and Analysis Software 6.2.1	Perkin-Elmer

2.1.6 Cell lines and viruses

Table 2.11 Cell lines

Cell line	Source
A549	American Type Culture Collection
C6/36	Dr. Sonia Best (NIH Rock Mountain Laboratory)
HEK 293T	American Type Culture Collection
Huh 7	American Type Culture Collection
Vero (CCL81)	American Type Culture Collection
Vero E6 (CRL-1586)	American Type Culture Collection

Table 2.12 Viruses

Virus	Source
Mayaro virus (MAYV) serotype D (strain 07-18066-99)	Brandy Russell (Center for Disease Control and Prevention)
Semliki Forest virus (SFV; strain SFV6.1)	Dr. Andres Merit (University of Tartu)

Virus	Source
Sendai virus (SeV; Cantell Strain #10100774)	Charles River Laboratories
Severe Acute Respiratory Syndrome Coronavirus 2 (SARS-CoV-2; strain CANADA/VIDO01/2020)	Dr. Darryl Falzarano (Vaccine and Infectious Disease Organization)
Sindbis virus (SINV; Toto1101 molecular clone)	Dr. Charles Rice (Rockefeller University)

2.2 Methods

2.2.1 Molecular biology

2.2.1.1 Isolation of plasmid DNA from Escherichia coli

E. coli cultures harboring desired plasmids were grown in LB media (Table 2.5) containing ampicillin (100 µg/ml; Table 2.1) or kanamycin (50 µg/ml; Table 2.1) at 37 °C on a shaker at 225 rpm for 16 h. Plasmid DNA from small batch cultures (5 ml) were isolated using QIAprep Spin Miniprep Kit (Table 2.4). Plasmid DNA from large batch (400 ml) cultures were isolated using NucleoBond Xtra Maxi Kit (Table 2.4). The concentration of isolated plasmid DNA were measured using a NanoDrop ND-1000 Spectrophotometer (Table 2.10) and then stored at -20°C until required for use.

2.2.1.2 Polymerase chain reaction (PCR)

PCR amplification of DNA was performed using Platinum *Taq* Polymerase High Fidelity (Table 2.3). Typical reactions consisted of 1X High Fidelity PCR buffer, 2 mM of $MgSO_4$, 200 µM of dNTP mix, 200 nM of forward and reverse primers, 50 ng/ml of template DNA, and 0.02 U/µl of Platinum *Taq* Polymerase High Fidelity. The annealing temperature was set according to

the predicted melting temperature of the primers, while the duration of extension was set according to the length of the PCR product. The reaction performed for 25 to 35 cycles using T100 Thermo Cycler (Table 2.10).

2.2.1.3 Agarose electrophoresis

Ultrapure agarose (0.8-1% [w/v], Table 2.1) was dissolved in TAE buffer with 0.5 µg/ml of ethidium bromide. After solidification, the agarose gels were submerged into electrophoresis tank containing TAE buffer. DNA samples were mixed with 6X loading dye (Table 2.1), loaded into wells adjacent to GeneRuler 1kb Plus (Table 2.2), and then separated by running gels at 100 V for 45-60 min. The DNA bands were visualized using a ultraviolet Transilluminator (Table 2.10) and then excised for further manipulations such as ligation.

2.2.1.4 Restriction endonuclease digestion

Restriction digestion of PCR products and plasmid DNA were typically performed at 37°C for 1 h in 50 µl reactions containing 2 µg of DNA, 2 U of restriction endonucleases (Table 2.3) and the corresponding manufacturer-supplied digestion buffers. In some cases, digested DNA fragments were dephosphorylated using CIP (Table 2.3) at 37°C for 45 min.

2.2.1.5 Purification of DNA fragments

PCR products were purified using QIAquick PCR Purification Kits (Table 2.4). DNA fragments from restriction endonuclease digestion were separated by agarose gel electrophoresis

and the desired DNA fragments excised from gel and purified using QIAEX II Gel Extraction Kit (Table 2.4).

2.2.1.6 Ligation reaction

Inserts and vectors were combined in 1:1 and 1:5 molar ratios (20 to 100 ng of vector) in a 20 µl reaction containing ligase buffer (1X) and 1 U of T4 DNA ligase (Table 2.3). The mixtures were incubated at 22°C for 30 min prior to transformation of bacteria.

2.2.1.7 Transformation of E. coli

Subcloning Efficiency DH5α Competent Cells (Invitrogen) and One Shot Stbl3 Chemically Competent *E. coli* (Invitrogen) were used for transformation of plasmid DNA. Plasmid DNA (up to 100 ng) was added to 50 µl of competent cells on ice, then heat-shocked for 45 sec in 42°C water bath. SOC medium (Table 2.1) was then added to the transformation mixtures and then incubated at 37°C for 45 min in an orbital shaker (225 rpm). The transformed cells were plated onto LB agar containing appropriate antibiotics and then incubated at 37°C for 16 h.

2.2.1.8 Construction of recombinant plasmids

Construction of 3XFLAG-tagged MAYV protein expression plasmids

MAYV protein expression plasmids were generated from cDNA templates prepared from RNA isolated from MAYV-infected Vero cells using SuperScript III Reverse Transcriptase (Table 2.3). Viral gene-specific cDNAs with C-terminal 3XFLAG-tags were cloned between NheI and

FseI restriction sites in pcDNA 3.1(-) 3XFLAG plasmid (Kumar et al., 2016). Due to the auto-protease activity of capsid protein which cleaves tags off of its C-terminus, a 3XFLAG sequence was added in frame to the N-terminal region of the protein. The primers used for these PCR reactions are listed in Table 2.8. The sequence integrities of all constructs were confirmed by Sanger sequencing.

Construction of plasmids encoding 3XFLAG-tagged SARS-CoV-2 proteins

SARS-CoV-2 protein expression plasmids were generated from cDNA template prepared from RNA extracted from SARS-CoV-2 infected Vero E6 cells using SuperScript III Reverse Transcriptase (Table 2.3) and PCR. Viral gene-specific cDNAs with C-terminal 3X FLAG tag cassettes were cloned between NheI and FseI restriction sites in pcDNA 3.1(-) 3XFLAG plasmid (Kumar et al., 2016). Due to the instability of the C-terminally tagged NSP10 construct in bacteria, a 3XFLAG sequence was added in frame to the coding region for the N-terminal region of the protein. The primers used for cloning are listed in Table 2.8. All constructs were verified by Sanger sequencing.

2.2.1.9 Site directed mutagenesis

To generate MAYV NSP2 and SARS-CoV-2 NSP1 mutants, two-step PCR was used for site directed mutagenesis. In addition to the flanking primers used for cloning wild type viral gene constructs, fusion primers (Table 2.8) that contained desired mutant sequence were used for these reactions. Two PCR reactions were performed for the first step, using pcDNA3.1(-) 3XFLAG plasmid with the wild type gene and either combination of flanking and fusion primers. For the

second PCR step, the two PCR products from the first step were used as templates, while only using the flanking primers. The PCR products from the second step which contained the introduced point mutation were cloned back into pcDNA3.1(-) 3XFLAG plasmid between NheI and FseI restriction sites. All constructs were verified by Sanger sequencing.

2.2.2 Cell culture and transfection

2.2.2.1 Cell culture maintenance

A549, HEK 293T, Huh7, Vero (CCL-81), and Vero E6 (CRL-1586) cells were cultured in DMEM (Table 2.1) supplemented with 100 U/ml penicillin and streptomycin (Table 2.1), 1 mM HEPES (Table 2.1), 2mM glutamine (Table 2.1), and 10% (v/v) heat-inactivated FBS (Table 2.1) at 37°C in 5% CO_2. C6/36 cells were cultured in MEM (Table 2.1) containing 100 U/ml penicillin and streptomycin, 2mM glutamine, 10% (v/v) heat-inactivated FBS, and 1x non-essential amino acid (Table 2.1) at 32°C in 5% CO_2.

2.2.2.2 Transfection of mammalian cell lines

Transient transfection of A549, HEK 293T, and Huh7 cells were performed using Lipofectamine 2000 or TransIT-LT1 (Table 2.1). Cells were seeded 24 h prior to transfection so that they would be 80% confluent at the time of transfection. For A549 and Huh7 cells in 12-well plates, 1 µg of DNA and 2 µl of Lipofectamine 2000 or 0.5 µg of DNA and 1 µl of TansIT-LT1 were added to OptiMEM (Table 2.1). For HEK 293T cells in 12-well plates, 2 µg of DNA and 4 µl of Lipofectamine 2000 were mixed in OptiMEM. Where indicated 2 µg of poly(I:C) and 3 µl

of TransIT-LT1 in OptiMEM were used for transfection of cells. Transfected cells were incubated for 12 to 24 h, after which media was changed.

2.2.3 Virology techniques

2.2.3.1 Virus infection

Cells were infected with viral stocks diluted in DMEM (Table 2.1) media containing 3% FBS for 1 h at 37°C in a 5% CO_2 atmosphere. Virus-containing media were replaced with complete growth media and incubated at 37°C in a 5% CO_2 until the endpoint of the infection experiments. Infection with MAYV, SeV, SFV, and SINV were performed following CL-2 procedures. Infection with SARS-CoV-2 was performed following CL-3 procedures.

2.2.3.2 Plaque assay

Vero (CCL-81) or Vero E6 (CRL-1586) cells (1.5 x 10^5 cells/well) were seeded onto 24-well plates 24 h before infection with MAYV or SARS-CoV-2, respectively. The culture media containing MAYV or SARS-CoV-2 were serially diluted in serum-free DMEM. To each well, 100 µl of serum-free DMEM and 100 µl of virus-containing dilution were added. After 1 h at 37°C in a 5% CO_2 atmosphere, the virus-containing media were aspirated and replaced with 1 ml of DMEM containing 0.5% methylcellulose followed by incubation at 37°C in a 5% CO_2 atmosphere for two (MAYV) or three (SARS-CoV-2) days. Cells were then fixed by adding 1 ml of 10% formaldehyde to each well. After 30 min at room temperature, formaldehyde-containing culture media were removed after which the wells were rinsed with water and then dried by tapping the plates over a paper towel before staining with 1% (w/v) crystal violet (Table 2.1) in 20% (v/v)

methanol (Table 2.1) for 30 min at room temperature. After removing the staining solution, the wells were rinsed with water and then air-dried. Plaques in each well were counted to determine the number of infectious viral particles (plaque forming unit (PFU)/ml) in the original sample using the formula below. To accurately estimate the number of infectious viral particles in a given sample, wells that were appropriate to account for had more than three plaques, while no more than 30 of them in a single well.

$$\frac{\text{Average \# of plaques}}{\text{dilution factor} \times \text{volume of diluted virus added}} = \text{PFU/ml}$$

2.2.4 Protein gel electrophoresis and immunoblotting

2.2.4.1 Sodium dodecyl-sulphate polyacrylamide gel electrophoresis (SDS-PAGE)

Unless otherwise indicates, cell lysates for immunoblotting were washed once with PBS (Table 2.5) followed by lysis with SDS-Sample buffer (Table 2.5) supplemented with 0.1% (v/v) of Benzonase (Table 2.1). The acrylamide gels were prepared by overlaying 5% stacking gel (5% (v/v) acrylamide/bis-acrylamide, 0.1% (v/v) SDS, 125 mM Tris (pH 6.8), 0.1% (v/v) APS, and 0.1% (v/v) TEMED) on 8-15% resolving gels (8~15% (v/v) acrylamide/bis-acrylamide, 0.1% (v/v) SDS, 375 mM Tris (pH 8.8), 0.1% (v/v) APS, and 0.1% (v/v) TEMED). Cell lysates were heated at 95°C for 10 min and then loaded onto acrylamide gels which were bathed in SDS-PAGE running buffer (Table 2.5). To separate proteins, gels were subjected to 100 V until the dye front reached the resolving gel after which the voltage was increased to 150 V and ran until the dye fronts reached the bottom of the gels.

2.2.4.2 Immunoblotting

Following SDS-PAGE, proteins were transferred from the gels to PVDF membranes (Table 2.1). PVDF membranes were activated by incubating in methanol (Table 2.1) for 10 min and protein transfer was carried out by subjecting the gel and membrane under 40 mA in Transfer buffer (Table 2.5) for 16 h at room temperature. The PVDF membranes were then incubated in Blocking buffer (Table 2.5) for 30 min at room temperature before incubating with primary antibodies (Table 2.6) diluted in Blocking buffer for at least an hour at room temperature. Membranes were washed three times with PBS-Tween (Table 2.5) for 10 min each and then incubated with secondary antibodies (Table 2.7) diluted in Blocking buffer for 1 h at room temperature in the dark. The membranes were washed three more times with PBS-Tween and proteins were visualized using an Odyssey Infrared Imaging System (Table 2.10). Processing of the images and quantification of proteins were performed using Image Studio Lite (Table 2.10).

2.2.5 Analysis of protein-protein interactions

2.2.5.1 Co-immunoprecipitation (co-IP)

HEK 293T cells were seeded into T25 flasks for 24 h such they were 80% confluent at the time of transfection. Cells were transfected with 6 µg of FLAG-tagged viral protein encoding plasmids and 12 µl of Lipofectamine 2000 (Table 2.1) mixed in OptiMEM (Table 2.1). Twenty-four hours later, cells were lysed by with ice-cold IP buffer (Table 2.5) and then placed on a rotator at 4°C for 30 min. During cell lysis, 10 µl of anti-Flag magnetic beads (Table 2.1) were incubated in Blocking buffer (Table 2.5) at 4°C for 10 min, then washed twice with IP buffer by rotating at 4°C for 10 min each. The lysates were clarified by centrifugation at 16,000 g for 15 min at 4°C,

after which the supernatants were incubated with beads on a rotator at 4°C for 2 h. After three washes with IP buffer, proteins bound to magnetic beads were processed for mass spectrometry (LC-MS/MS), or SDS sample buffer (Table 2.5) was added to the beads, which were then incubated at 95°C for 10 min, separated by SDS-PAGE and analyzed by immunoblotting.

2.2.6 Microscopy

2.2.6.1 Indirect immunofluorescence confocal microscopy

A549 and Huh7 cells were seeded onto 12-well plate (4.5 x 10^4 cells/well) with coverslips 24 h prior to transfection using TransIT-LT1 (Table 2.1) or virus infection. After experimental endpoints, cells were washed three times with PBS (Table 2.5), fixed with 4% PFA (Table 2.1) in PBS for 10 min at room temperature, then washed three more times with PBS. Cells were permeabilized with 0.5% (v/v) Triton X-100 (Table 2.1) in PBS for 10 min, followed by three washes in PBS. Cells were incubated in Blocking buffer (Table 2.5) for 30 min, after which they were incubated in primary antibodies (Table 2.6) diluted in Blocking buffer for 1 h at room temperature. Cells were then washed three times with PBS and incubated with secondary antibodies (Table 2.7) and 1 µg/ml of DAPI (Table 2.1) in Blocking buffer for 45 min at room temperature in darkness. After staining with secondary antibodies, coverslips were washed three more times with PBS and mounted on microscope slides using ProLong Gold Antifade Mounting Reagent (Table 2.1) and then stored at 4°C protected from light. Cells on coverslips were imaged using an IX-81 spinning-disc confocal microscope (Table 2.10) equipped with 60X/1.42 numerical aperture (NA) PlanApo N oil objective. Images were acquired, processed, and analyzed using Volocity software (Table 2.10).

2.2.7 RNA techniques

2.2.7.1 RNA isolation

RNA was isolated from cells using NucleoSpin RNA Mini Kit (Table 2.4) and then quantitated with a NanoDrop ND-1000 Spectrophotometer (Table 2.10) before use in cDNA synthesis reactions or storage at -80°C.

2.2.7.2 cDNA synthesis

Purified RNA was reverse transcribed into cDNA using SuperScript III Reverse Transcriptase (Table 2.3) or Improm-II Reverse Transcriptase System (Table 2.3) which were used for cloning viral genes into plasmids or for qRT-PCR, respectively. cDNAs that were to be analyzed by qRT-PCR were diluted 1:5 with water and stored at -20°C.

2.2.7.3 Quantitative real time polymerase chain reaction (qRT-PCR)

Typically, qRT-PCR reaction mixtures (15 µl) contained 5 µl of cDNA template, 100 nM of appropriate forward and reverse primers (Table 2.9) and 1X PerfeCTa SYBR Green Super Mix with Low ROX (Table 2.3) and were amplified for 40 cycles (30 sec 94°C, 40 sec at 55°C, and 20 sec at 68°C) in CFX96 Real-Time PCR Detection System (Table 2.10). The CT values were normalized to that of *ACTB* mRNA which served as an internal control (ΔCT). The ΔΔCT values were determined by normalizing to the appropriate control group ΔCT values and the relative RNA levels were calculated using the formula $2^{(-\Delta\Delta CT)}$.

2.2.8 Luciferase reporter assay

HEK 293T cells were seeded onto 12-well plates (4 x 10^5 cells/well) 24 h prior to transfection. To assess IFN induction, cells were transfected with viral protein-encoding plasmids, CMV promoter-controlled *Renilla* luciferase construct (pRL-TK; Promega), and either IFN-β promoter-driven (p125-Luc; provided by T. Taniguchi, University of Tokyo Japan), IRF3-controlled promoter-driven (p55-CIB-Luc; provided by T. Taniguchi, University of Tokyo Japan), or NFκB-controlled promoter-driven (pNF-kB-Luc; Stratagene) *Firefly* luciferase construct. The IFN induction pathway was activated by infecting cells with 50 hemagglutinating units (HAU)/ml of SeV (Table 2.12) for 16 h. Cells were transfected with viral protein-encoding plasmids, CMV promoter-controlled *Renilla* luciferase construct, and either IFN-stimulated responsive element (ISRE) promoter-driven (pGL4-ISRE; Promega) or IFN-ɣ-activated site (GAS) promoter-driven (pGAS-Luc; Stratagene) *Firefly* luciferase constructs to measure IFN signaling potentiated by type I (100 U/ml of IFN-α) or type II IFNs (10 U/ml of IFN-ɣ), respectively. To activate the IFN signaling pathway, cells were treated with the indicated IFN types for 16 h. At experimental endpoints, cells were lysed with 250 µl of Luciferase lysis buffer (Table 2.5) and either rocked in room temperature for 15 min or stored at -80°C until analysis.

For luciferase assays, 50 µl of lysate were aliquoted into 96-well microplates in duplicate for measuring each *Firefly* and *Renilla* luminescence activity. To measure *Firefly* luciferase activity, 100 µl of luciferase assay buffer (Table 2.5) supplemented with 70 µM D-luciferin (Table 2.1) and 2 mM ATP (Table 2.1) was added into each well which were then incubated for 5 min at room temperature after which luciferase activities were measured using a Synergy HTX Plate Reader (Table 2.10) using an exposure time of 1 sec. For *Renilla* luciferase, 100 µl of Luciferase assay buffer supplemented with 1.4 µM of coelenterazine (Table 2.1) was added to each well and

luciferase activities was measured immediately with a Synergy HTX Plate Reader using an exposure time of 0.5 sec. The *Firefly* luciferase reporter values were normalized against *Renilla* luciferase reporter values and further normalized to appropriate negative control groups in which IFN pathways were not stimulated.

2.2.9 Enzyme-link immunosorbent assay (ELISA) for IFN-β detection

A549 cells (1.2×10^5) and HEK 239T cells (4×10^5) were seeded onto 12-well plate 24 h prior to viral infection or transfection of viral protein-encoding plasmids. At indicated time points, 50 HAU/ml of SeV (Table 2.12) were added to each well to activate the IFN induction pathway. Sixteen hours later, cell culture supernatants were collected and the concentrations of IFN-β were measured using a Human IFN-beta Quantikine ELISA kit (Table 2.4) according to manufacturer's protocol. The absorbance were measured using a Synergy HTX Plate Reader (Table 2.10).

Chapter 3

Mayaro virus non-structural protein 2 circumvents the induction of interferon in part by depleting host transcription initiation factor IIE subunit 2.

Portions of this chapter have been published as:

Ishida, R., Cole, J., Lopez-Orozco, J., Fayad, N., Felix-Lopez, A., Elaish, M., Luo, S.Y., Julien, O., Kumar, A., and Hobman, T.C. 2021. Mayaro Virus Non-Structural Protein 2 Circumvents the Induction of Interferon in Part by Depleting Host Transcription Initiation Factor IIE Subunit 2. Cells 10 (12). doi: doi.org/10.3390/cells10123510.

3. 1 Rationale

Mayaro virus (MAYV) is an emerging mosquito-transmitted alphavirus that is anticipated to cause large outbreaks as other arboviruses such as Zika, Dengue, and Chikungunya (CHIKV) viruses have in the past. Most MAYV infections in human lead to debilitating arthralgia and myalgia that persist for several months to years (Yue et al., 2019). Despite these concerns, our understanding of MAYV biology is very limited there are no specific treatments or vaccines available to control outbreaks.

One important aspect of MAYV biology that is poorly understood is how it affects the IFN response; virtually no studies have looked at this process thus far (Figueiredo et al., 2019). It is known that viral RNAs from other alphaviruses are sensed by both RIG-I and MDA5 (Akhrymuk et al., 2016), while the secretion of IFNs is almost completely blocked during infection of fibroblasts (Burke et al., 2009; Bhalla et al., 2019; Akhrymuk et al., 2018). Furthermore, the non-structural protein 2 (NSP2) of CHIKV and Sindbis virus (SINV) is directly linked to the proteasomal degradation of Rpb1, a component of cellular RNA polymerase II (Akhrymuk et al., 2019; Fros et al., 2013; Frolova et al., 2002; Gorchakov et al., 2005; Breakwell et al., 2007). This is thought to mediate global shutoff of host transcription, including IFN and ISG mRNAs. Lastly, a recent study by Goertz et al. revealed that NSP2 of CHIKV interferes with the IFN signaling pathway by facilitating nuclear export of STAT1 (Goertz et al., 2018). While some IFN response evasion strategies may be conserved among all alphaviruses, it is possible that MAYV and other alphaviruses have evolved additional mechanism(s) of suppressing this host antiviral defence system.

Since MAYV is closely related to other alphavirus that suppress IFN induction and can establish productive infections in mammals (Powers et al., 2001; Forrester et al., 2012; Roundy et

al., 2017), we hypothesized that one or more proteins encoded by this virus is able to efficiently block IFN induction. I dissected the IFN induction pathway during MAYV infection and was able to identify the viral protein responsible for suppressing IFN induction during infection. I was also able to elucidate a novel mechanism by which MAYV antagonizes this cellular pathway.

3.2 Results

3.2.1 MAYV suppresses production of type I and III IFNs

To determine if/how IFN induction is affected during MAYV infection, type I IFN (*Ifnb*) and viral genomic RNA were quantitated by qRT-PCR at 4, 8, 12 and 24 hours after A549 cells were infected with MAYV or Sendai virus (SeV). Despite robust virus replication, induction of *Ifnb* mRNA in MAYV-infected cells was delayed and dramatically suppressed compared to cells infected with SeV (Figure 3.1A-B), a potent inducer of IFN production (Elco et al., 2005). However, treatment of cells with type I IFN prior to infection significantly inhibited MAYV in a dose-dependent manner (Figure 3.1C) indicating that the virus is sensitive to IFN.

Next, we assessed whether the relatively low levels of *Ifnb* mRNA in MAYV-infected cells are the result of active suppression of IFN induction pathways. MAYV infected cells were transfected with poly(I:C), a dsRNA analog that induces IFN following detection by RIG-I-like receptors (Okamoto et al., 1998). Transcripts encoding type I (*Ifnb*) and type III (*Ifnl2*) IFNs were then quantified by qRT-PCR. Poly(I:C) transfection robustly induced *Ifnb* and *Ifnl2* but levels of these transcripts were ~50-fold lower in MAYV-infected cells compared to mock-infected cells (Figure 3.2A and B). MAYV infection alone resulted in a relatively modest increase (~100-fold) in *Ifnb* and *Ifnl2* which were further increased ~10-fold by poly(I:C) challenge. In comparison,

SeV infection resulted in ~10,000-fold increased levels of *Ifnb* but this effect was dampened in cells that were first infected with MAYV (Figure 3.2C). IFN-β was not detected in the media of MAYV-infected cells regardless of whether they were challenged with SeV or not (Figure 3.2D). The observation that levels of SeV genomic RNA were higher in MAYV-infected cells suggests that impaired IFN induction during MAYV infection was not due to poor replication of SeV in those cells (Figure 3.2E).

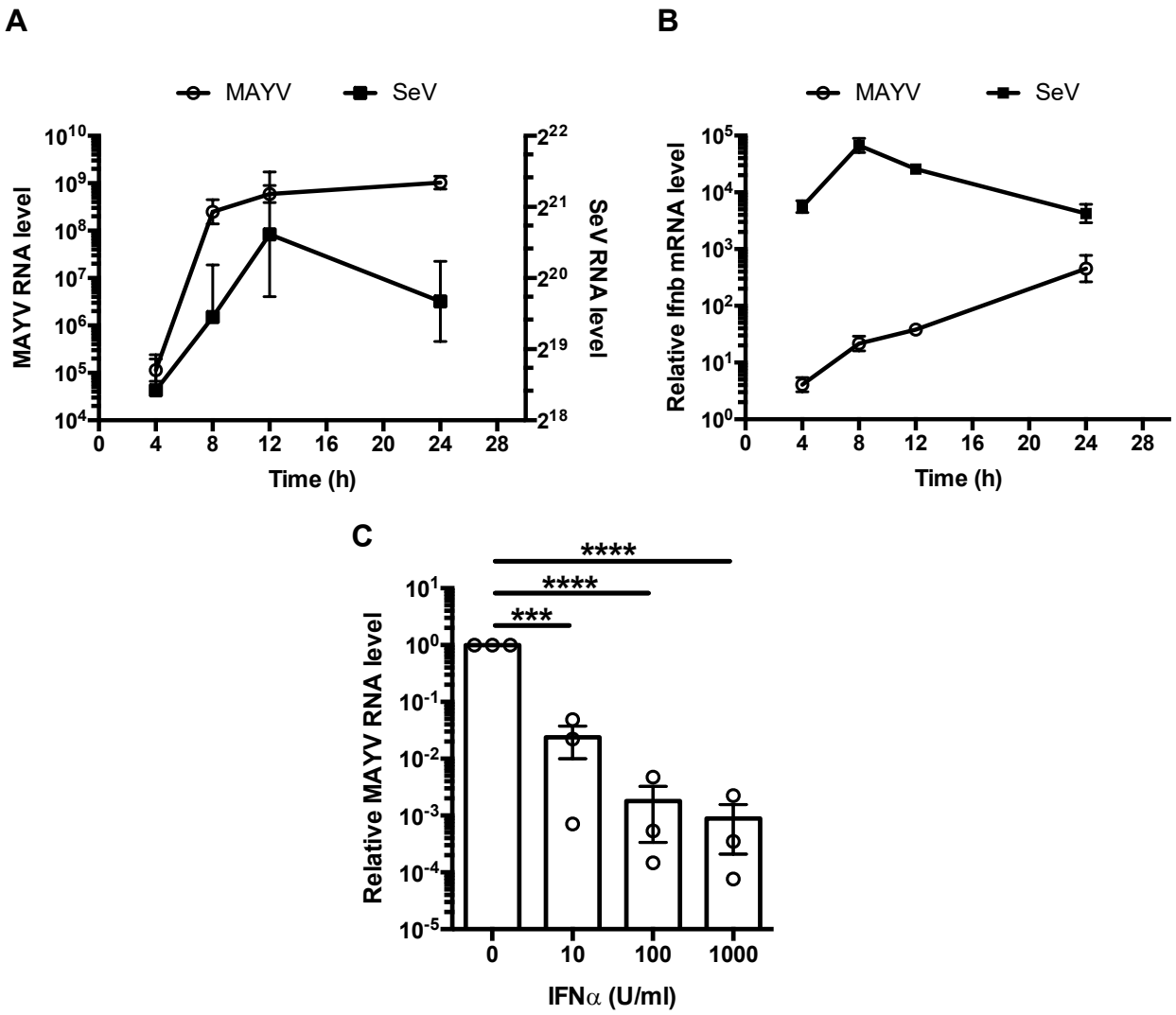

Figure 3.1 MAYV is sensitive to pre-treatment of type-I IFNs. A and **B**. A549 cells were infected with either MAYV (MOI=3) or SeV (50 HAU/ml). Total RNA was collected at 4-hour intervals for up to 24-hours post-infection (hpi). Viral RNA (A) and Ifnb mRNA (B) were quantitated by qRT-PCR and expressed as fold mock infected cells normalized to Actb mRNA levels. N = 3. **C**. A549 cells were treated with IFN-α (0, 10, 100, and 100 U/ml) for 6 h and infected with MAYV (MOI=1). At 24 hpi, relative levels of MAYV RNA in total cellular RNA samples were quantitated by qRT-PCR (normalized to Actb) and expressed as folds of replication to cells not treated with IFN-α. *** $P < 0.001$, **** $P < 0.0001$; N = 3.

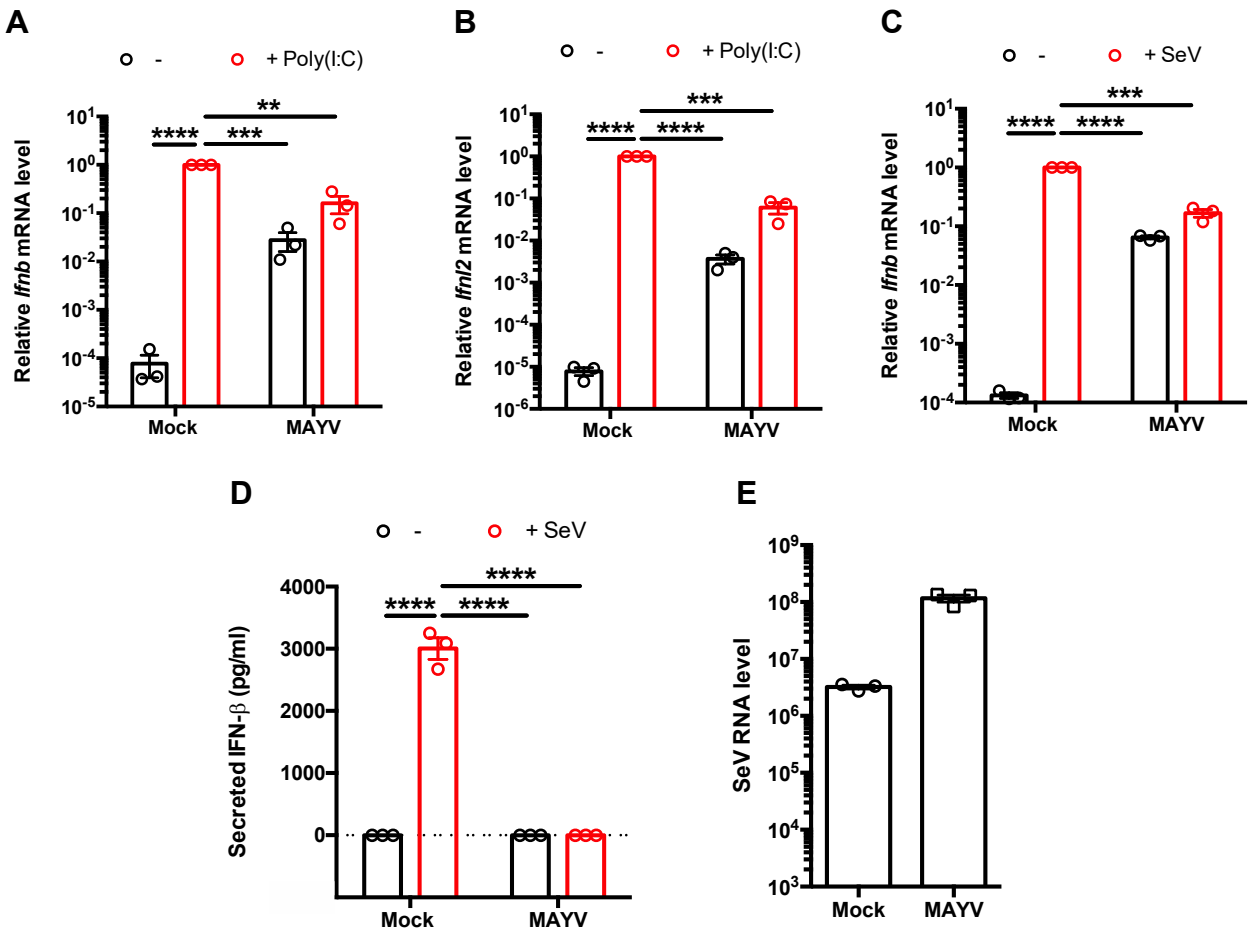

Figure 3.2 MAYV suppresses induction of type I and III IFNs. A and **B**. A549 cells were infected with MAYV (MOI=3) for 24 h, then treated with 2 µg/ml of poly(I:C). After 16 h, total RNA was collected and *Ifnb* (A) and *Ifnl2* (B) mRNA were measured by qRT-PCR and normalized to *Actb* mRNA level and expressed as folds to mock infected cells. ** $P < 0.01$, *** $P < 0.001$, **** $P < 0.0001$; N = 3. **C** and **D**. A549 cells were infected with MAYV (MOI=3) for 24 h, then challenged with (SeV) (50 HAU/ml) for 16 h. *Ifnb* transcripts in cells and IFN-β in cell culture supernatants was measured by qRT-PCR (C) and enzyme linked immunosorbent assay (D) respectively. *** $P < 0.001$, **** $P < 0.0001$; N = 3. E. A549 cells were infected with MAYV (MOI=3) for 24 h, then infected with SeV (50 HAU/ml) for 16 h. Total RNA was collected and SeV viral RNA level were measured by real time qRT-PCR and normalized to *Actb* mRNA level and expressed as folds of mock infected cells. N = 3.

3.2.2 MAYV suppresses the IFN induction pathway downstream of IRF3 nuclear translocation.

Next, we examined whether nuclear translocation of the antiviral transcription factor IRF3, which is required for production of IFN-β mRNA, was affected by MAYV infection. In contrast to SeV infection which induced translocation of IRF3 into nuclei, IRF3 remained in the cytoplasm of MAYV-infected cells (Figure 3.3). However, when MAYV infected cells were subsequently infected with SeV, IRF3 localized to the nucleus (Figure 3.3), indicating that the IFN induction pathway is at least partially intact in MAYV infected cells up to the IRF3 nuclear translocation step. Taken together, these data are compatible with a scenario where MAYV efficiently avoids detection of its RNA by RIG-I-like receptors (RLRs), and/or partially blocks the IFN induction pathway upstream of IRF3 nuclear transport to prevent IFN production in infected cells. Since SeV induced IRF3 nuclear translocation was unaffected (Figure 3.3) but the production of IFN transcripts and secreted IFNs were blocked in MAYV infected cells (Figure 3.2A, B, C and D), the virus likely targets additional steps in the IFN induction pathway, downstream of IRF3 nuclear translocation.

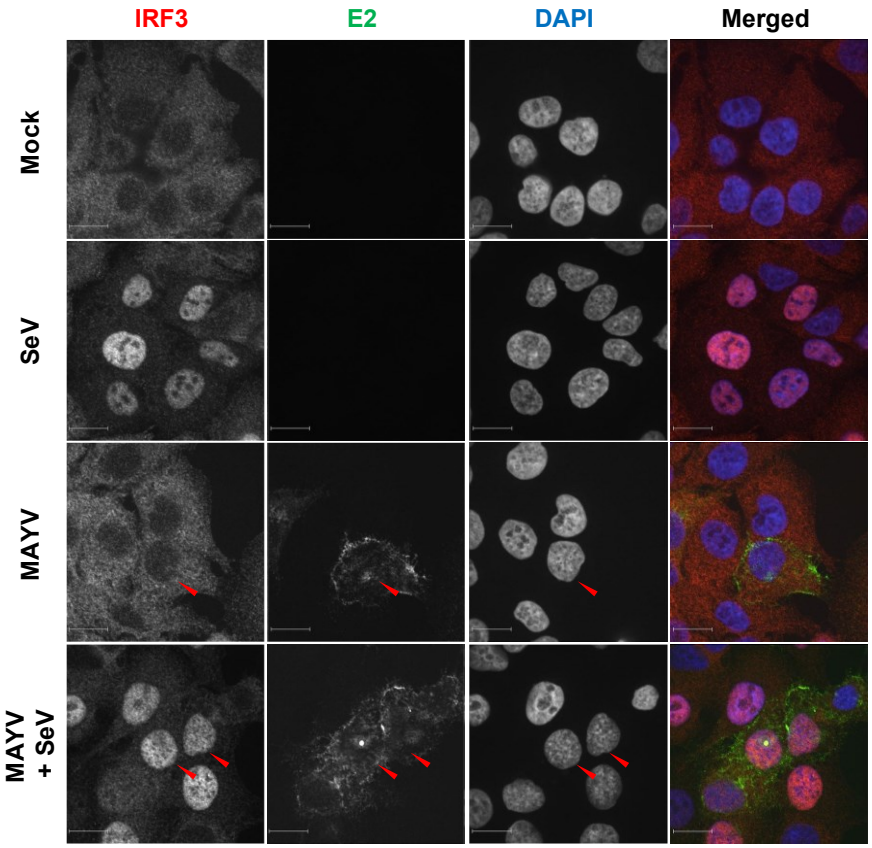

Figure 3.3 MAYV does not block nuclear translocation of IRF3. A549 cells were infected with MAYV (MOI=1) for 24 h and then infected with 50 HAU/ml of SeV for 8 h. The subcellular localization of IRF3 in MAYV-infected cells was assessed by confocal microscopy after staining with antibodies against IRF3 and MAYV E2 protein.

3.2.3 Cloning of 3xFLAG-tagged MAYV proteins into pcDNA3.1(-)

To identify the viral protein(s) responsible for suppression of the IFN induction pathway during MAYV infection, we generated expression plasmids encoding individual epitope-tagged MAYV proteins. With the exception of the capsid protein which was tagged on the N-terminus, all MAYV proteins were tagged at their C-termini with 3xFLAG epitope. It was not feasible to tag the C-terminus of MAYV capsid because like other alphavirus capsid proteins, it has auto-protease activity which cleaves the hydrophobic signal peptide at its C-terminus (Melancon and Garoff 1987). Expression of the tagged viral proteins in transfected HEK 293T cells was authenticated by immunoblotting (Figure 3.4A).

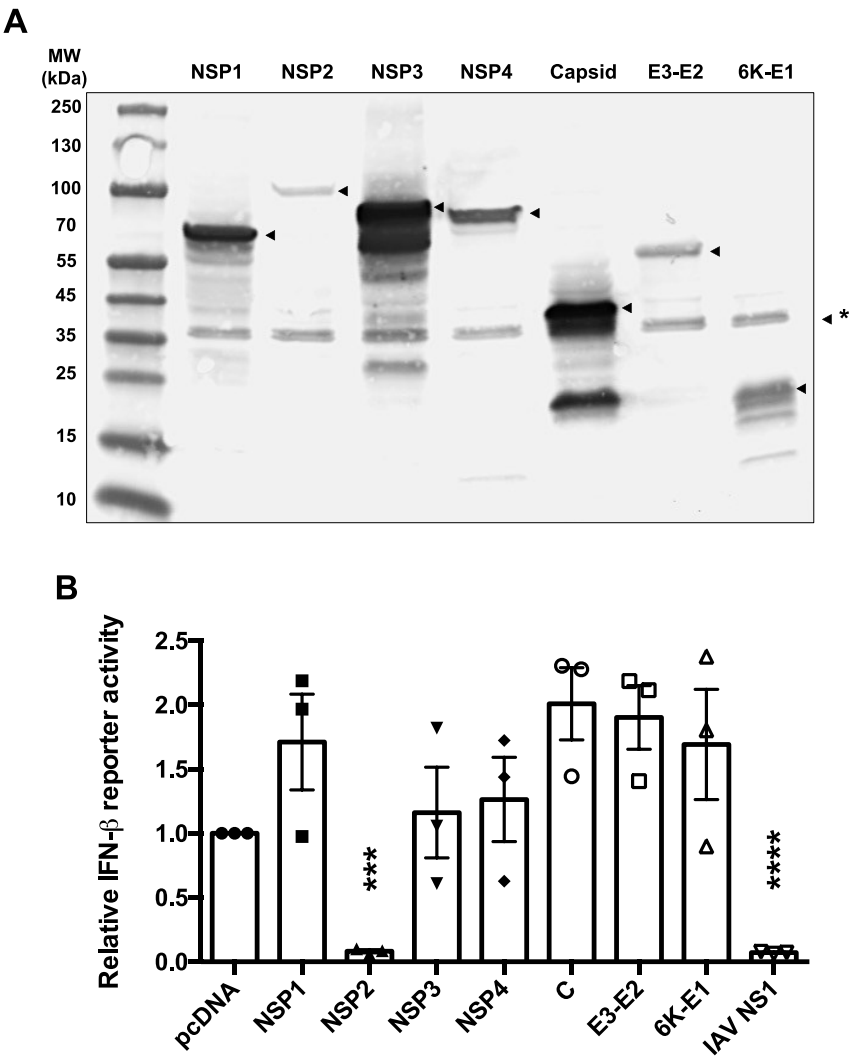

Figure 3.4 MAYV NSP2 antagonizes the induction of IFNs. A. HEK 293T cells were transfected with pcDNA 3.1 (-) plasmids encoding the indicated 3xFLAG-tagged MAYV proteins. After 24 h, cell lysates were subjected to immunoblotting with anti-FLAG antibody. The positions of the epitope tagged viral proteins are indicated with arrowheads. A non-specific protein recognized by the anti-FLAG or secondary antibody is indicated by *. **B**. HEK 293T cells were co-transfected with plasmids encoding the indicated MAYV proteins, empty vector (pcDNA) or Influenza A virus NSP1 as well as a plasmids encoding IFN-β *Firefly* luciferase and constitutively expressed control *Renilla* luciferase. After 24 h, cells were infected with 50 HAU/ml of SeV and then *Firefly* and *Renilla* luciferase activities were measured 16h later. *** $P < 0.001$, **** $P < 0.0001$; N = 3.

3.2.4 MAYV NSP2 reduces interferon induction downstream of IRF3 activation

Next, the effect of MAYV protein expression on IFN induction in response to SeV infection was evaluated using a IFN-β-promoter-based luciferase reporter assay. NSP2 was the only MAYV protein whose expression significantly blocked IFN-β promoter activity (Figure 3.4B). Despite its relatively low expression compared to the other Flag-tagged MAYV proteins (Figure 3.4A), NSP2 suppressed IFN-β promoter activity almost as efficiently as the NS1 protein of Influenza A virus (IAV), a known suppressor of the IFN induction (Gack et al., 2009) and the positive control for these experiments. Because activation of IRF3 and NFκB is critical for induction of *Ifnb* (Fensterl 2015), we assessed whether NSP2 blocks the activities of these two transcription factors using IRF3 and NFκB promoter-based luciferase reporters. Compared to the vector control and MAYV capsid protein, NSP2 reduced IRF3- and NFκB-dependent luciferase expression by as much as 10-fold (Figure 3.5A and B). To determine the step in the IFN induction pathway targeted by NSP2, we assessed how overexpressing individual components in the pathway (RIG-I (2xCARD), TBK1, IKKε, IRF3, and constitutively active IRF3 (IRF3-5D)) affected NSP2-dependent inhibition. None of these components rescued the NSP2 blockade of the IFN induction pathway (Figure 3.5C), suggesting that this viral protein acts downstream of the IRF3 phosphorylation step. Interestingly, IRF3 nuclear translocation in response to SeV infection was not affected by NSP2 expression though (Figure 3.5D and E). These data are consistent with those shown in Figure 3.2 and 3.3 in which MAYV infection was able to block IFN induction downstream of IRF3 nuclear translocation.

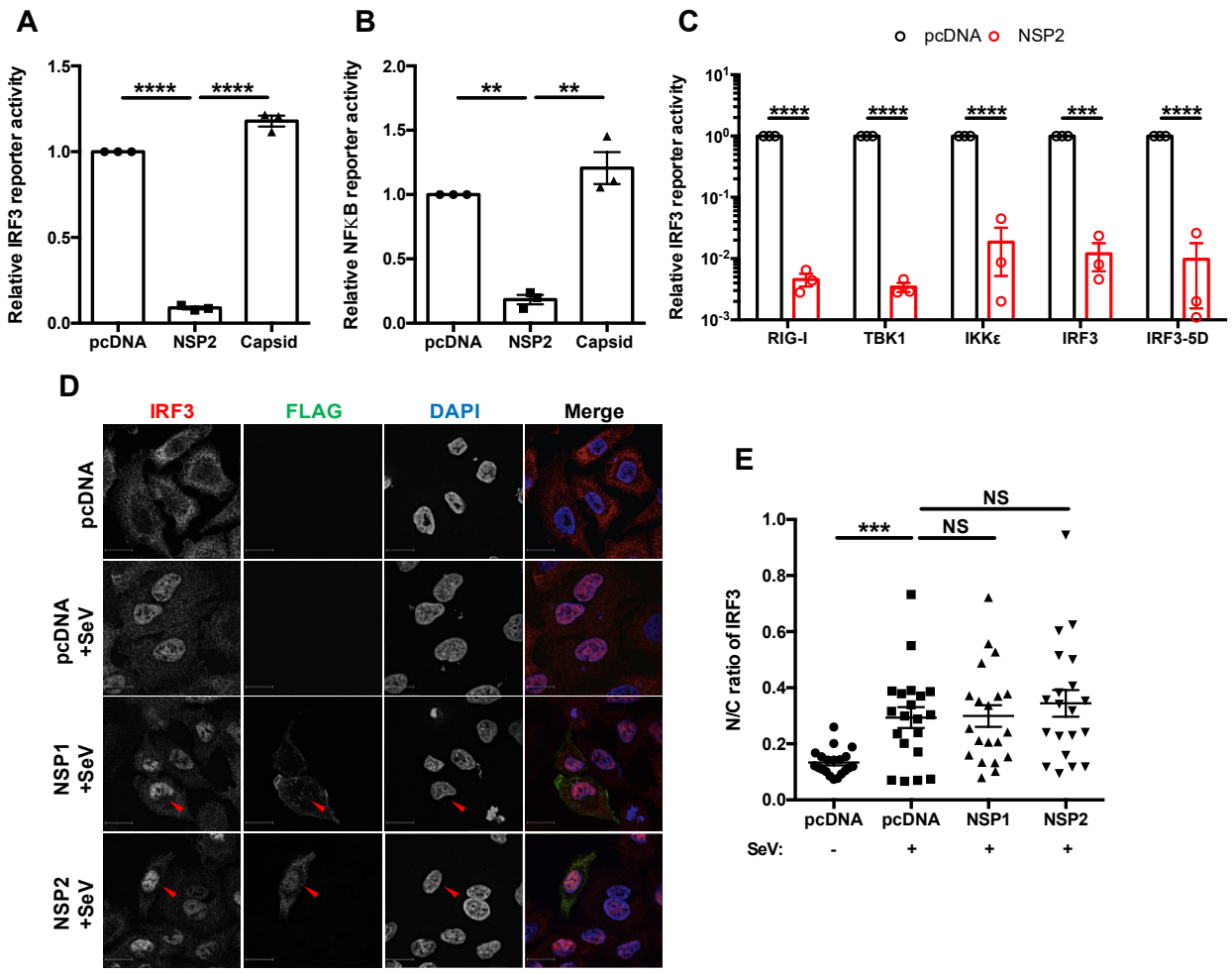

Figure 3.5 MAYV NSP2 blocks IFN induction downstream of IRF3 activation. A and **B**. HEK 293T cells were co-transfected with plasmids encoding NSP2 or capsid proteins and *Firefly* luciferase under the control of IRF3- (A) or NFκB- (B) responsive promotors as well as a plasmid encoding constitutively expressed *Renilla* luciferase. After 24 h, cells were challenged with 50 HAU/ml of SeV for 16 h after which *Firefly* and *Renilla* luciferase activities were measured. ** $P < 0.01$, **** $P < 0.0001$; N = 3. **C**. HEK 293T cells were co-transfected with plasmids encoding NSP2, and RIG-I (2xCARD), IKKε, TBK1, IRF3, IRF3-5D or empty vector, IRF3-promotor *Firefly* luciferase and constitutively expressed *Renilla* luciferase. Samples were harvested at 24 h post transfection after which *Firefly* and *Renilla* luciferase activities were measured. *** $P < 0.001$, **** $P < 0.0001$; N = 3. **D** and **E**. A549 cells were transfected with indicated 3xFLAG-tagged protein-encoding plasmids. After 24 h, cells were challenged with SeV infection (50 HAU/ml) for 8 h, then fixed and stained with antibodies against FLAG and IRF3 followed by confocal microscopy. The cytoplasmic and nuclear IRF3 signals were quantified using Volocity software. *** $P < 0.001$, **** $P < 0.0001$; N = 20.

3.2.5 The effect of NSP2 on interferon induction is partially mediated by transcriptional shutoff

Alphavirus NSP2 proteins contain a helicase domain at the N-terminus with RNA-dependent NTPase activity (Gomez de Cedron et al., 1999; Vasiljeva et al., 2000), a papain-like cysteine protease domain (Strauss et al., 1992), and a C-terminal methyltransferase domain (Russo et al., 2006) (Figure 3.6A). To determine which domain(s) of NSP2 was important for blocking IFN induction, expression constructs encoding NSP2 lacking NTPase ($NSP2^{K197N}$) (Vasiljeva et al., 2000), protease activity ($NSP2^{C478A}$) (Strauss et al., 1992), helicase domain ($NSP2^{\Delta helicase}$) or protease domain ($NSP2^{\Delta protease}$) were generated (Figure 3.6A). Both $NSP2^{K197N}$ and $NSP2^{C478A}$ reduced IFN induction in response to SeV infection similar to wildtype NSP2 and IAV NS1 protein (Figure 3.7A), indicating that NTPase and protease activities are not required to block IFN induction. However, constructs lacking the protease ($NSP2^{\Delta protease}$) or helicase ($NSP2^{\Delta helicase}$) domains were unable to block IFN induction in response to SeV infection (Figure 3.7A).

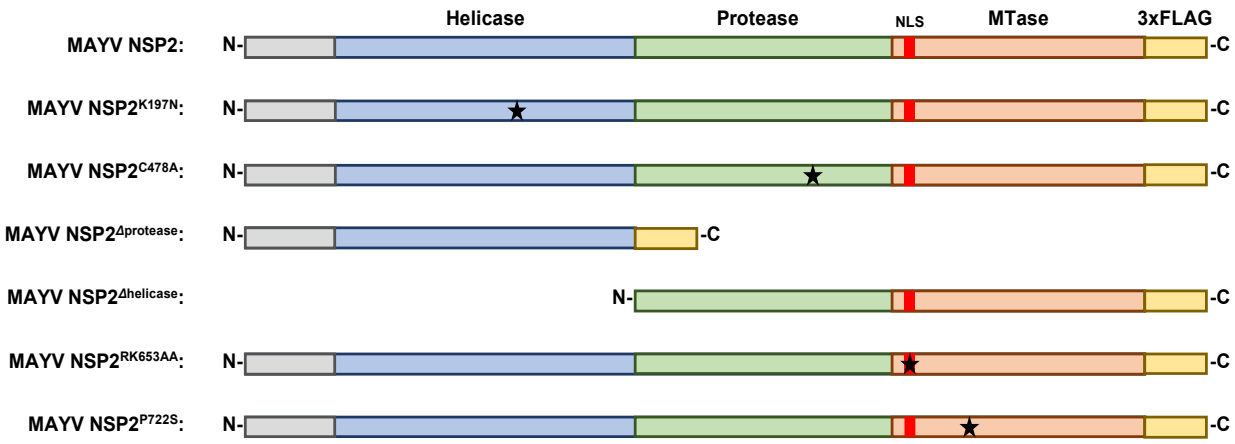

Figure 3.6 Schematic representation of 3xFLAG-tagged MAYV NSP2 constructs. From top, 3xFLAG-tagged wild type NSP2, NTPase mutant NSP2^{K197N}, protease-dead NSP2^{C478A}, helicase only NSP2$^{\Delta protease}$, protease only NSP2$^{\Delta helicase}$, NLS-deficient NSP2^{RK653AA}, and host transcription shutoff deficient NSP2^{P722S}.

Previous studies have shown that other alphavirus NSP2 proteins translocate to the nucleus and inhibits host transcription by depleting Rpb1, a component of the RNA polymerase II complex (Akhrymuk et al., 2012; Fros et al., 2013). To determine if these processes were important for the ability of MAYV NSP2 to antagonize IFN induction, site-directed mutagenesis was used to generate nuclear localization signal (NLS)-deficient ($NSP2^{RK653AA}$) (Breakwell et al., 2007) and transcriptional shutoff deficient ($NSP2^{P722S}$) (Akhrymuk et al., 2012) mutants of NSP2 (Fig 3.6A). Confocal microscopy analyses confirmed that $NSP2^{RK653AA}$ was not able to translocate into the nucleus whereas wildtype and $NSP2^{P722S}$ were detected in nuclei and the cytoplasm (Figure 3.7C). However, while both $NSP2^{RK653AA}$ and $NSP2^{P722S}$ significantly blocked IFN induction, $NSP2^{P722S}$ was ~4-fold less effective than wildtype NSP2 (Figure 3.7B). Furthermore, in cells over-expressing a constitutively active form of IRF3 (IRF3-5D) and $NSP2^{RK653AA}$ or $NSP2^{P722S}$, levels of IFN transcripts were higher than in cells expressing wild type NSP2 (Figure 3.7D). Unlike wildtype NSP2 and $NSP2^{RK653AA}$, $NSP2^{P722S}$ did not reduce IRF3-5D expression in co-transfected cells (Figure 3.7E and F). While these data suggest that NSP2 supresses IFN induction in part by mediating host cell transcriptional shutoff, it appears to function through a second mechanism that is independent from its nuclear function or ability to abrogate transcription.

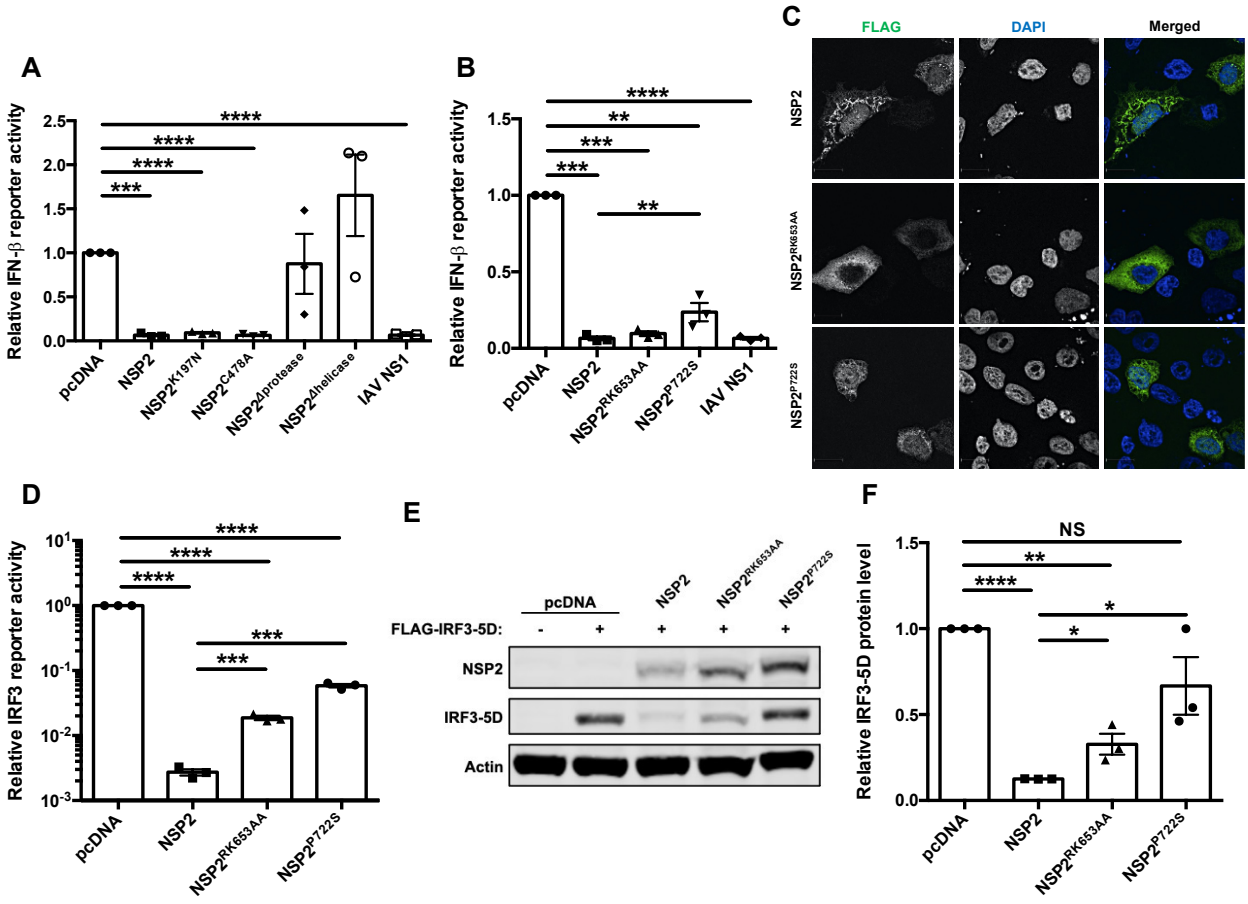

Figure 3.7 Inhibition of IFN induction by MAYV NSP2 is partially mediated by transcriptional shutoff. A and **B**. HEK 293T cells were transfected with the indicated viral NSP2 constructs, IFN-β *Firefly* luciferase reporter and a control *Renilla* reporter. After 24 h, cells were infected with 50 HAU/ml of SeV for 16 h, after which relative *Firefly* and *Renilla* luciferase activities were measured. ** $P < 0.01$, *** $P < 0.001$, **** $P < 0.0001$; N = 3. **C**. A549 cells were transfected with indicated MAYV NSP2 constructs. After 24 h, cells were fixed and stained using α-FLAG antibody and imaged by confocal microscopy. Nuclei are stained with DAPI. **D-F**. HEK 293T cells were transfected with indicated viral NSP2 constructs, FLAG-IRF3-5D, IRF3-promotor *Firefly* luciferase reporter and a control *Renilla* reporter. After 24 h, *Firefly* and *Renilla* luciferase activities were measured (D). Cell whole lysate were also analyzed by immunoblotting using antibodies against FLAG and actin (E and F). * $P < 0.05$, ** $P < 0.01$, *** $P < 0.001$, **** $P < 0.0001$; N = 3.

3.2.6 NSP2 interacts with and downregulates the levels of host transcription mediators Rpb1 and TFIIE2

To further investigate how MAYV affects the host antiviral response, co-immunoprecipitation (co-IP) followed by tandem mass spectrometry (LC-MS/MS) was used to identify host cell proteins that interact with NSP2. Putative NSP2-binding host proteins were subjected to analyses using Molecular Interaction Search Tool (MiST) and key cellular processes associated with NSP2 interactors were assessed through Gene Ontology (GO) enrichment analysis. One of the key enriched GO terms was "RNA polymerase II holoenzyme complex" (Figure 3.8A), which consists of proteins involved in transcription by RNA polymerase II. Two members of this complex were identified in the NSP2 co-IP. Specifically, Rpb1 (also known as POLR2A), a component of RNA polymerase II that was previously shown to interact with other alphavirus NSP2 proteins (Akhrymuk et al., 2012; Fros et al., 2013), and TFIIE2, an integral factor that functions in transcription initiation (Vannini and Cramer 2012). Until this study, TFIIE2 was not known to interact with alphavirus NSP2. Interestingly, the transcriptional shutoff mutant $NSP2^{P722S}$ formed a stable interaction with Rpb1 but not TFIIE2 (Figure 3.8B-C). Confocal microscopy analyses revealed that in cells transfected with NSP2, expression levels of Rpb1 and TFIIE2 were significantly reduced (Figure 3.9A, B, C, and D). The NLS mutant $NSP2^{RK653AA}$ reduced TFIIE2 but not Rpb1 levels, whereas the transcriptional shutoff mutant $NSP2^{P722S}$ did not affect levels of either protein (Figure 3.9A, B, C, and D). Accordingly, nuclear localization of NSP2 appears to be important for depleting Rpb1 but not for suppressing TFIIE2 expression.

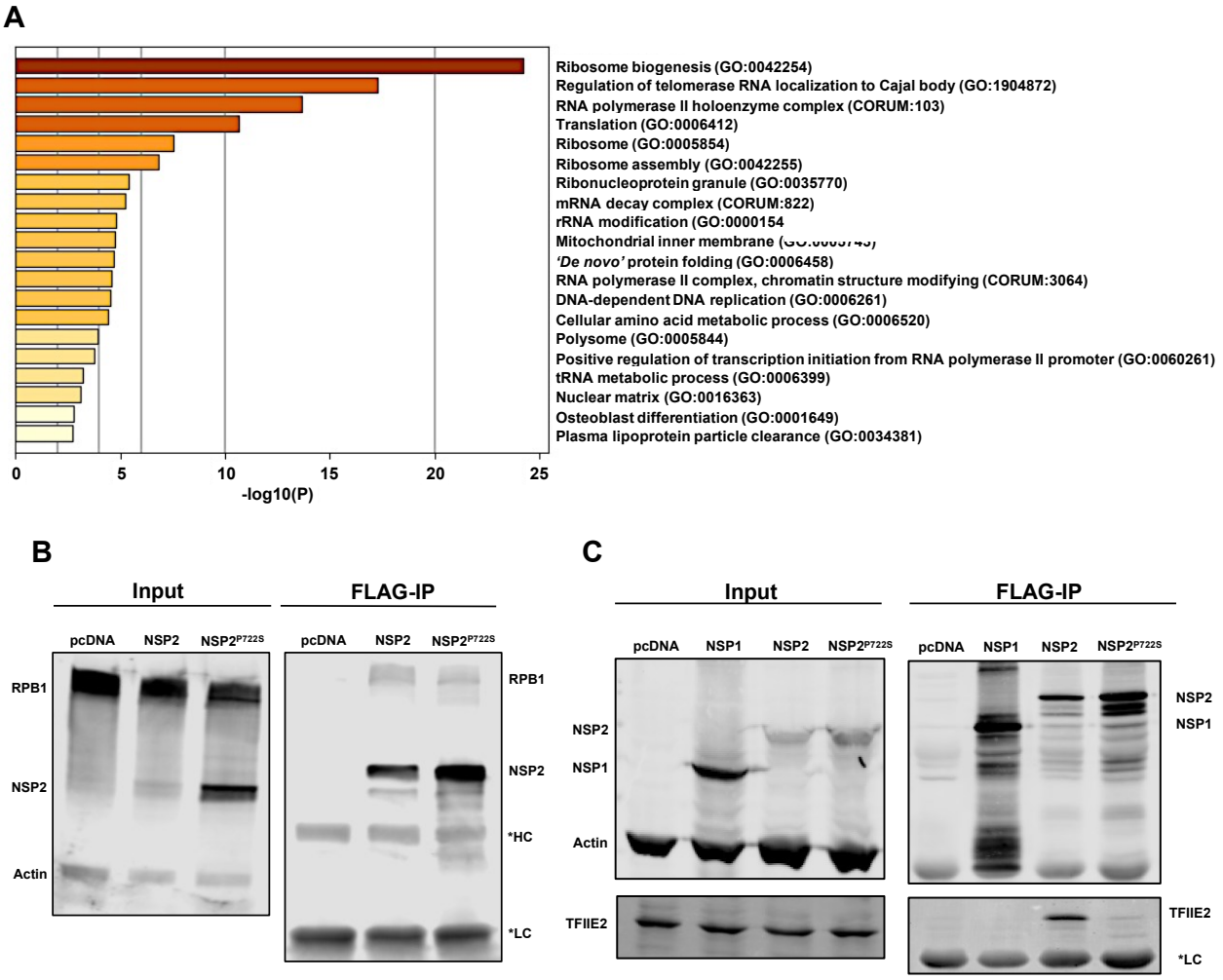

Figure 3.8 MAYV NSP2 interacts with key transcription mediators, Rpb1 and TFIIE2. A. Heatmap of GO term enrichment analysis. HEK 293T cells were transfected with pcDNA empty vector or NSP2 for 24h, after which whole cell lysates were immunoprecipitated using magnetic beads coated with anti-FLAG. NSP2-interacting proteins were identified by liquid chromatography-tandem mass spectrometry and the protein-protein interactions from three independent experiments were scored by MiST analysis. NSP2 interacting host proteins with MiST score of ≥0.8 were selected to perform the GO enrichment analysis using the Metascape software. **B** and **C**. HEK 293T cells were transfected with the indicated viral protein constructs and 24h later, whole cell lysates were immunoprecipitated with magnetic beads coated with anti-FLAG and then subjected to immunoblot analysis using antibodies against FLAG, RPB1, and actin (B), or FLAG, TFIIE2, and actin (C). Representative blots from three independent experiments are shown.

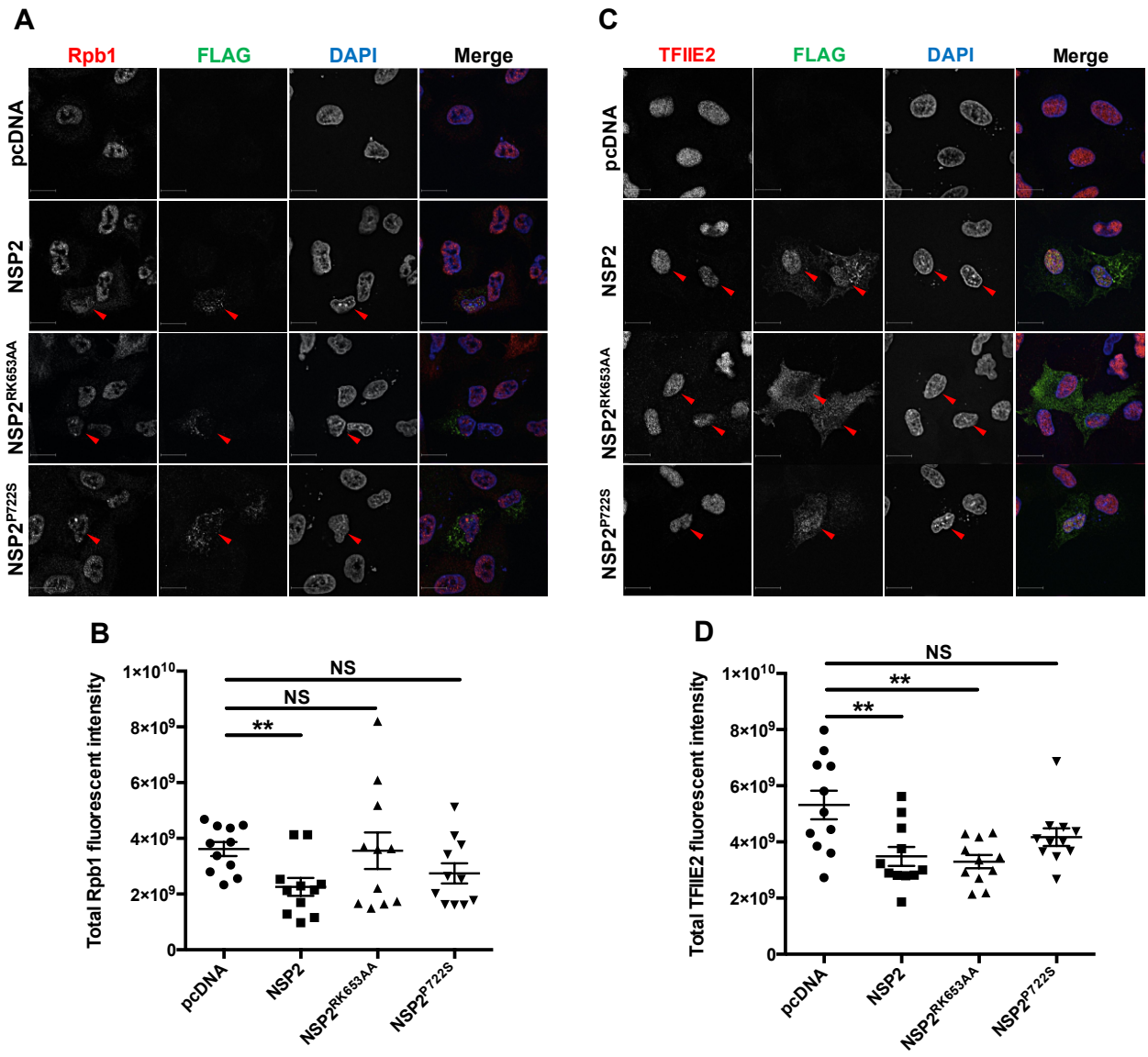

Figure 3.9 MAYV NSP2 downregulates Rpb1 and TFIIE2. A and **B**. WT MAYV NSP2 downregulates Rpb1. A549 cells were transfected with NSP2 WT or NSP2^{RK653AA} (NLS-deficient), or NSP2^{P722S} (host transcription shutoff deficient) constructs. After 24h, cells were fixed and stained using α-FLAG and α-Rpb1 antibodies and imaged by IF microscopy. The total Rpb1 fluorescent intensities were quantified using Volocity software. ** $P < 0.01$, NS= not significant; N = 11. **C** and **D**. A549 cells were transfected with indicated NSP2 constructs. After 24 h, cells were fixed and stained using antibodies to FLAG and and TFIIE2 followed by confocal microscopy imaging. The total TFIIE2 fluorescent intensities were quantified using Volocity software. ** $P < 0.01$, NS= not significant; N = 11.

3.2.7 Some but not all alphaviruses reduce levels of TFIIE2

Quantitative confocal analyses confirmed that MAYV infection resulted in significant loss of Rpb1 and TFIIE2 proteins at 24 hpi (Figure 3.10 A, B, C, and D). To elucidate how this occurs, MAYV-infected cells were treated with inhibitors of proteasomal- (epoxomicin) and lysosomal- (bafilomycin A1) dependent degradation followed by immunoblot analyses. Loss of Rpb1 protein during MAYV infection was significantly inhibited by epoxomicin (Figure 3.10E and F), which is consistent with previous findings that old world alphavirus NSP2-dependent depletion of Rpb1 involves the proteasome (Akhrymuk et al., 2012). Conversely, neither epoxomicin nor bafilomycin significantly blocked MAYV-induced loss of TFIIE2 protein (Figure 3.10E and G). Next, we examined the levels of Rpb1 and TFIIE2 proteins in SFV- and Sindbis virus (SINV)-infected cells. Similar to what was observed during MAYV infection, Rpb1 and TFIIE2 levels were both reduced at 24 hpi in SFV-infected cells (Figure 3.11A, B, and C). However, in cells infected with SINV, Rpb1 but not TFIIE2 levels were lower (Figure 3.11A, B, and C).

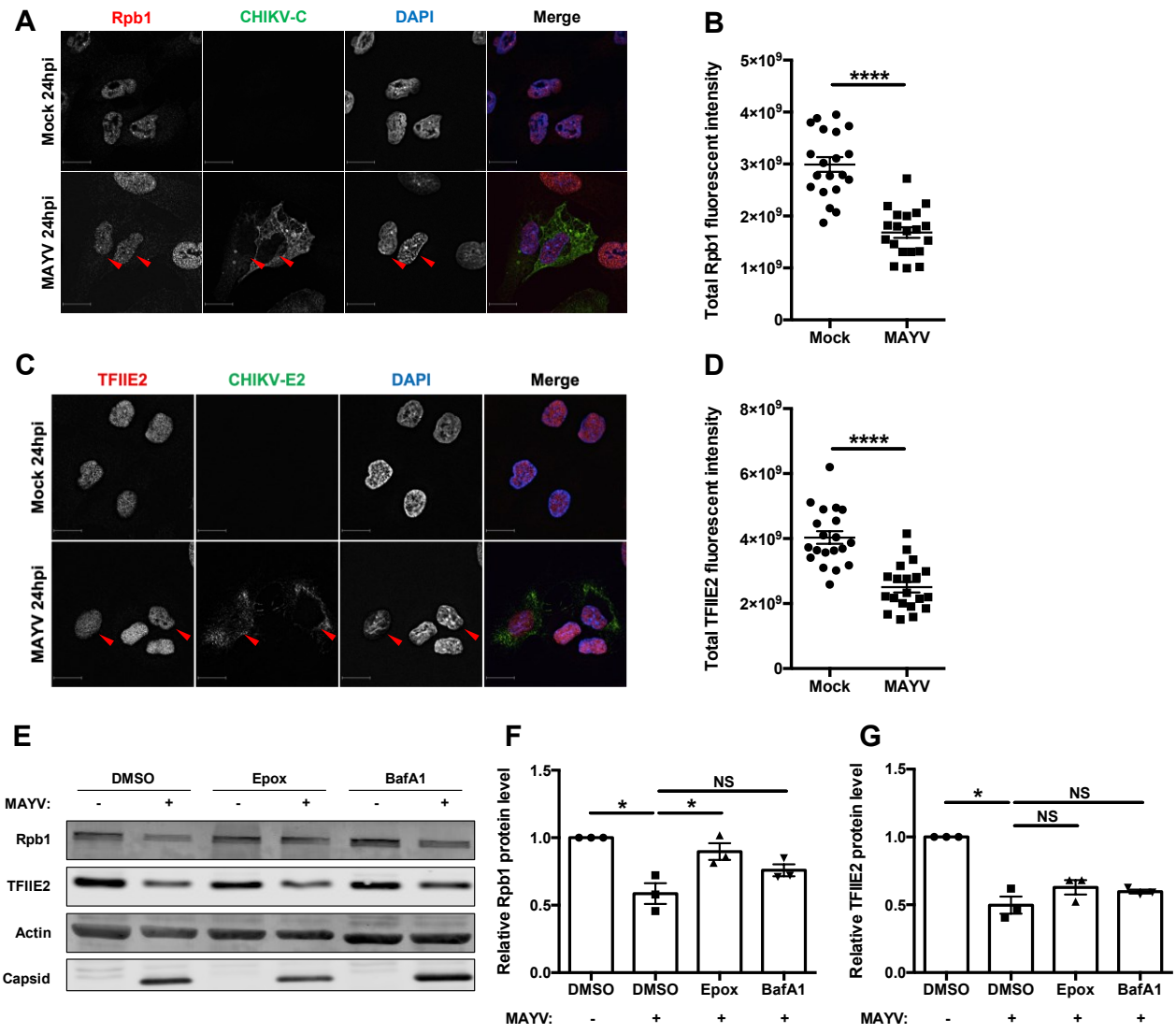

Figure 3.10 Levels of Rpb1 and TFIIE2 are reduced during MAYV infection. A-D. A549 cells were infected with MAYV (MOI=1) for 24 h and then fixed and stained with antibodies to CHIKV-Capsid and Rpb1 (A, B) or TFIIE2 (C, D) followed by confocal imaging. The total Rpb1 and TFIIE2 fluorescent intensities were quantified using Volocity software. **** $P < 0.0001$; N = 20. **E-G**. A549 cells were infected with MAYV (MOI=3) for 8 h, then treated with epoxomicin or bafilomycin (100 μM) for 24 h. Cell lysates were then subjected to immunoblotting using antibodies to Rpb1, TFIIE2, actin, CHIKV-capsid, and SFV-capsid proteins. The intensities of the protein bands were quantified using Image Studio software and then normalized to actin levels and expressed as folds of mock infected control. * $P < 0.05$, NS= not significant; N = 3.

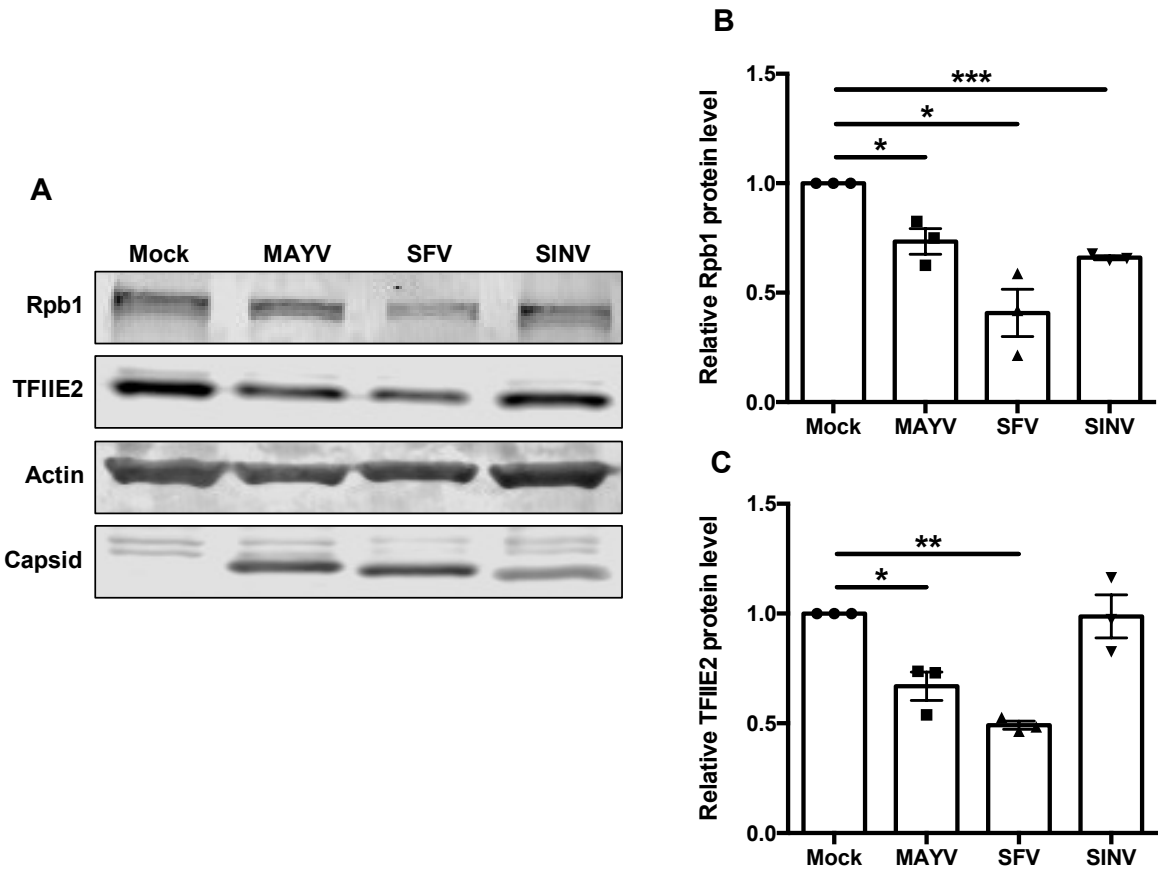

Figure 3.11 Some but not all alphaviruses downregulate TFIIE2 protein levels. A-C. A549 cells were infected with either MAYV, SFV, or SINV (MOI=1) for 24 h after which cell lysates were processed for immunoblotting using antibodies against Rpb1, TFIIE2, actin, CHIKV-capsid, and SFV-capsid proteins. The intensities of the protein bands were quantified using Image Studio software and then normalized to actin levels and expressed as folds of mock infected control. * $P < 0.05$, ** $P < 0.01$, *** $P < 0.001$; N = 3.

3.2.8 MAYV suppresses global transcription during infection

Finally, as a first step toward understanding how MAYV infection affects host cell transcription, we assessed bulk levels of RNA as well as transcripts of housekeeping genes following infection. As expected, total cellular RNA was greatly reduced at 48 hpi (Figure 3.12A), while housekeeping gene transcripts were lower at 24 hpi (Figure 3.12B, C, and D). One possibility to explain the lack of substantial decrease in total RNA level at 24 hpi may be due to increasing levels of viral RNA during this time period. Indeed we observed a significant increase in viral RNA from 8 to 24 hpi (Figure 3.12E). Together, these results suggest that MAYV infection circumvents IFN induction in part by blocking global transcription through NSP2-mediated depletion of transcription factors TFIIE and Rpb1.

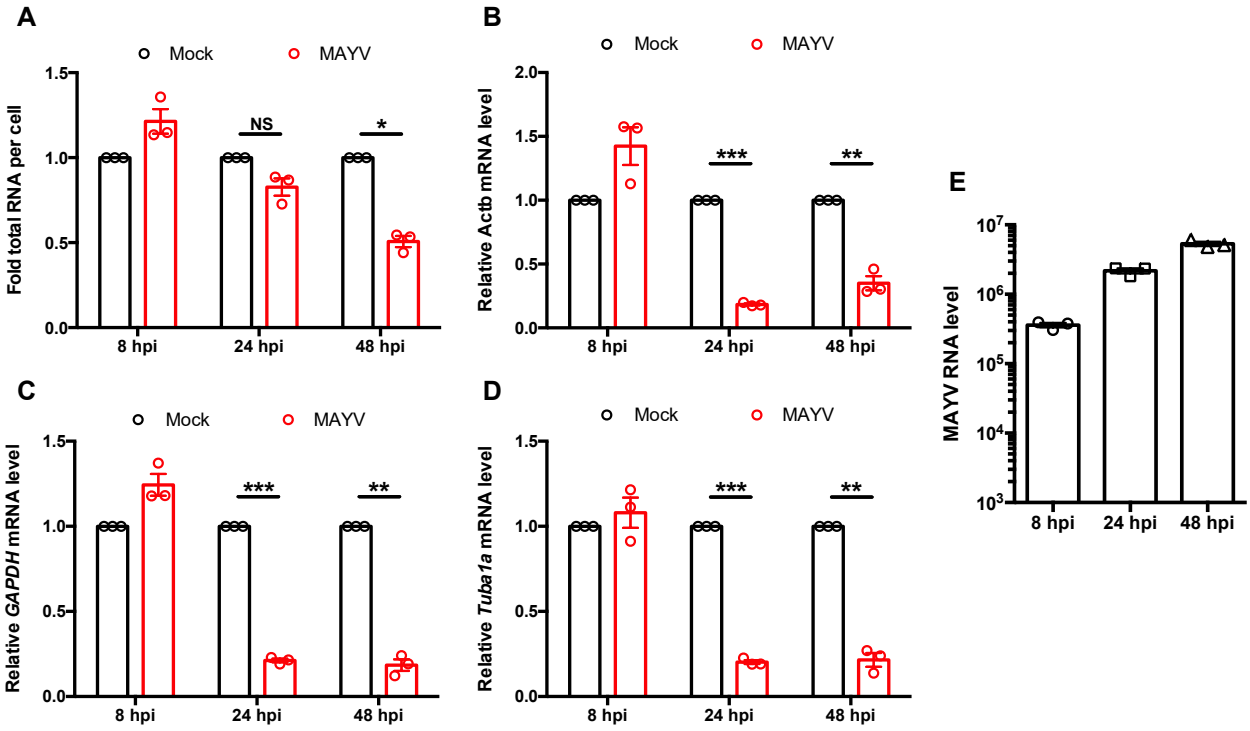

Figure 3.12 MAYV blocks global transcription during infection. A-E. A549 cells were infected with MAYV (MOI=3) for 8, 24, and 48 h after which total cellular RNA was extracted and quantified using a spectrophotometer (A). Relative levels of *ACTB* (B), *GAPDH* (C), *Tuba1a* (D), MAYV RNA (E) were measured by qRT-PCR and normalized by cell count and expressed as fold mock infected cells. * $P < 0.05$, ** $P < 0.01$, *** $P < 0.001$. NS= not significant; N = 3.

3.3 Summary

In this chapter, I analyzed how MAYV affects the induction phase of the IFN response. I observed that MAYV infection inhibits production of *Ifnb* transcripts and secretion of IFNs. Intriguingly, MAYV did not block SeV-induced IRF3 nuclear translocation, suggesting that it blocks IFN induction at a post-IRF3 nuclear translocation step. NSP2 was the only MAYV protein that prevented IFN induction. In parallel to what was observed in MAYV-infected cells, expression of NSP2 did not block nuclear translocation of IRF3 but did subvert IRF3-5D-mediated IFN induction. This evidence suggests that NSP2 blocks induction IFN downstream of IRF3 phosphorylation and nuclear translocation. Mutational analyses indicated that the transcriptional shutoff function of NSP2 is at least in part responsible for blocking IFN induction. NSP2 was found to bind and downregulate Rpb1 and TFIIE2; two host proteins that are important for RNA polymerase II mediated transcription. Rpb1 is depleted via a proteasomal-dependent mechanism, during MAYV infection whereas the mechanism by which TFIIE2 levels are decreased is not clear. Interestingly, unlike Rpb1 which is depleted during infection with MAYV, SFV and SINV, targeted loss of TFIIE2 was not observed during SINV infection. Together, these results provide novel insight into how MAYV suppresses the induction arm of the IFN response. This information may be important when considering development of therapeutics against MAYV and other alphaviruses.

Chapter 4

SARS-CoV-2 non-structural protein 1 inhibits the interferon response by causing depletion of key host signaling factors.

Portions of this chapter have been published as:

Kumar, A.*, Ishida, R.*, Strilets, T.*, Cole, J., Lopez-Orozco, J., Fayad, N., Felix-Lopez, A., Elaish, M., Evseev, D., Magor, K.E., Mahal, L.K., Nagata, L.P., Evans, D.H., and Hobman, T.C. 2021. SARS-CoV-2 Nonstructural Protein 1 Inhibits the Interferon Response by Causing Depletion of Key Host Signaling Factors. J Virol 95 (13): doi: 10.1128/JVI.00266-21.

*Authors contributed equally

A. Kumar performed experiments for Figure 4.1 B, C, D, and F; Figure 4.8 A, B, C, and D. T. Strilets performed experiments for Figure 4.3 C; Figure 4.10 A and B. J. Cole performed experiments for Figure 4.2 A and B. D. Evseev performed experiments for Figure 4.7 D.

4.1 Rationale

The emergence of severe acute respiratory syndrome coronavirus 2 (SARS-CoV-2), first reported in 2019 in Wuhan, China, is responsible for the ongoing COVID-19 pandemic (Wang et al., 2020; Zhu et al., 2020), which has resulted in over 5 million deaths thus far. The virus is readily transmitted via respiratory droplets (Prem et al., 2020), and as it continues to spread among the human population, genetic drift drives the rise of new variants of concern (VOCs) that can be more transmissible and/or virulent (Khateeb et al., 2021; Bano et al., 2021; Kumar, Singh, et al., 2021). While most SARS-CoV-2 infections are asymptomatic or mild, severe cases can manifest as acute respiratory distress syndrome, thromboembolism, and multiorgan failure (Mir et al., 2021). Although multiple SARS-CoV-2 vaccines are now licensed for use, it remains important to further understand the biology of the virus in order to guide development of novel antivirals and to make informed decisions for disease management.

Extensive research efforts have focused on understanding how SARS-CoV-2 affects the host IFN response. In cell culture models, the virus is highly sensitive to pre-treatment with IFNs (Vanderheiden et al., 2020a; Miorin et al., 2020), consistent with the observation that early administration of type I IFNs has some therapeutic benefit (Davoudi-Monfared et al., 2020; Monk et al., 2021; Alavi Darazam et al., 2021). Moreover, a significant number of patients with severe COVID-19 have either underlying defects in their capacity to produce IFNs or have auto-antibodies that neutralize type I IFNs (Zhang et al., 2020; Bastard et al., 2020; Bastard et al., 2021), thereby further highlighting the importance of the IFN response during SARS-CoV-2 infection. Data from many studies suggest that more than half of the proteins encoded by the virus can interfere with the immune response (Banerjee et al., 2020; Shin et al., 2020; Thoms et al., 2020; Li et al., 2020; Jiang et al., 2020; Lei et al., 2020; Yuen et al., 2020; Acharya et al., 2020; Miorin

et al., 2020; Xia et al., 2020; Mu et al., 2020b; Shemesh et al., 2021; Gori Savellini et al., 2021; Zhao et al., 2021). However, the data in these studies are not consistent among each other, and the complete picture by which SARS-CoV-2 suppresses the IFN response is not clear.

To further understand how SARS-CoV-2 infection affects the IFN response, we analyzed both IFN induction and signalling during SARS-CoV-2 infection as well as in transfected cells expressing individual viral proteins. Our study was the first to assess the suppression of IFN response using plasmids encoding *bona fide* SARS-CoV-2 proteins as opposed to codon-optimized plasmids used in other studies (Li et al., 2020; Xia et al., 2020; Lei et al., 2020; Yuen et al., 2020; Shin et al., 2020; Jiang et al., 2020; Miorin et al., 2020; Shemesh et al., 2021). As such, it can be argued that our strategy better represents the viral protein expression levels seen during infection. As part of this work, we describe mechanisms by which the SARS-CoV-2 non-structural protein 1 (NSP1) and nucleocapsid protein (N) suppress the IFN response.

4.2 Results

4.2.1 SARS-CoV-2 blocks IFN induction

To understand how the host cell responds to SARS-CoV-2 infection, we assessed the transcriptional induction of *Ifnb* mRNA and secretion of IFN-β from ACE2-expressing HEK 293T (HEK 293T-ACE2) cells using qRT-PCR and ELISA, respectively. While robust replication of the virus was observed in these cells, similar to levels seen in Vero E6 cells, by 24 and 48 hpi (Figure 4.1A), no significant increase in *Ifnb* mRNA (Figure 4.1B) or secreted IFN-β (Figure 4.1C) were observed. Conversely, infection of these cells with Sendai virus (SeV) resulted in increased secretion of IFN-β into culture media. In contrast, cells which were first infected with SARS-CoV-

2 secreted very low levels IFN-β in response to SeV infection (Figure 4.1C). Similarly, no induction of the ISG IFIT1 was observed in SARS-CoV-2 infected cells and significantly lower levels were induced when challenged with SeV or poly(I:C) (Figure 4.1D and E). These results are in agreement with a recent study describing human airway epithelial cell cultures infected with SARS-CoV-2 (Vanderheiden et al., 2020a).

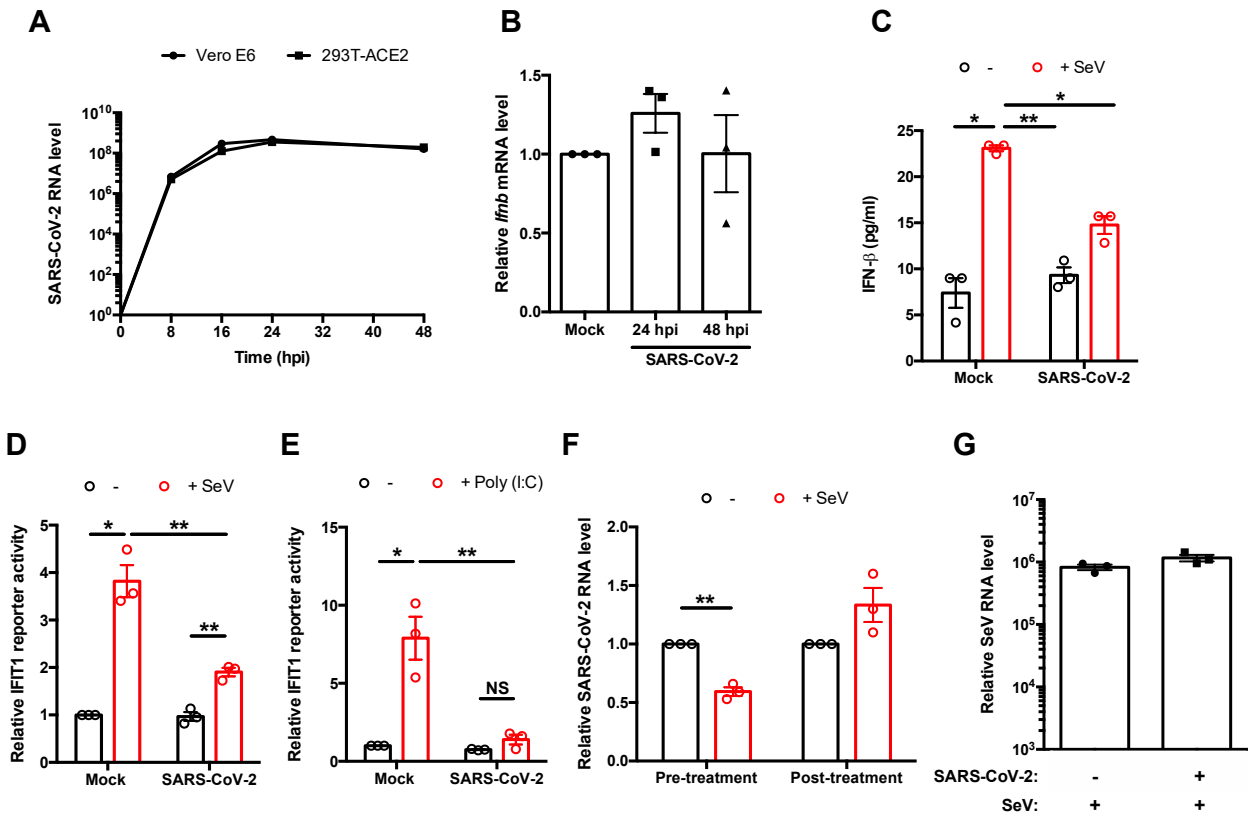

Figure 4.1 SARS-CoV-2 blocks IFN induction. A. Vero E6 and HEK 293T-ACE2 cells were infected with SARS-CoV-2 (MOI=1) and total RNA was harvested at 0, 8, 16, 24, and 48 hours post infection (hpi). Viral RNA level was measured by qRT-PCR and normalized to *ACTB* mRNA level and expressed as folds of mock-infected cells. N = 3. **B**. HEK 293T-ACE2 cells were infected with SARS-CoV-2 (MOI=1) and total RNA was harvested at 24 and 48 hours post infection (hpi). *Ifnb* level was measured by qRT-PCR and normalized to *ACTB* mRNA level and expressed as folds of mock-infected cells. N= 3. **C**. Mock or SARS-CoV-2 infected (30 hpi) HEK 293T-ACE2 cells were challenged with 50 HAU/ml Sendai virus (SeV) for 16 h. IFN-β in cell culture supernatants was measured by enzyme linked immunosorbent assay (ELISA). * $P < 0.05$, ** $P < 0.01$; N = 3. **D** and **E**. HEK 293T-ACE2 cells were infected with SARS-CoV-2 (MOI=1). After 24 h, the cells were transfected with IFIT1 *Firefly* luciferase reporter and control *Renilla* reporter plasmids and then challenged with 100 HAU/ml of SeV (D) or 2 μg/ml of poly(I:C) (E) for 16 h. *Firefly* and *Renilla* luciferase activities were measured in cell lysates after which the IFIT1 reporter luciferase activity was normalized against *Renilla* reporter values and were further normalized to uninduced mock infected cells. * $P < 0.05$, ** $P < 0.01$, NS = not significant ; N = 3. **F**. HEK 293T-ACE2 cells infected with SeV (50 HAU/ml) for 8 h pre-infection (pre-treatment) or 16 h post-infection (post-treatment) were subsequently infected with SARS-CoV-2 (MOI=1). Total RNA was harvested 48 hpi. SARS-CoV-2 genomic RNA was measured by qRT-PCR and normalized to *ACTB* mRNA level and expressed as folds of mock-infected cells. ** $P < 0.01$; N = 3. **G**. HEK 293T cells were infected with SARS-CoV-2 (MOI=1). After 24 h, cells were infected with SeV (50HAU/ml) for 16 h, after which total RNA was harvested. SeV genomic RNA was measured by qRT-PCR and normalized to *ACTB* mRNA level and expressed as folds of mock-infected cells. N = 3.

Next, we examined the ability of SARS-CoV-2 to infect cells in which type I IFN had been induced by SeV either 8 h pre-infection or 16 h post-infection. Replication of SARS-CoV-2 was significantly impaired in cells that were previously infected with SeV for 8 h (Figure 4.1F). In contrast, addition of SeV to cells 16 h post-infection with SARS-CoV-2 had little effect on its replication indicating that this coronavirus actively blocks IFN induction (Figure 4.1F). Of note, similar amounts of intracellular SeV RNA were detected in mock- and SARS-CoV-2-infected cells (Figure 4.1G), indicating that SARS-CoV-2-infected cells are as permissive for SeV infection as mock-infected cells. The suppression of IFN induction during SARS-CoV-2 infection was further evident from the lack of phosphorylation of IRF3 (Figure 4.2A) and absence of SeV-induced-IRF3 transport into the nucleus (Figure 4.2B).

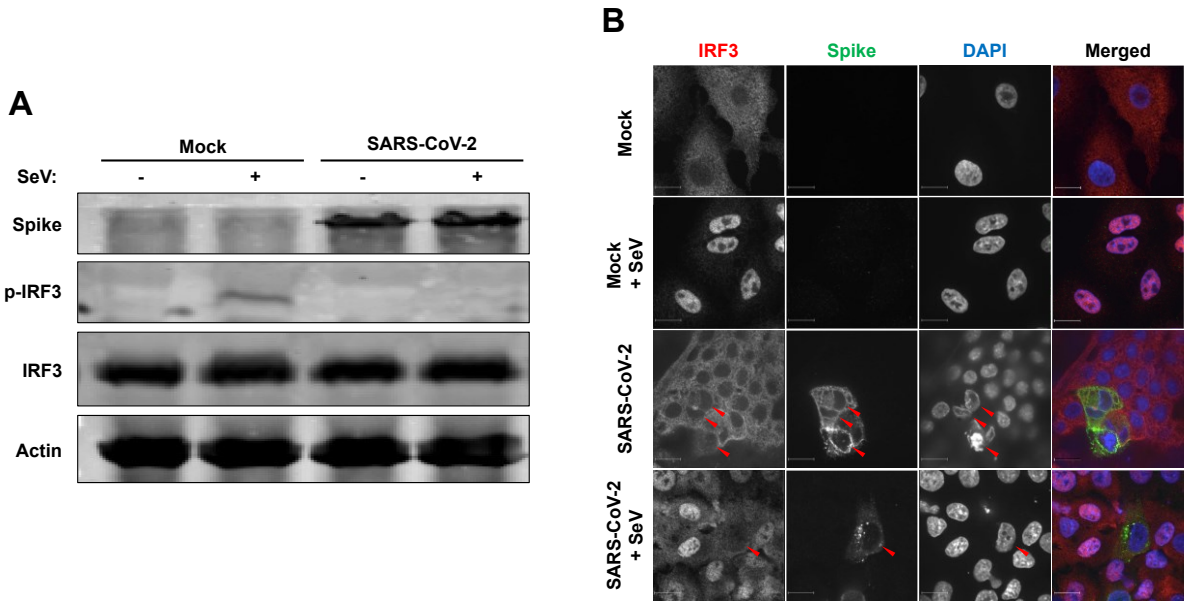

Figure 4.2 SARS-CoV-2 blocks IRF3 phosphorylation and nuclear translocation. A. HEK 293T-ACE2 cells were infected with SARS-CoV-2 (MOI=1) for 16 h, then infected with mock or 50 HAU/ml of SeV for 8 h. Cell lysates were subjected to immunoblotting using antibodies against Spike, IRF3, phospho-IRF3 and actin. **B**. A549 were electroporated with plasmid encoding ACE2 and then infected with SARS-CoV-2 (MOI=1) for 16 h followed by challenge with 50 HAU/ml of SeV for 8 h. Cells were fixed and Spike and IRF3 localization were determined by indirect-immunofluorescence analysis.

4.2.2 Cloning of 3XFLAG-tagged SARS-CoV-2 proteins into pcDNA3.1(-)

To determine which viral proteins were responsible for antagonizing type I IFN induction, we constructed expression plasmids for all known proteins of SARS-CoV-2 with C-terminal 3XFLAG tags using cDNA generated from infected cell lysates. NSP10 was tagged with 3X FLAG on its N-terminus due to the instability of the C-terminally tagged version. The expression and molecular weights of most sequence-verified constructs was determined by immunoblotting (Figure 4.3A). Expression of NSP6 and ORF10 were verified by immunoprecipitation coupled with immunoblotting (Figure 4.3B) whereas expression of NSP3 (>250 kDa) was confirmed by indirect immunofluorescence (IF) (Figure 4.3C).

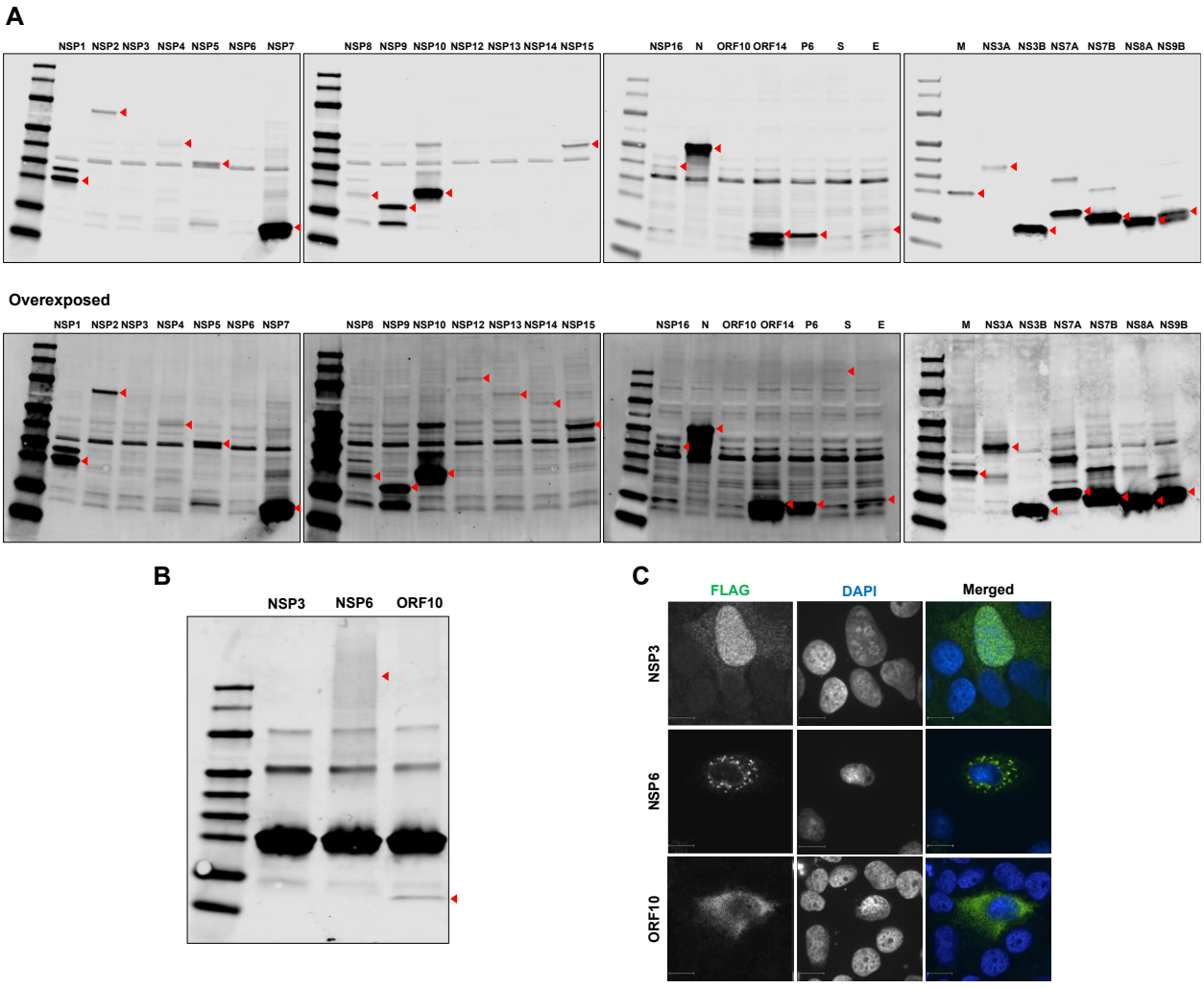

Figure 4.3 Expression of pcDNA3.1(-) 3XFLAG-tagged SARS-CoV-2 protein constructs. A. Huh7 cells were transfected with plasmids encoding the indicated viral proteins with 3XFLAG tags. After 24 h, cell lysates were subjected to immunoblotting with antibodies against FLAG. The positions of the FLAG-tagged viral proteins are indicated with red arrowheads. **B**. HEK 293T cells were transfected with plasmids encoding FLAG-tagged SARS-CoV-2 NSP3, NSP6, and ORF10 which protein expressions were not confirmed by western blot. Cells were harvested 24 h post-transfection, immunoprecipitated with anti-FLAG antibody, and subjected to western blot analysis immunostaining with antibody against FLAG. **C**. Huh7 cells were transfected with NSP3, NSP6, and ORF10 for 48 h, fixed and imaged by IF microscopy after staining using antibody against FLAG.

4.2.3 SARS-CoV-2 NSP1 and N block IFN induction

The effect of SARS-CoV-2 proteins on SeV-induced IFN induction was assessed using an IFN-β luciferase reporter assay and ELISA. Expression of the N and NSP1 proteins reduced IFN-β reporter activity by 70% and 30% respectively (Figure 4.4A). Secretion of IFN-β was also significantly impaired in cells expressing these viral proteins (Figure 4.4B). As the antiviral transcription factors IRF3 and NFκB are important for IFN induction (Fensterl 2015), we assessed whether N or NSP1 affected their activities. Whereas both viral proteins inhibited IRF3-dependent transcription by >50%, NFκB reporter activity was more strongly affected by NSP1 (64% reduction) (Figure 4.4C and D). We next examined whether localization of IRF3 was affected in SeV-infected cells expressing N protein or NSP1. IRF3 did not translocate to the nuclei of NSP1 expressing cells which is consistent with the observation that this viral protein inhibits IFN induction (Figure 4.5A and B). Conversely, nuclear accumulation of IRF3 was not significantly affected in cells expressing N protein nor the control protein NS3A (Figure 4.5A and B). Mapping studies using overexpression of IFN induction pathway components suggest that a critical step targeted by NSP1 is the phosphorylation of IRF3 (Figure 4.5C). Specifically, NSP1-mediated reduction in IRF3 signaling was rescued by expression of a constitutively active form of IRF3 (IRF3-5D). We also tested how expression of an NSP1 mutant (KH164AA) that is unable to suppress translation (Narayanan et al., 2008) affected induction of type I IFNs. The KH164AA mutant did not reduce IFN-β reporter activity (Figure 4.6A and B) which was consistent with the observation that it did not block translocation of IRF3 into nuclei (Figure 4.6C and D). Together, these data suggest that NSP1 mediated suppression of IFN production is linked to its ability to block host cell translation and inhibit nuclear transport of IRF3.

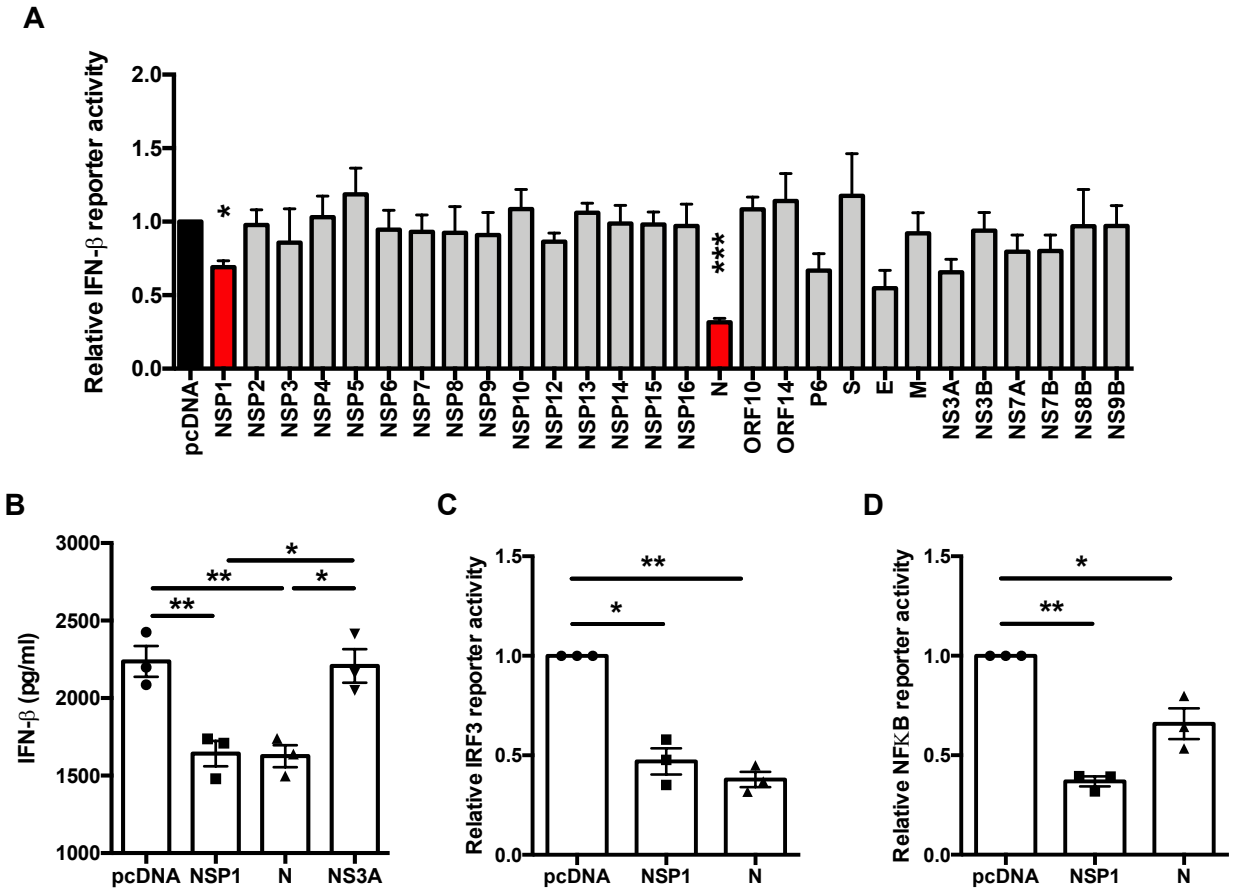

Figure 4.4 SARS-CoV-2 NSP1 and N block IFN induction. A. HEK 293T cells were transfected with plasmids encoding the indicated viral proteins, IFN-β *Firefly* luciferase reporter and control *Renilla* reporter. Twenty-four hours later cells were infected with 100 HAU/ml of SeV for 16 h after which *Firefly* and *Renilla* luciferase activities were measured in cell lysates. IFN-β reporter activity was normalized against *Renilla* reporter values and the data are presented as folds activity to pcDNA empty vector control. * $P < 0.05$, *** $P < 0.001$; N = 3. **B**. HEK 293T cells were transfected with plasmids encoding NSP1, NS3A or N, and 24 h later challenged with 100 HAU/ml of Sendai virus for 16 h. The culture supernatants were harvested and IFN-β levels determined by ELISA. * $P < 0.05$, ** $P < 0.01$; N = 3. **C** and **D**. HEK 293T cells were transfected with plasmids encoding NSP1 or N proteins and *Firefly* luciferase under the control of IRF3- (C) or NFκB- (D) responsive promotors as well as a constitutively expressed *Renilla* luciferase reporter. Twenty-four hours later cells were challenged with 100 HAU/ml of SeV for 16 h after which *Firefly* and *Renilla* luciferase activities were measured in cell lysates. The *Firefly* luciferase activity was normalized against *Renilla* luciferase values and the data is presented as folds activity to pcDNA empty vector control. * $P < 0.05$, ** $P < 0.01$; N = 3.

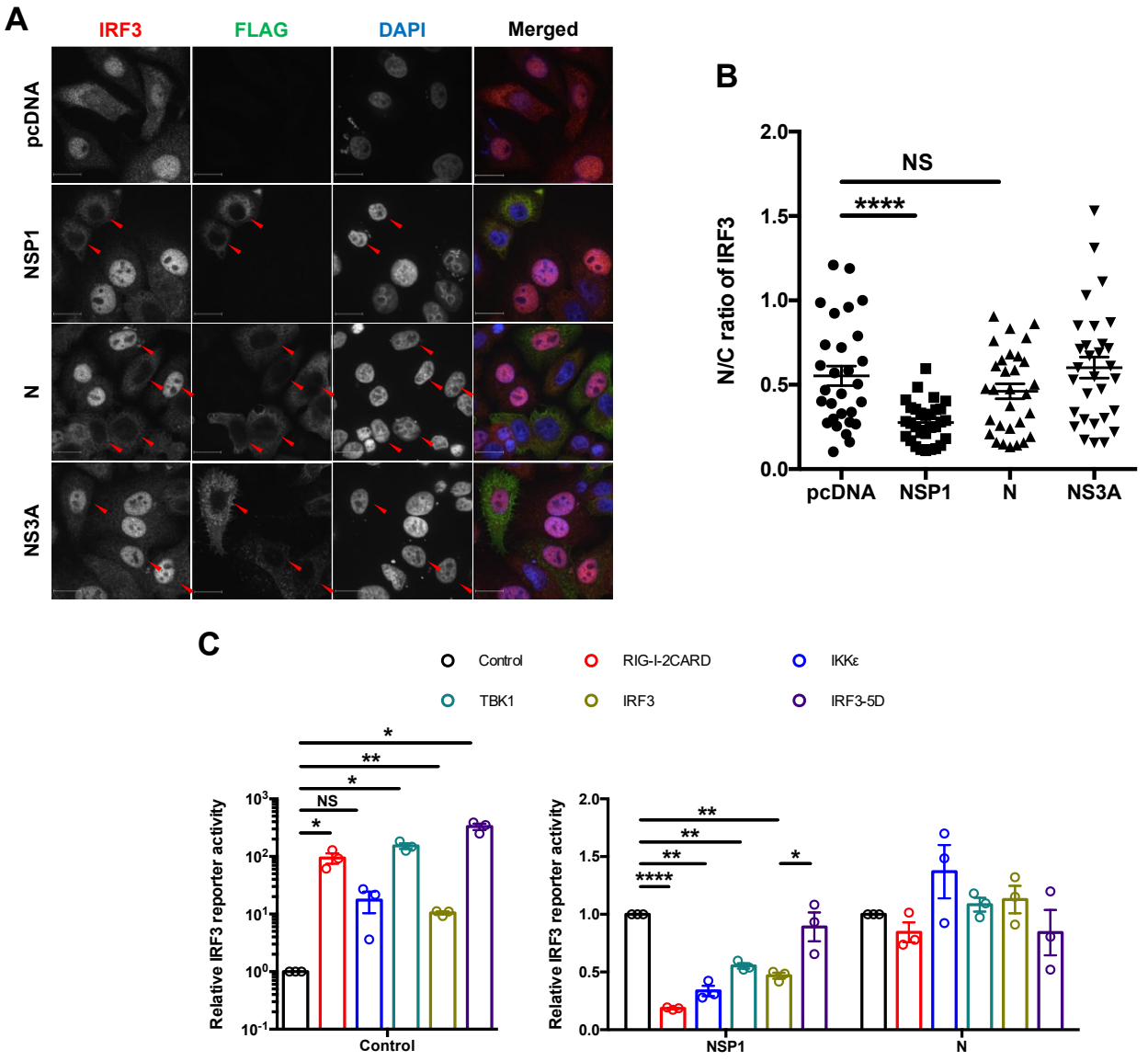

Figure 4.5 SARS-CoV-2 blocks activation of IRF3. A and **B**. A549 cells were transfected with plasmids encoding NSP1, N, or NS3A and 24 h later challenged with 100 HAU/ml of SeV for 8 h. The cells were then processed for indirect immunofluorescence using antibodies against FLAG and IRF3. The cytoplasmic and nuclear IRF3 signal were quantitated using Volocity software. **** $P < 0.0001$, NS = not significant; N = 30. **C**. HEK 293T cells were transfected with plasmids encoding NSP1 or N and RIG-I, IKKε, TBK1, IRF3, or IRF3-5D, IRF3-promotor *Firefly* luciferase reporter, and constitutively expressed *Renilla* luciferase reporter. Samples were harvested at 24 h post transfection after which *Firefly* and *Renilla* luciferase activities were measured in cell lysates. The *Firefly* luciferase activity was normalized against *Renilla* luciferase values and the data are presented as folds activity to pcDNA empty vector control. * $P < 0.05$, ** $P < 0.01$, **** $P < 0.0001$, NS = not significant; N = 3.

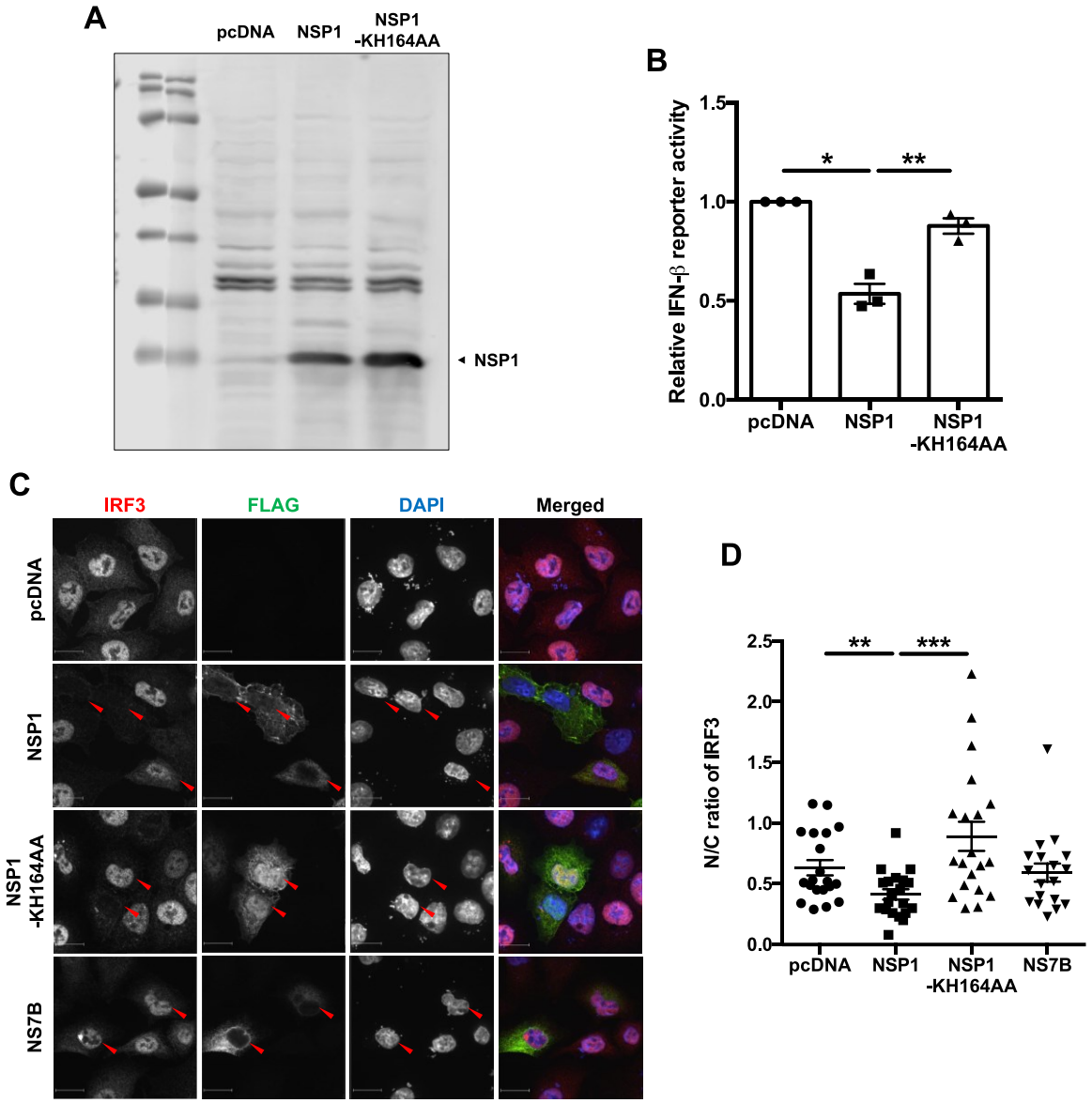

Figure 4.6 SARS-CoV-2 NSP1 blocks IFN induction through translational shutoff. A. HEK 293T cells were transfected with either empty vector and plasmids encoding wild type NSP1 or mutant NSP1-KH164AA for 24 h. Cell lysates were then subjected to immunoblotting with antibodies against FLAG. **B**. HEK 293T cells were transfected with empty vector or plasmids encoding wild type NSP1 or mutant NSP1-KH164AA, IFN-β-responsive *Firefly* luciferase reporter and control *Renilla* reporter. After 24 h, the cells were challenged with 100 HAU/ml of SeV for 16 h and then harvested for luciferase assays. The *Firefly* reporter activities were normalized against *Renilla* reporter values and the data are presented as folds activity to uninduced empty vector control. * $P < 0.05$, ** $P < 0.01$; N = 3. **C** and **D**. A549 cells were transfected with plasmid encoding wild type NSP1, mutant (KH164AA) NSP1 or NS7B for 24 h after which cells were challenged with 100 HAU/ml of SeV for 8 h. Samples were then processed for indirect immunofluorescence microscopy using antibodies against FLAG and IRF3. The fluorescent intensities in the nucleus and cytoplasm were measured using Volocity software. ** $P < 0.01$, *** $P < 0.001$; N = 20.

4.2.4 SARS-CoV-2 N protein interacts with TRIM25, but does not block ubiquitination of RIG-I.

To further understand how N protein blocked IFN induction, we probed for interaction between SARS-CoV-2 N protein and TRIM25. Previously it was reported that the N protein of the closely related coronavirus SARS-CoV, inhibits TRIM25-mediated ubiquitination of RIG-I (Hu et al., 2017), an essential step in RIG-I activation. Stable interaction between N protein and TRIM25 was observed by co-immunoprecipitation (Figure 4.7A) and the importance of TRIM25 in restricting SARS-CoV-2 replication was demonstrated by overexpression of TRIM25 (Figure 4.7B and C). However, N protein did not impair ubiquitination of RIG-I by TRIM25 *in vitro* (Figure 4.7D). Accordingly, the mechanism of N-mediated suppression of IFN-β induction remains to be elucidated.

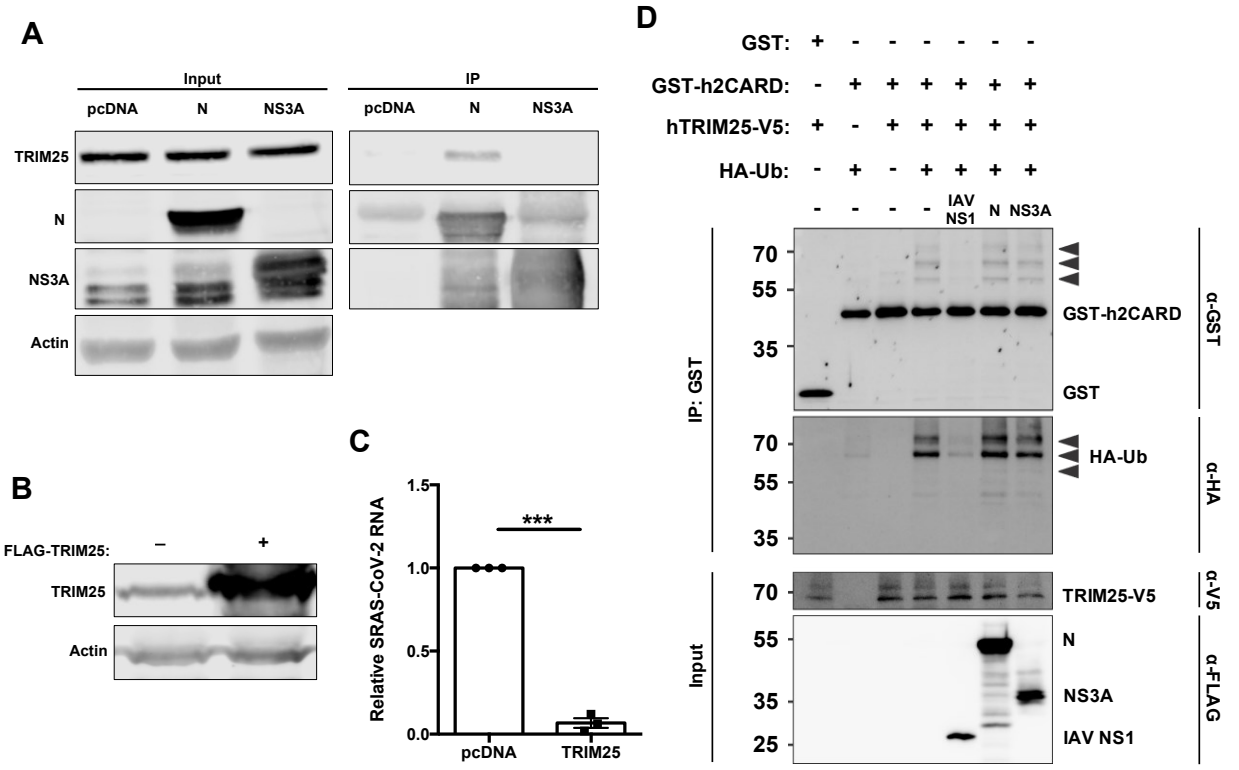

Figure 4.7 SARS-CoV-2 N protein interacts with TRIM25 without blocking RIG-I ubiquitination. A. HEK 293T cells were transfected with plasmids encoding SARS-CoV-2 N or NS3A proteins or empty vector. After 48 h, cell lysates were immunoprecipitated with anti-FLAG antibody and then subjected immunoblot analysis using antibodies against FLAG, TRIM25, and actin. **B**. HEK 293T cells were transfected with a plasmid encoding FLAG-TRIM25 or empty vector for 48 h after which cell lysates were subjected to immunoblot analysis using antibodies against TRIM25 and actin. **C**. HEK 293T-ACE2 cells were transfected with a plasmid encoding FLAG-tagged TRIM25 or empty vector for 48 h. Cells were then infected with SARS-CoV-2 (MOI=1) for 48 h, after which total RNA was harvested and subjected to qRT-PCR to quantify viral genomic RNA which was normalized to *ACTB* mRNA level and expressed as folds of pcDNA empty vector transfected cells. *** $P < 0.001$; N = 3. **D**. HEK 293T cells were transfected with plasmids encoding GST-tagged human RIG-I CARD domains (GST-h2CARD) or GST alone, together with HA-tagged ubiquitin (HA-Ub), V5-tagged human TRIM25 (hTRIM25-V5), and the indicated FLAG-tagged viral proteins. Clarified whole cell lysates were subjected to GST pulldown (IP: GST), followed by immunoblot analysis with anti-GST, anti-HA, anti-V5, and anti-FLAG antibodies. Influenza A virus (IAV) NS1 serves as a positive control for blocking TRIM25-mediated ubiquitination of the RIG-I CARD domains.

4.2.5 SARS-CoV-2 blocks ISG induction

To investigate how SARS-CoV-2 affects the signaling arm of the IFN response, we first assessed induction of ISGs in SARS-CoV-2 infected HEK 293T-ACE2 cells. While robust viral replication was observed in these cells (Figure 4.1A), no significant induction of the ISG *Ifit1* mRNA was detected (Figure 4.8A). Treatment of HEK 293T-ACE2 cells with IFN-α strongly upregulated *Ifit1* expression indicating the presence of a functional IFN signaling pathway in these cells (Figure 4.8B). Next, we examined the sensitivity of SARS-CoV-2 to pre- and post-infection treatment with IFN-α, IFN-γ and IFN-λ. Consistent with recent reports (Mantlo et al., 2020; Felgenhauer et al., 2020; Miorin et al., 2020; Vanderheiden et al., 2020a), replication of SARS-CoV-2 was strongly inhibited by pre-treatment with IFN-α, whereas post-treatment had only a moderate effect (Figure 4.8B). Interestingly, neither pre- nor post-treatment of cells with IFN-γ reduced viral replication whereas IFN-λ inhibited virus replication but not to the same degree as IFN-α. These results were further confirmed by IFN-stimulated response element (ISRE) promoter reporter assays where strong inhibition was observed in SARS-CoV-2 infected cells (Figure 4.8C). In contrast, GAS promotor activity was not inhibited in SARS-CoV-2 infected cells treated with IFN-γ (Figure 4.8D). We next examined how SARS-CoV-2 affected levels of cellular proteins involved in type I IFN signaling. Immunoblot analysis revealed that levels of STAT2 and Tyk2 were significantly reduced during infection whereas IFNAR1, Jak1 and STAT1 levels were largely unaffected (Figure 4.9A and B).

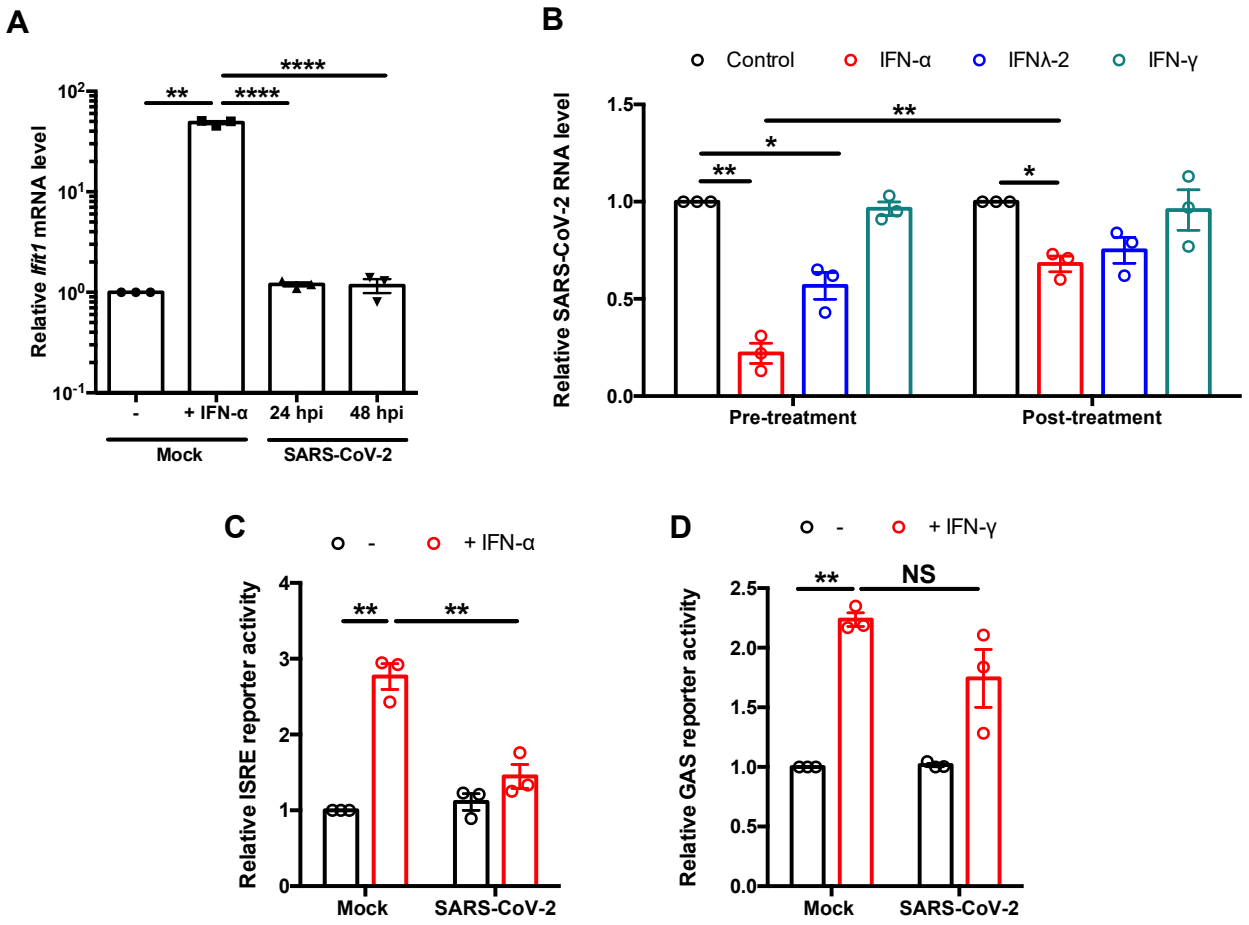

Figure 4.8 SARS-CoV-2 block ISG induction. A. HEK 293T-ACE2 cells were infected with SARS-CoV-2 (MOI=2) and total RNA was harvested at 24 and 48 hpi. Mock-infected cells were treated with IFN-α (100 U/ml) for 16 hours as control. *Ifit1* level was measured by qRT-PCR and normalized to *ACTB* mRNA level. ** $P < 0.01$, **** $P < 0.0001$; N = 3. **B**. HEK 293T-ACE2 cells treated with IFN-α (100 U/ml), IFN-λ (100 ng/ml), or IFN-γ (10 U/ml) for 6 h pre-infection (pretreatment) or 16 hpi (post-treatment) of SARS-CoV-2 (MOI=1). Total RNA was harvested 48 hpi and viral genomic RNA was measured by qRT-PCR. All values are expressed as fold of mock infected samples. * $P < 0.05$, ** $P < 0.01$; N = 3. **C**. HEK 293T-ACE2 cells were infected with SARS-CoV-2 (MOI=1) and 24 h later transfected with ISRE *Firefly* luciferase reporter and control *Renilla* reporter plasmids and then induced with 100 U/ml of IFN-α for 16 h. The samples were harvested and processed by luciferase assay. The ISRE reporter activity was normalized against *Renilla* reporter values which were further normalized to the uninduced mock infected cells. * $P < 0.05$, ** $P < 0.01$; N = 3. **D**. HEK 293T-ACE2 cells were infected with SARS-CoV-2 (MOI=1) and then 24 h later transfected with IFN-γ-responsive (GAS) *Firefly* luciferase reporter and control *Renilla* reporter and induced with 10 U/ml of IFN-γ. After 16 h, luciferase activities were measured and GAS-dependent luciferase activities were normalized against *Renilla* reporter values and the data are presented as folds activity to mock samples. ** $P < 0.01$, NS = not significant; N = 3.

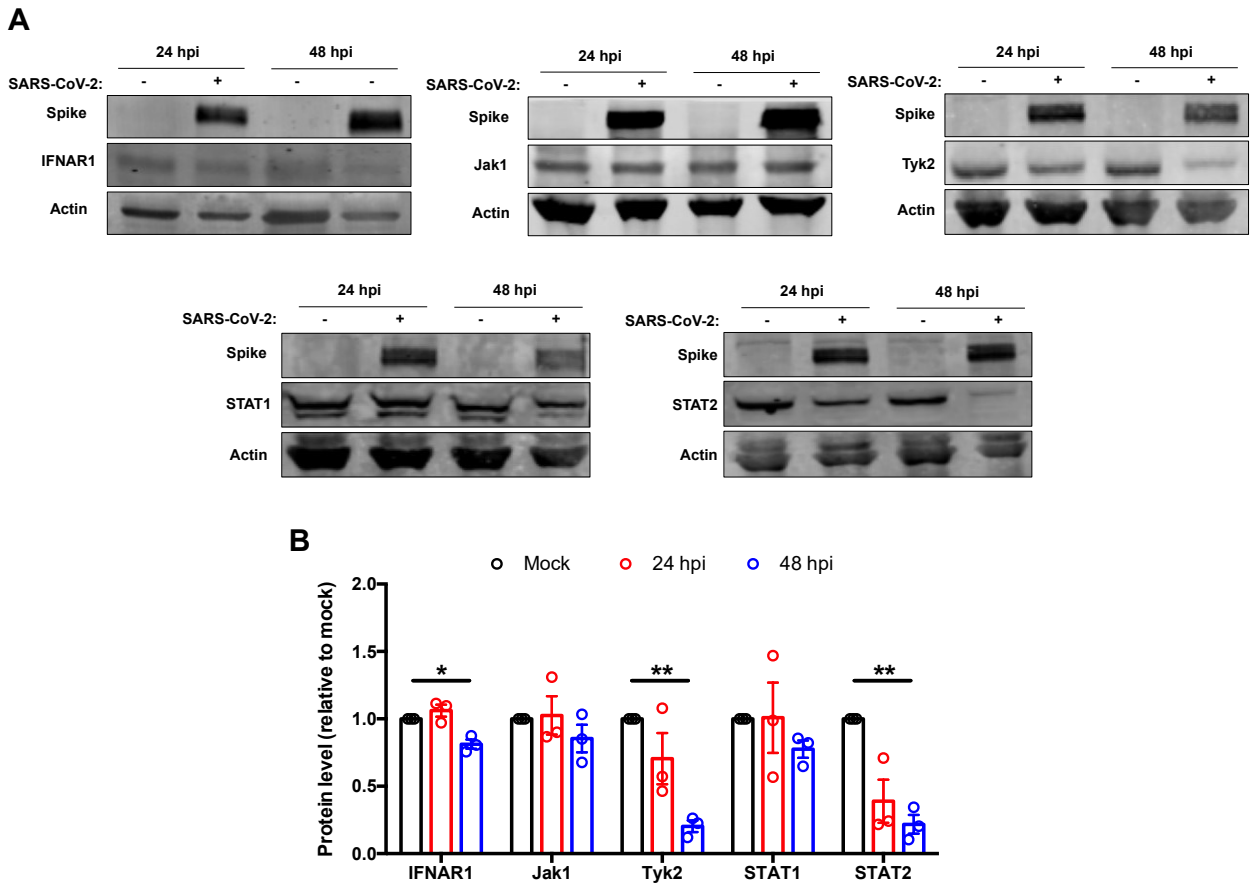

Figure 4.9 SARS-CoV-2 downregulates Tyk2 and STAT2 protein levels. A and **B**. HEK 293T-ACE2 cells were infected with SARS-CoV-2 (MOI=1) and cell lysates collected 24 and 48 hpi were subjected to immunoblotting using antibodies against Spike, IFNAR1, Jak1, Tyk2, STAT1, STAT2, and actin. The intensities of the protein bands were measured using Image Studio software, normalized to actin level and expressed as folds of mock infected control. * $P < 0.05$, ** $P < 0.01$; N = 3.

4.2.6 Tyk2 and STAT2 are depleted during SARS-CoV-2 infection

Next, infected cells were treated with IFN-α or IFN-γ for 2 h, after which localization of STAT1 and STAT2 were examined by confocal microscopy. Compared to uninfected cells, STAT2 fluorescence was greatly diminished in infected cells, and nuclear translocation of the protein in response to IFN treatment was not observed (Figure 4.10A). In contrast, neither the STAT1 fluorescent signal nor its nuclear translocation were noticeably affected by SARS-CoV-2 infection (Figure 4.10B). To determine the mechanism by which STAT2 depletion occurred during infection, we treated infected cells with inhibitors of proteasomal- (epoxomicin) and lysosome- (bafilomycin A1) dependent degradation. Epoxomicin treatment partially rescued STAT2 levels suggesting that depletion of this transcription factor during SARS-CoV-2 infection is mediated at least in part by proteasomal degradation (Figure 4.10C and D). As SARS-CoV-2 is known to suppress host cell translation (Schubert et al., 2020), we assessed whether the loss of STAT2 and potentially other antiviral host factors were due to this effect. When green fluorescent protein (GFP)-expressing cells were infected with SARS-CoV-2, there was no reduction in GFP mRNA but a 30% decrease in protein levels was observed (Figure 4.11A, B, and C). Treatment of uninfected cells with cycloheximide resulted in reduction of STAT2 and Tyk2 protein levels comparable to those seen during infection (Figure 4.11D and E), suggesting that virus-mediated suppression of host cell translation is important for blocking IFN signaling.

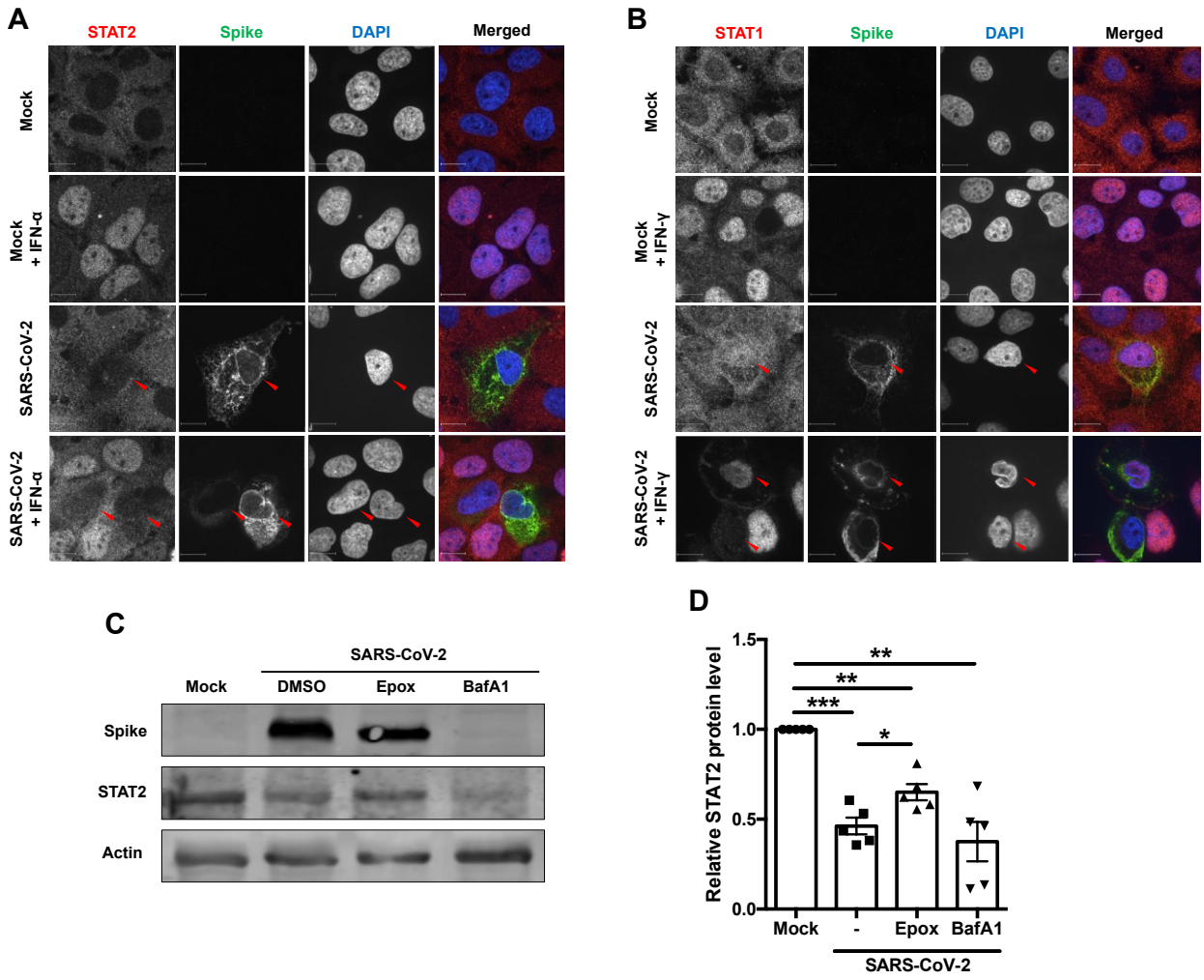

Figure 4.10 STAT2 is depleted during SARS-CoV-2 infection. A and **B**. Huh7 cells were infected with SARS-CoV-2 (MOI=0.5) and at 46 hpi treated with IFN-α (100 U/ml) for 2 h. Cells were then processed for indirect immunofluorescence using antibodies against Spike and STAT2 (A) or STAT1 (B). **C** and **D**. HEK 293T-ACE2 cells were infected with SARS-CoV-2 (MOI=2) and 16 hpi treated with either DMSO, 100 μM of epoxomicin or Bafilomycin A1 for 36 h. Cell lysates were subjected to immunoblotting using antibodies against Spike, STAT2 and actin. The intensities of the protein bands were measured using Image Studio software, normalized to actin level and expressed as folds of uninfected control * $P < 0.05$, ** $P < 0.01$, *** $P < 0.001$; N = 5.

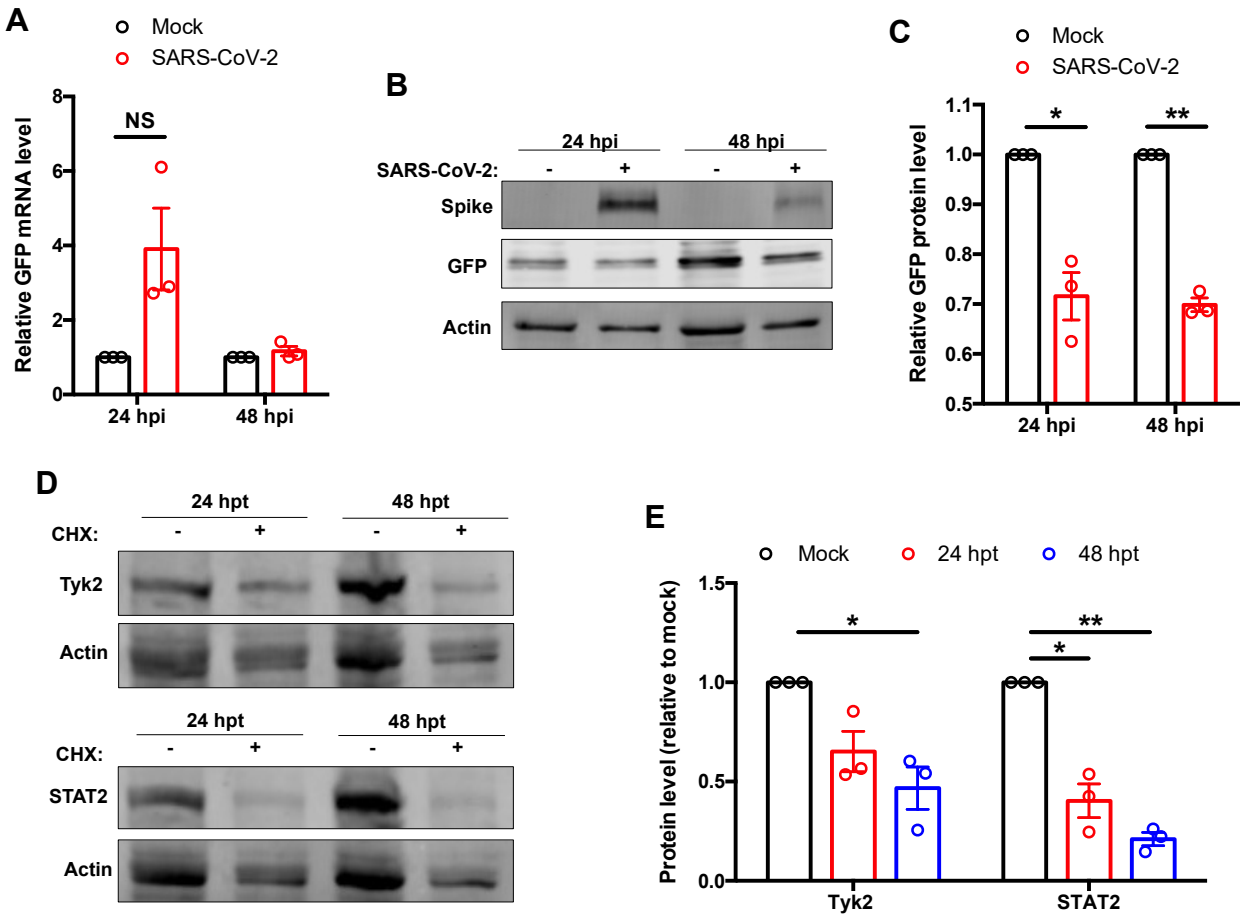

Figure 4.11 SARS-CoV-2 mediated translational shutoff can reduce Tyk2 and STAT2 during infection. A-C. HEK 293T-ACE2 cells were transduced with a lentivirus encoding AcGFP for 4 h and then infected with SARS-CoV-2 (MOI=1). Total RNA and proteins were extracted at 24 and 48 hpi and relative GFP transcript (normalized to *ACTB* mRNA; A) and protein (normalized to actin; B and C) levels were determined by qRT-PCR and immunoblotting, respectively. * $P < 0.05$, ** $P < 0.01$; N = 3. **D** and **E**. HEK 293T cells were treated with 100 µM of cycloheximide for 24 or 48 h, after which cell lysates were subjected to immunoblotting using antibodies against STAT2, Tyk2, and beta-actin. The intensities of the protein bands were measured using Image Studio software, normalized to β-actin level and expressed as folds of uninfected control. * $P < 0.05$, ** $P < 0.01$; N = 3.

4.2.7 SARS-CoV-2 NSP1 blocks IFN signaling

To identify the viral proteins that inhibit IFN signaling, we performed ISRE reporter assays in cells expressing individual SARS-CoV-2 proteins. NSP1 was the only viral protein that significantly suppressed ISRE reporter activity (Figure 4.12A). To examine the mechanism behind this phenomenon, we again employed the NSP1 mutant KH164AA that is unable to inhibit host cell translation. The mutant NSP1 did not block ISRE-dependent transcription (Figure 4.12B) which is consistent with a role for viral translational suppression in preventing IFN induction (Banerjee et al., 2020; Kamitani et al., 2006; Narayanan et al., 2008). STAT2 expression in cells expressing NSP1 was also examined by confocal microscopy. Compared to cells expressing SARS-CoV-2 NS7B or NSP1 KH164AA mutant, the STAT2 signal was significantly reduced in cells expressing wild type NSP1 (Figure 4.12C and D). These results are consistent with immunoblotting data in which levels of ectopically expressed STAT2-GFP were reduced by wild type NSP1, but not by the KH164AA mutant (Figure 4.13A and B). Furthermore, in cells co-expressing *Renilla* luciferase and wild type NSP1, a 40% reduction in luciferase reporter activity was observed (Figure 4.14A). Similarly, in cells expressing GFP and NSP1, there was no significant reduction in mRNA level but a 40-45% reduction GFP protein level was observed (Figure 4.14B, C, and D) demonstrating an inhibitory effect of NSP1 on overall protein production. NSP1-mediated depletion of STAT2 could be partially rescued by treatment with epoxomicin (Figure 4.14G and H) indicating that proteasome-mediated degradation plays a role in STAT2 depletion. However, although statistically insignificant, epoxomicin treatment also increased STAT2 protein levels in control samples (Figure 4.14G and H), indicating that STAT2 is normally turned over via the proteasomal machinery. Our data are consistent with a scenario where virus-

induced global translational shutdown leads to depletion of critical host antiviral factors with short half-lives, such as STAT2 and Tyk2 that are needed for induction of ISGs.

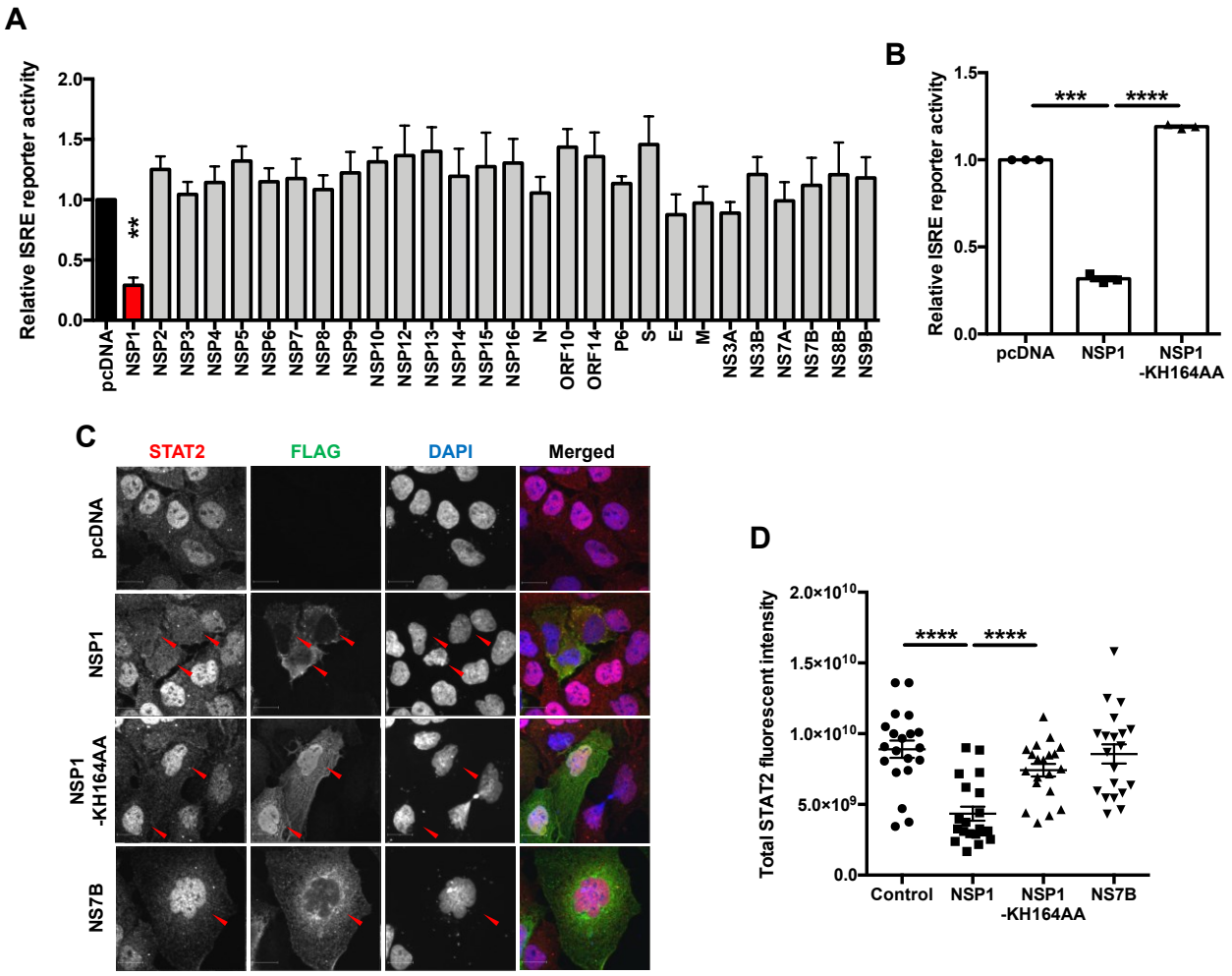

Figure 4.12 SARS-CoV-2 NSP1 blocks IFN signaling. A. HEK 293T cells were transfected with plasmids encoding the indicated viral proteins, ISRE *Firefly* luciferase reporter and control *Renilla* luciferase reporter. Twenty-four hours later cells were induced with 100 U/ml of IFN-α for 16 h. *Firefly* and *Renilla* reporter activity was measured by luciferase assay. The ISRE reporter activity was normalized against *Renilla* reporter values and the data is presented as folds activity to empty vector control. ** $P < 0.01$; N = 3. **B**. HEK 293T cells were transfected with pcDNA carrying indicated proteins, and ISRE *Firefly* luciferase reporter and control *Renilla* reporter. 24 h later the cells were induced with 100 U/ml of IFN-α for 16 h and then *Firefly* and *Renilla* luciferase activities were measured. The ISRE reporter activity was normalized against *Renilla* reporter values and the data are presented as folds activity to pcDNA empty vector control. *** $P < 0.001$, **** $P < 0.0001$; N = 3. **C** and **D**. Huh7 cells were transfected with plasmids encoding the indicated SARS-CoV-2 proteins. Twenty-four hours later cells were induced with 100 U/ml of IFN-α for 2 h and then processed for indirect immunofluorescence microscopy with antibodies against FLAG and STAT2. The total fluorescent intensity of STAT2 was measured using Volocity software. **** $P < 0.0001$; N = 20.

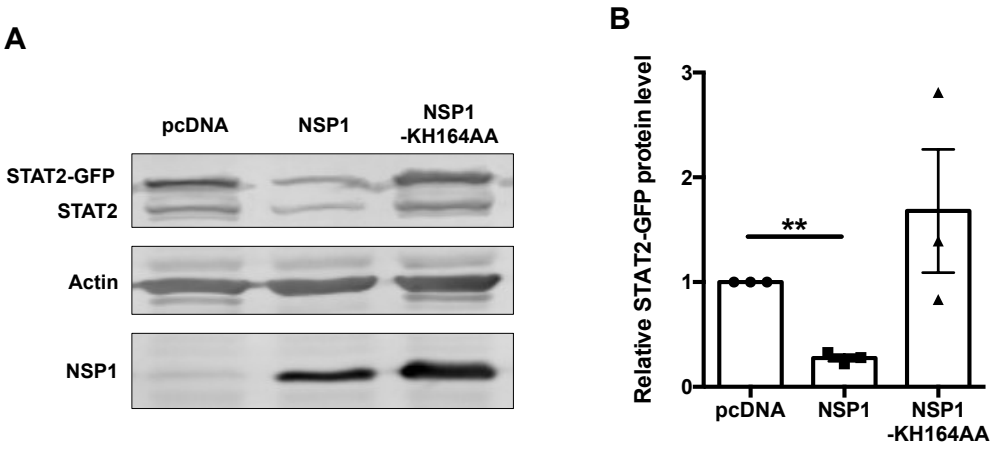

Figure 4.13 SARS-CoV-2 NSP1 reduces STAT2 through translational shutoff. A and **B**. HEK 293T cells were transfected with plasmids encoding wild type or mutant (KH164AA) NSP1 proteins and STAT2-GFP for 24 h after which lysates were subjected to immunoblotting with antibodies against FLAG, STAT2, and actin. The intensities of the bands were calculated using Image Studio software, normalized to actin levels and expressed as folds compared to empty vector transfected samples. ** $P < 0.01$; N = 3.

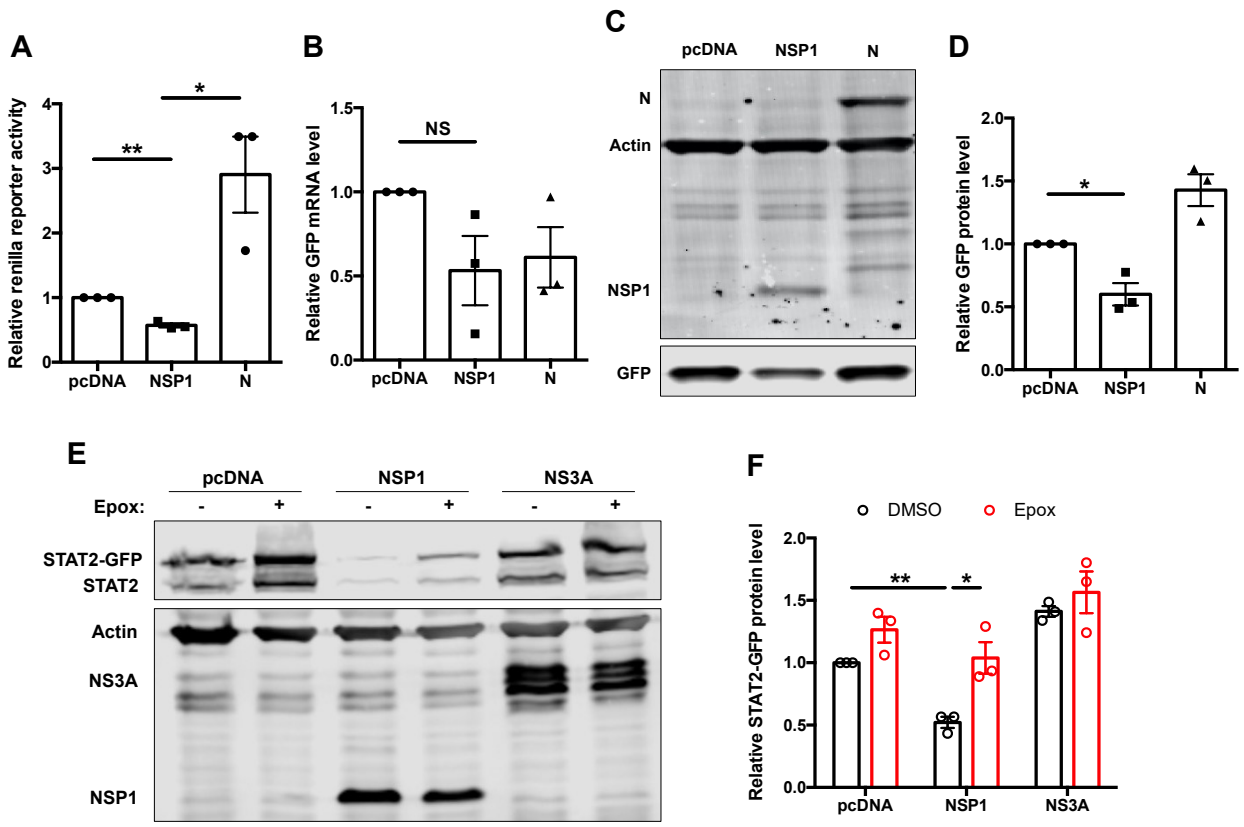

Figure 4.14 SARS-CoV-2 NSP1 interferes with host translational machinery. A. HEK 293T cells were transfected with plasmids encoding NSP1 or N protein or empty vector and *Renilla* luciferase reporter. After 24 h, cell lysates were subjected to luciferase assay. The data are presented as folds activity to empty vector control. * $P < 0.05$, ** $P < 0.01$; N =3. **B**-**D**. HEK 293T cells were transduced with lentivirus encoding AcGFP for 4 h and then transfected with plasmids encoding NSP1 or N protein for 24 h. Total RNA and protein were harvested and GFP transcript (normalized to *ACTB* mRNA; B) and protein (normalized to actin; C and D) levels were determined by qRT-PCR and immunoblotting, respectively. * $P < 0.05$, NS = not significant; N =3. **E** and **F**. HEK 293T cells were transfected with plasmids encoding NSP1 or NS3A and STAT2-GFP. After 24 h, cells were treated with either DMSO or 100 μM of epoxomicin for 24 h. Cell lysates were then processed by immunoblotting with antibodies against FLAG, STAT2 and actin. * $P < 0.05$, ** $P < 0.01$; N =3.

4.3 Summary

In this chapter, the effect of SARS-CoV-2 infection on the IFN response was systematically analyzed. Circumvention of both induction and the signaling arms of the IFN response was observed during SARS-CoV-2 infection. While the virus was sensitive to pre-treatment of cells with SeV and IFNs, it was impervious to these treatments once infection was established. With respect to the underlying mechanisms, nuclear translocation of IRF3 and STAT2 were impaired in SARS-CoV-2-infected cells. Furthermore, levels of STAT2 and Tyk2 were significantly reduced during infection.

SARS-CoV-2 NSP1 and N suppressed the induction of IFNs, however only NSP1 inhibited the IFN signaling pathway. N protein was shown to interact with TRIM25, but without impairing its function of activating RIG-I, which is normally required to initiate IFN induction. Expression of NSP1 inhibited nuclear translocation of IRF3 and blunted the effects of IRF3 overexpression on IFN induction suggesting that this viral protein interferes with activation of IRF3. Analyses indicated that translational shutoff by NSP1 is indispensable for antagonizing IFN and ISG induction. Indeed, similar to what was observed in SARS-CoV-2-infected cells, ectopic expression of NSP1 led to the abrogation of STAT2, while the mutant NSP1-KH164AA did not reduce STAT2 in transfected cells. Together, our study demonstrates that during SARS-CoV-2 infection, NSP1-mediated translational shutoff leads to the reduction of key IFN response mediators including STAT2 and Tyk2, thereby efficiently blocking the expression of IFNs and ISGs.

Chapter 5

Discussion

5.1 Synopsis

Emerging positive-strand RNA viruses have the potential to cause great damage to public health systems and the global economy. These viruses account for the majority of emerging human pathogens (Carrasco-Hernandez et al., 2017), which can be attributed to their high mutations rates (Duffy et al., 2008; Holmes 2009) that allow them to adapt to new hosts more readily than other pathogens. Proactively studying these pathogens will undoubtedly leave us in a better position for future epidemics and pandemics. For my thesis work, I studied how two emerging positive-strand RNA viruses from two different families, namely MAYV (*Togaviridae*) and SARS-CoV-2 (*Coronaviridae*), affect the IFN response, a critical arm of the antiviral immune response. In chapter 3, I showed that MAYV antagonizes the induction of IFNs in part by viral NSP2-mediated transcriptional shutoff. Expression of MAYV NSP2 reduces level of Rpb1 and TFIIE2, two key proteins necessary for RNA polymerase II-dependent transcription, thereby limiting host gene expression including transcription of IFNs. In chapter 4, I investigated how SARS-CoV-2 infection affects the IFN response. While viral NSP1 and N proteins suppressed IFN induction, NSP1 was the only viral protein that impeded ISG induction. Finally, it was shown that SARS-CoV-2 NSP1-mediated shutoff of host translation is important for suppression of the IFN response.

5.2 Antagonism of IFN induction by MAYV

Given that the IFN response is critical for controlling viral infection, viruses have evolved strategies to evade and suppress this response to infect mammalian cells (reviewed in (Garcia-Sastre 2017)). The IFN response is also critical for controlling alphavirus infections, including MAYV (Figueiredo et al., 2019; Gardner et al., 2010; Schilte et al., 2010; Couderc et al., 2008; Lane et al., 2018; Fros et al., 2010; Reynaud et al., 2015). While substantial research has focused

on how alphavirus suppress the signaling arm of the IFN response (Fros et al., 2010; Fros et al., 2013; Goertz et al., 2018), comparatively little is known on how these viruses suppress the induction arm of the IFN responses.

5.2.1 Interaction between MAYV and the IFN induction pathway

My data showed that pre-treatment of cells with type I IFNs significantly impairs MAYV replication which is in agreement with previous studies on other alphaviruses (Fros et al., 2010; Reynaud et al., 2015; Lane et al., 2018). I also observed that induction of *Ifnb* transcripts in MAYV-infected cells was delayed and suppressed compared to cells infected with another RNA virus, SeV. Earlier studies showed that multiple alphaviruses including CHIKV, SINV, RRV, Easter Equine Encephalitis virus, and Venezuelan Equine Encephalitis virus also suppressed IFN induction during infection (Assi et al., 2015; Burke et al., 2009; Schilte et al., 2010). It is worth noting that while MAYV activated the IFN induction later during infection, these IFNs will have little impact on MAYV infected cells since alphaviruses are known to suppress ISG induction (Fros et al., 2010; Fros et al., 2013; Goertz et al., 2018).

Our team was the first to assess how IFN induction was affected in alphavirus-infected that were challenged with potent IFN inducers such as poly(I:C) treatment or SeV infection. We observed that MAYV actively suppresses the transcription of type I IFN genes and secretion of IFN. Lack of IFN secretion during alphavirus infection was reported earlier but these studies suggest that this effect is cell type-dependent. Specifically, it was only observed in fibroblasts and epithelial cells but not in monocytes (Burke et al., 2009; Akhrymuk et al., 2018; Bhalla et al., 2019). Type I IFN secretion in immune cells is reportedly IRF7-dependent and MAVS-independent (Webster et al., 2018; Bhalla et al., 2019). Therefore, induction of type I IFNs in

innate immune cells is likely mediated by TLR7/8, which signals through MyD88 (Kawai and Akira 2009). It will be of interest to systematically study the interaction between MAYV and the IFN induction pathway in their *in vivo* target cells such as synovial fibroblasts, monocytes, and macrophages.

The observation that MAYV does not block SeV-induced nuclear translocation of IRF3 suggest that the virus blocks the IFN induction downstream of this step. Similarly, SFV which blocks IFN induction, does not affect nuclear translocation of IRF3 and NFκB (Breakwell et al., 2007). This leaves transcription and translation of IFNs as the steps that could be affected by MAYV and SFV. Since *Ifnb* and *Ifnl2* levels are lower in MAYV-infected cells, it is reasonable to assume that the virus interferes with the transcription of IFN genes.

5.2.2 Suppression of IFN induction and host transcription by MAYV NSP2

Several studies have implicated alphavirus NSP2 proteins as important suppressors of the IFN response (Bae et al., 2019; Akhrymuk et al., 2019; Breakwell et al., 2007; Goertz et al., 2018; Fros et al., 2010; Fros et al., 2013). Similarly, we found that expression of MAYV NSP2 in the absence of other viral proteins was sufficient to block IFN induction (Ishida et al, 2021). Of note, a study by Bae et al. found that CHIKV envelope protein also suppresses IFN induction in addition to NSP2 (Bae et al., 2019), but this was not the case with our MAYV envelope protein expression constructs. This discrepancy may be due to the differences between MAYV and CHIKV envelope proteins and/or the fact that our viral protein constructs are made of *bona fide* sequences rather than the codon-optimized ones used by Bae et al. It is also worth noting that the transmembrane protein (TF; transframe protein) of SINV has been reported to compromise the IFN response

(Rogers et al., 2020). However, this ribosomal frameshift product of MAYV was not included in our assays.

Expression of MAYV NSP2 blocks IFN induction but does not prevent IRF3 nuclear translocation, a result that mirrored what occurs during MAYV infection. Based on these observations, NSP2 likely affects one or more steps downstream of IRF nuclear translocation such as transcription, nuclear export of transcripts, and/or translation of IFNs. Indeed, IFN induction was less affected by a transcriptional shutoff mutant of NSP2 ($NSP2^{P722S}$). These observations are consistent with other reports that found that shutoff of host transcription by alphavirus NSP2 is necessary for suppressing the host IFN response (Frolova et al., 2002; Gorchakov et al., 2005; Fros et al., 2013; Akhrymuk et al., 2019). Of note, $NSP2^{P722S}$ suppressed IFN induction significantly, but not as efficiently as wild-type NSP2, suggesting a transcriptional shutoff-independent mechanism of IFN antagonism. While a few studies reported that alphavirus NSP2 proteins interfere with host translation (Frolova et al., 2002; Bhalla et al., 2016), others suggest that this effect is due to sequestration of translational machinery by viral RNA (Sanz et al., 2015; Carrasco et al., 2018). Although results from my thesis work showed that MAYV completely blocked the translation and/or secretion of IFNs (Ishida et al., 2021), future studies are required to determine exactly how this occurs.

NSP2 proteins of Old World alphaviruses impede host transcription by depleting Rpb1, a component of RNA polymerase II, through proteasomal degradation (Akhrymuk et al., 2012). Our analyses found that MAYV NSP2 binds and depletes not only Rpb1 (Ishida et al., 2021), but also TFIIE2, which is required for initiating RNA polymerase II-mediated transcription (Vannini and Cramer 2012). Interestingly, while the transcriptional shutoff mutant $NSP2^{P722S}$ binds Rpb1, it did not form a stable complex with TFIIE2, suggesting that the interaction between NSP2 and TFIIE2

is important for transcriptional shutoff. Of note, while NSP2 must translocate to the nucleus to deplete Rpb1, the NLS of NSP2 is dispensable for depleting TFIIE2. Therefore, unlike Rpb1, the interaction between NSP2 and TFIIE2 may occur in both the cytoplasm and the nucleus.

MAYV infection or expression of NSP2 alone reduced expression of levels of Rpb1 and TFIIE2. Moreover, we found that the degradation of Rpb1 during MAYV infection was dependent on the proteasome (Ishida et al., 2021) which is consistent with an earlier study (Akhrymuk et al., 2012). However, I was unable to discern how MAYV infection results in depletion of TFIIE2 as neither proteasomal nor lysosomal inhibitors rescued levels of this host protein. Furthermore, it is unlikely that TFIIE2 is cleaved by the protease activity of NSP2 since the protease-dead NSP2^{C478A} suppressed IFN induction as efficiently as wildtype NSP2. It should also be noted that TFIIE2 lacks the cleavage site that is normally targeted by alphavirus NSP2 (Saisawang et al., 2015).

Rpb1 is also depleted during infection by other alphaviruses such as SFV and SINV (Akhrymuk et al., 2012). Interestingly, while I observed that levels of TFIIE2 were lower in MAYV- and SFV-infected cells, SINV infection did not result in loss of this host protein. Thus, while NSP2-mediated depletion of Rpb1 appears to be ubiquitous during alphavirus infection, this is not the case for TFIIE2. A comprehensive pan-alphavirus study is required to understand the difference in host transcriptional shutoff strategies used by different alphaviruses.

In summary, our study demonstrated that the induction arm of the IFN response is strongly suppressed by MAYV, a process that is mediated largely by NSP2. Transcriptional shutoff plays an integral role in suppressing the IFN induction pathway, and the viral NSP2 mediates this by depleting key host transcription mediators, namely Rpb1 and TFIIE2. Given that this emerging alphavirus has the potential to cause large outbreaks similar to CHIKV (Hotez and Murray 2017; Brustolin et al., 2018; Wiggins et al., 2018), there is considerable interest in developing therapeutic

and prophylactic therapies against MAYV (Langendries et al., 2021; Powers et al., 2021; Hoque et al., 2021; Rafael et al., 2020; Campos et al., 2020). The findings presented in this thesis further our understanding of the biology of MAYV and may be of help when developing therapeutics against this pathogens and potentially other alphaviruses.

5.3 Evasion of IFN response by SARS-CoV-2

In the early days of the COVID-19 pandemic, much of the studies on SARS-CoV-2 were guided by what we knew about the closely related pathogen SARS-CoV, which emerged in 2002 (Sun et al., 2020; Wu et al., 2020). The pathogenesis of SARS-CoV is closely tied to the IFN response (Cameron et al., 2007; Cameron et al., 2008; Channappanavar et al., 2016) and of note, almost half of known SARS-CoV proteins were implicated in suppressing this antiviral system (Totura and Baric 2012; Kindler et al., 2016). As such, we predicted that outcomes of SARS-CoV-2 infection are also affected by the IFN response, and that this virus employs multiple strategies to circumvent this immune response. Since many reports on SARS-CoV-2 and the IFN response have now been published, here I will compare them with findings from my thesis research.

5.3.1 Suppression of IFN induction by SARS-CoV-2

SARS-CoV, and in recent studies SARS-CoV-2, evade host antiviral defenses by multiple mechanisms. First, coronaviruses, including SARS-CoV and SARS-CoV-2, replicate their genomes in double-membrane vesicles, thereby preventing the recognition of dsRNA by PRRs (van Hemert et al., 2008; Knoops et al., 2008; Snijder et al., 2020). In addition, multiple viral proteins including NSP1, NSP3, NSP6, NSP12, NSP13, NSP14, NSP15, N, M, NS3B, P6, NS7B,

NS8B, and NS9B of SARS-CoV-2 have been reported to suppress IFN induction through different independent mechanisms (Table 5.1) (Li et al., 2020; Xia et al., 2020; Lei et al., 2020; Yuen et al., 2020; Shin et al., 2020; Jiang et al., 2020; Miorin et al., 2020; Zheng et al., 2020; Gori Savellini et al., 2021; Shemesh et al., 2021; Zhao et al., 2021; Oh and Shin 2021; Wang et al., 2021; Rashid et al., 2021). While there are many consistencies among these studies, discrepancies remain and therefore, additional studies are required to elucidate exactly how SARS-CoV-2 antagonizes the IFN induction pathway.

Table 5.1 SARS-CoV-2 proteins involved in subversion of IFN induction

Viral Protein	Mechanism	Reference
NSP1	Suppression of nuclear export of mRNA, inhibition of mRNA translation	(Banerjee et al., 2020; Lei et al., 2020; Thoms et al., 2020; Xia et al., 2020; Yuan et al., 2020; Shemesh et al., 2021; Zhang et al., 2021)
NSP3	Proteolytic cleavage of ISG15 from IRF3	(Shin et al., 2020; Lei et al., 2020)
NSP5	Unknown	(Shemesh et al., 2021)
NSP6	Binds TBK1 and prevent IRF3 phosphorylation	(Xia et al., 2020; Shemesh et al., 2021)
NSP12	Disrupts IRF3 nuclear translocation	(Lei et al., 2020; Wang et al., 2021)
NSP13	Binds TBK1 and block its phosphorylation	(Xia et al., 2020; Yuen et al., 2020; Lei et al., 2020)
NSP14	Unknown	(Yuen et al., 2020; Lei et al., 2020)
BSP15	Unknown	(Yuen et al., 2020; Shemesh et al., 2021)
N	Sequester TRIM25, preventing RIG-I activation	(Li et al., 2020; Gori Savellini et al., 2021; Oh and Shin 2021; Zhao et al., 2021)
M	Binds RIG-I, MDA5, and TBK1 and prevent activation of IRF3	(Lei et al., 2020; Zheng et al., 2020)
NS3B	Unknown	(Konno et al., 2020)
P6	Binds Rae1-Nup98 complex and disrupts IRF3 nuclear transport	(Lei et al., 2020; Li et al., 2020; Miorin et al., 2020; Xia et al., 2020; Yuen et al., 2020; Addetia et al., 2021; Shemesh et al., 2021)
NS7B	Unknown	(Shemesh et al., 2021)
NS8B	Unknown	(Li et al., 2020)
NS9B	Sequester TOM70, impeding MAVS-mediated IFN induction	(Jiang et al., 2020)

There is a growing consensus among studies that SARS-CoV-2 is a poor inducer of IFNs and ISGs during infection, as observed in cell culture, animal models, and in patients (Neufeldt et al., 2020; Israelow et al., 2020; Hadjadj et al., 2020; Blanco-Melo et al., 2020; Vanderheiden et al., 2020b; Miorin et al., 2020). Our team's findings are consistent with these studies as we found very little induction of IFNs during SARS-CoV-2 infection. Moreover, we found that SARS-CoV-2 infection is sensitive to pre-treatment with IFN-inducing stimuli, but resistant to the same stimuli once infection has been established. Similarly, several studies have indicated that SARS-CoV-2 is very sensitive to IFN pre-treatment, while resistant to post-infection treatment with IFNs (Mantlo et al., 2020; Felgenhauer et al., 2020; Miorin et al., 2020; Vanderheiden et al., 2020b; Lokugamage et al., 2020). Using SeV and poly(I:C) as IFN agonists, we confirmed that SARS-CoV-2 impairs the induction of IFNs during infection in part by inhibiting phosphorylation and nuclear translocation of IRF3.

In our studies, only NSP1 and N proteins were found to significantly block the IFN response, far fewer than what has been reported by other groups (Li et al., 2020; Xia et al., 2020; Lei et al., 2020; Yuen et al., 2020; Shin et al., 2020; Jiang et al., 2020; Zheng et al., 2020; Shemesh et al., 2021; Wang et al., 2021; Rashid et al., 2021). Some of these discrepancies may be explained by the differences in protein expression constructs employed. Our study used original SARS-CoV-2 protein-encoding sequences to create the expression constructs, in contrast to the codon-optimized viral protein constructs used in most other studies. The expression level of codon-optimized viral protein constructs was higher than that observed from our constructs and likely *bona fide* viral protein levels during viral infection. Specifically, our NSP3, NSP6, NSP12, NSP13, and NSP14 constructs expressed poorly compared to other studies that found these proteins suppress the induction of IFNs (Yuen et al., 2020; Lei et al., 2020; Shin et al., 2020; Xia et al.,

2020; Shemesh et al., 2021). Furthermore, proteins expressed from codon-optimized plasmids may have altered conformations since the expedited translation alters the kinetics of protein folding (Liu 2020). On the other hand, by not optimizing codon usage in our expression constructs, we may have limited the expression of certain SARS-CoV-2 proteins, especially for ones with cryptic splice sites. Indeed, Hosseini *et al.* have found cryptic splice sites in SARS-CoV-2 NSP3, 12, 13, and 14 (Hosseini Rad Sm and McLellan 2020), which were poorly expressed in our hands. Nevertheless, further investigations are required to determine whether proteins from codon-optimized constructs truly play a role in suppressing IFN induction during SARS-CoV-2 infection. Another variable that may have affected the outcomes of these studies is the type, size, and location of epitope tags that were used to label the viral proteins. For instance, the C-terminal region of SARS-CoV-2 P6 is important for binding Nup98-Rae1 complex which is necessary for blocking the bidirectional nucleocytoplasmic transport of molecules including IRF3 and STAT1/2 (Miorin et al., 2020; Xia et al., 2020; Addetia et al., 2021). We may have prevented this interaction by attaching a 3xFLAG tag to the C-terminus of our P6 construct, therefore compromising P6-mediated inhibition of IFN response.

My findings indicate that SARS-CoV-2 NSP1 blocks IFN induction via a mechanism that is dependent on host translational shutoff. NSP1 proteins of coronaviruses have been reported to suppress host translation through a number of different mechanisms. NSP1 of SARS-CoV and MERS-CoV target host mRNA for degradation by an as yet unknown mechanism, while sparing viral transcripts from the same fate (Narayanan et al., 2008; Huang et al., 2011; Lokugamage et al., 2015). NSP1 of SARS-CoV and SARS-CoV-2 can also disrupt nuclear translocation of host mRNAs by sequestering Nup93, which is normally found at the nuclear pore complex (Gomez et al., 2019; Zhang et al., 2021). Lastly, NSP1 of SARS-CoV and SARS-CoV-2 directly binds to 40S

ribosomal subunit, preventing host translation while allowing translation of leader sequence-containing viral transcripts (Kamitani et al., 2006; Narayanan et al., 2008; Kamitani et al., 2009; Thoms et al., 2020; Banerjee et al., 2020; Yuan et al., 2020; Schubert et al., 2020). Here, we found that SARS-CoV-2 NSP1 prevents nuclear translocation of IRF3 in response to IFN inducers such as SeV by blocking phosphorylation of IRF3. A translational shutoff mutant NSP1^{KH164AA} did not inhibit nuclear translocation of IRF3 or IFN induction. The NSP1-mediated block in translation may result in rapid depletion of labile factors that are required for IRF3 phosphorylation but it is also important to consider the possibility that mutations that affect the translational shutoff ability of NSP1 could alter other functions of this protein. Indeed, Jauregui et al. found that most mutations in SARS-CoV NSP1 resulted in altering more than one of its functions (Jauregui et al., 2013). As such, understanding how NSP1 hinders nuclear translocation of IRF3 requires further investigations.

Unfortunately, we were unable to pinpoint the precise mechanism by which SARS-CoV-2 N antagonized IFN induction. While we showed that N protein stably interacted with TRIM25, unlike SARS-CoV N protein which disrupts activation of RIG-I by sequestering TRIM25 (Hu et al., 2017), N protein of SARS-CoV-2 did not affect ubiquitination of RIG-I in our hands. Of note, two recent studies showed that the SARS-CoV-2 N protein also suppressed RIG-I activation by sequestering TRIM25 (Gori Savellini et al., 2021; Oh and Shin 2021). Yet another group reported that low concentrations of N of SARS-CoV and SARS-CoV-2 inhibits of IFN induction by sequestering TRIM25, when present at higher levels, N protein accentuates the IFN response resulting in the production of proinflammatory cytokines (Zhao et al., 2021).

5.3.2 Suppression of IFN signaling by SARS-CoV-2

Thus far NSP1, NSP3, NSP6, NSP7, NSP13, NSP14, N, M, S, NS3A, P6, NS7A, NS7B, and NS8B of SARS-CoV-2 have been reported to impede IFN signaling (Table 5.2) (Li et al., 2020; Yuen et al., 2020; Lei et al., 2020; Xia et al., 2020; Miorin et al., 2020; Mu et al., 2020a). As with reports of how the virus affect the induction arm of the IFN pathway, many of these reports are inconsistent with each other, hence further studies are required to learn more about how SARS-CoV-2 affect expression of ISGs.

Table 5.2 SARS-CoV-2 proteins reported to antagonize IFN signaling

Viral Protein	Mechanism	Reference
NSP1	Suppression of nuclear export of mRNA, inhibition of mRNA translation, disruption of STAT1 phosphorylation	(Banerjee et al., 2020; Lei et al., 2020; Thoms et al., 2020; Xia et al., 2020; Yuan et al., 2020; Zhang et al., 2021)
NSP3	Unknown	(Lei et al., 2020)
NSP6	Suppression of STAT1/2 phosphorylation	(Xia et al., 2020)
NSP7	Unknown	(Xia et al., 2020)
NSP13	Suppression of STAT1/2 phosphorylation	(Lei et al., 2020; Xia et al., 2020)
NSP14	Unknown	(Lei et al., 2020)
N	Suppression of STAT1/2 phosphorylation	(Lei et al., 2020; Mu et al., 2020a)
M	Suppression of STAT1 phosphorylation	(Xia et al., 2020)
S	Unknown	(Lei et al., 2020)
NS3A	Suppression of STAT1 phosphorylation	(Xia et al., 2020)
P6	Binds Rae1-Nup98 complex and disrupts STAT1/2 nuclear transport	(Lei et al., 2020; Li et al., 2020; Miorin et al., 2020; Xia et al., 2020; Yuen et al., 2020; Addetia et al., 2021; Shemesh et al., 2021)
NS7A	Suppression of STAT2 phosphorylation	(Xia et al., 2020)

NS7B	Suppression of STAT1/2 phosphorylation	(Xia et al., 2020)
NS8B	Unknown	(Lei et al., 2020)

Consistent with other reports (Neufeldt et al., 2020; Israelow et al., 2020; Hadjadj et al., 2020; Blanco-Melo et al., 2020; Vanderheiden et al., 2020b; Miorin et al., 2020), we observed little to no induction of ISGs during SARS-CoV-2 infection, suggesting that the virus actively blocks IFN signaling. This was further corroborated by our observation that SARS-CoV-2 is resistant to treatment with type I, II, and III IFNs once the virus has established infection. Nevertheless, the virus is sensitive to pre-treatment of cells with type I and III IFNs, thus indicating that SARS-CoV-2 replication is inhibited by ISGs. Interestingly, SARS-CoV-2 infection does not block ISG induction by IFN-ɣ, but is resistant to ISGs induced by this type of IFN (Kumar, Ishida, et al., 2021), suggesting the virus does not need to suppress type II ISG induction in non-immune cell lines. In the course of my studies, I observed significant loss of Tyk2 and STAT2 during SARS-CoV-2 infection which could explain how the virus affects type I and III IFN signaling. Furthermore, the depletion of Tyk2 could explain the decreased STAT-phosphorylation in SARS-CoV-2 infected which was observed by others (Miorin et al., 2020; Xia et al., 2020; Yang et al., 2020).

In our hands, NSP1 was the only viral protein that significantly blocked IFN signaling (Kumar et al, 2021). Again, other reports suggest that there are more SARS-CoV-2 proteins that antagonize this pathway (Li et al., 2020; Yuen et al., 2020; Lei et al., 2020; Xia et al., 2020; Miorin et al., 2020; Mu et al., 2020a), but the above-mentioned variables, such as codon-optimization and the size/location of the epitope tag may explain these discrepancies. One of the SARS-CoV-2 proteins that is consistently reported to suppress ISG induction is accessory protein P6, which

binds to Nup98-Rae1 complex and blocks the nuclear translocation of STAT1/2 (Miorin et al., 2020; Xia et al., 2020; Addetia et al., 2021). While several other SARS-CoV-2 proteins are reported to antagonize induction of ISGs, the mechanism by which they suppress this pathway requires further investigation.

The NSP1 of SARS-CoV and SARS-CoV-2 have been consistently reported as potent antagonist of ISG induction by blocking the phosphorylation of STAT1 and shutting down host translation (Kamitani et al., 2006; Wathelet et al., 2007; Kamitani et al., 2009; Huang et al., 2011; Banerjee et al., 2020; Lei et al., 2020; Thoms et al., 2020; Xia et al., 2020). Similarly, we observed that SARS-CoV-2 NSP1 effectively impairs IFN signaling through translational shutoff. By impeding host translation, SARS-CoV-2 infected cells will produce less IFNs and ISGs. In addition, translational shutoff will result in the depletion of proteins with shorter half-lives such as Tyk2 and STAT2, thereby further impairing the IFN signaling pathway.

Overall, the present study with others shows that SARS-CoV-2 effectively suppresses the IFN response during infection. Several SARS-CoV-2 proteins are reported to be involved in suppressing the induction of IFNs and ISGs, including NSP1 and N which we described here. These findings should be taken into account when considering therapeutic options against SARS-CoV-2 and in the event of future coronavirus outbreaks. Lastly, given the rise of SARS-CoV-2 VOCs (Khateeb et al., 2021; Bano et al., 2021; Kumar, Singh, et al., 2021), it will of interest to study their interactions with the IFN system, since new strategies to antagonize this response may alter our treatment options against these variants.

References

Acharya, D., Liu, G., and Gack, M.U. 2020. Dysregulation of type I interferon responses in COVID-19. Nat Rev Immunol 20 (7): 397-398. doi: 10.1038/s41577-020-0346-x.

Addetia, A., Lieberman, N.A.P., Phung, Q., Hsiang, T.Y., Xie, H., Roychoudhury, P., Shrestha, L., Loprieno, M.A., Huang, M.L., Gale, M., Jr., Jerome, K.R., and Greninger, A.L. 2021. SARS-CoV-2 ORF6 Disrupts Bidirectional Nucleocytoplasmic Transport through Interactions with Rae1 and Nup98. mBio 12 (2). doi: 10.1128/mBio.00065-21.

Akhrymuk, I., Frolov, I., and Frolova, E.I. 2016. Both RIG-I and MDA5 detect alphavirus replication in concentration-dependent mode. Virology 487: 230-41. doi: 10.1016/j.virol.2015.09.023.

Akhrymuk, I., Frolov, I., and Frolova, E.I. 2018. Sindbis Virus Infection Causes Cell Death by nsP2-Induced Transcriptional Shutoff or by nsP3-Dependent Translational Shutoff. J Virol 92 (23). doi: 10.1128/JVI.01388-18.

Akhrymuk, I., Kulemzin, S.V., and Frolova, E.I. 2012. Evasion of the innate immune response: the Old World alphavirus nsP2 protein induces rapid degradation of Rpb1, a catalytic subunit of RNA polymerase II. J Virol 86 (13): 7180-91. doi: 10.1128/JVI.00541-12.

Akhrymuk, I., Lukash, T., Frolov, I., and Frolova, E.I. 2019. Novel Mutations in nsP2 Abolish Chikungunya Virus-Induced Transcriptional Shutoff and Make the Virus Less Cytopathic without Affecting Its Replication Rates. J Virol 93 (4). doi: 10.1128/JVI.02062-18.

Alavi Darazam, I., Shokouhi, S., Pourhoseingholi, M.A., Naghibi Irvani, S.S., Mokhtari, M., Shabani, M., Amirdosara, M., Torabinavid, P., Golmohammadi, M., Hashemi, S., Azimi, A., Jafarazadeh Maivan, M.H., Rezaei, O., Zali, A., Hajiesmaeili, M., Shabanpour Dehbsneh, H., Hoseyni Kusha, A., Taleb Shoushtari, M., Khalili, N., Soleymaninia, A., Gachkar, L., and Khoshkar, A. 2021. Role of interferon therapy in severe COVID-19: the COVIFERON randomized controlled trial. Sci Rep 11 (1): 8059. doi: 10.1038/s41598-021-86859-y.

Anderson, R.M., Fraser, C., Ghani, A.C., Donnelly, C.A., Riley, S., Ferguson, N.M., Leung, G.M., Lam, T.H., and Hedley, A.J. 2004. Epidemiology, transmission dynamics and control of SARS: the 2002-2003 epidemic. Philos Trans R Soc Lond B Biol Sci 359 (1447): 1091-105. doi: 10.1098/rstb.2004.1490.

Assi, M., Thon-Hon, V.G., Jaffar-Bandjee, M.C., Martinez, A., and Gasque, P. 2015. Regulation of type I-interferon responses in the human epidermal melanocyte cell line SKMEL infected by the Ross River alphavirus. Cytokine 76 (2): 572-576. doi: 10.1016/j.cyto.2015.07.003.

Auguste, A.J., Liria, J., Forrester, N.L., Giambalvo, D., Moncada, M., Long, K.C., Moron, D., de Manzione, N., Tesh, R.B., Halsey, E.S., Kochel, T.J., Hernandez, R., Navarro, J.C., and Weaver, S.C. 2015. Evolutionary and Ecological Characterization of Mayaro Virus

Strains Isolated during an Outbreak, Venezuela, 2010. Emerg Infect Dis 21 (10): 1742-50. doi: 10.3201/eid2110.141660.

Bae, S., Lee, J.Y., and Myoung, J. 2019. Chikungunya Virus-Encoded nsP2, E2 and E1 Strongly Antagonize the Interferon-beta Signaling Pathway. J Microbiol Biotechnol 29 (11): 1852-1859. doi: 10.4014/jmb.1910.10014.

Banerjee, A.K., Blanco, M.R., Bruce, E.A., Honson, D.D., Chen, L.M., Chow, A., Bhat, P., Ollikainen, N., Quinodoz, S.A., Loney, C., Thai, J., Miller, Z.D., Lin, A.E., Schmidt, M.M., Stewart, D.G., Goldfarb, D., De Lorenzo, G., Rihn, S.J., Voorhees, R.M., Botten, J.W., Majumdar, D., and Guttman, M. 2020. SARS-CoV-2 Disrupts Splicing, Translation, and Protein Trafficking to Suppress Host Defenses. Cell 183 (5): 1325-1339 e21. doi: 10.1016/j.cell.2020.10.004.

Bano, I., Sharif, M., and Alam, S. 2021. Genetic drift in the genome of SARS COV-2 and its global health concern. J Med Virol. doi: 10.1002/jmv.27337.

Bastard, P., Gervais, A., Le Voyer, T., Rosain, J., Philippot, Q., Manry, J., Michailidis, E., Hoffmann, H.H., Eto, S., Garcia-Prat, M., Bizien, L., Parra-Martinez, A., Yang, R., Haljasmagi, L., Migaud, M., Sarekannu, K., Maslovskaja, J., de Prost, N., Tandjaoui-Lambiotte, Y., Luyt, C.E., Amador-Borrero, B., Gaudet, A., Poissy, J., Morel, P., Richard, P., Cognasse, F., Troya, J., Trouillet-Assant, S., Belot, A., Saker, K., Garcon, P., Riviere, J.G., Lagier, J.C., Gentile, S., Rosen, L.B., Shaw, E., Morio, T., Tanaka, J., Dalmau, D., Tharaux, P.L., Sene, D., Stepanian, A., Megarbane, B., Triantafyllia, V., Fekkar, A., Heath, J.R., Franco, J.L., Anaya, J.M., Sole-Violan, J., Imberti, L., Biondi, A., Bonfanti, P., Castagnoli, R., Delmonte, O.M., Zhang, Y., Snow, A.L., Holland, S.M., Biggs, C., Moncada-Velez, M., Arias, A.A., Lorenzo, L., Boucherit, S., Coulibaly, B., Anglicheau, D., Planas, A.M., Haerynck, F., Duvlis, S., Nussbaum, R.L., Ozcelik, T., Keles, S., Bousfiha, A.A., El Bakkouri, J., Ramirez-Santana, C., Paul, S., Pan-Hammarstrom, Q., Hammarstrom, L., Dupont, A., Kurolap, A., Metz, C.N., Aiuti, A., Casari, G., Lampasona, V., Ciceri, F., Barreiros, L.A., Dominguez-Garrido, E., Vidigal, M., Zatz, M., van de Beek, D., Sahanic, S., Tancevski, I., Stepanovskyy, Y., Boyarchuk, O., Nukui, Y., Tsumura, M., Vidaur, L., Tangye, S.G., Burrel, S., Duffy, D., Quintana-Murci, L., Klocperk, A., Kann, N.Y., Shcherbina, A., Lau, Y.L., Leung, D., Coulongeat, M., Marlet, J., Koning, R., Reyes, L.F., Chauvineau-Grenier, A., Venet, F., Monneret, G., Nussenzweig, M.C., Arrestier, R., Boudhabhay, I., Baris-Feldman, H., Hagin, D., Wauters, J., Meyts, I., Dyer, A.H., Kennelly, S.P., Bourke, N.M., Halwani, R., Sharif-Askari, N.S., Dorgham, K., Sallette, J., Sedkaoui, S.M., AlKhater, S., Rigo-Bonnin, R., Morandeira, F., Roussel, L., Vinh, D.C., Ostrowski, S.R., Condino-Neto, A., Prando, C., Bonradenko, A., Spaan, A.N., Gilardin, L., Fellay, J., Lyonnet, S., Bilguvar, K., Lifton, R.P., Mane, S., Lab, H., Clinicians, C., Clinicians, C.-S., Group, N.I.R.t.C., Group, N.-C.S., Danish, C., Danish Blood Donor, S., St. James's, H., group, S.C.I., French, C.C.S.G., Imagine, C.-G., Milieu Interieur, C., Co, V.C.C., Amsterdam, U.M.C.C., Biobank, I., Effort, C.H.G., cohort, C., Study, C.D., Cerba, H.-C., Etablissement du Sang study, g., Anderson, M.S., Boisson, B., Beziat, V., Zhang, S.Y., Vandreakos, E., Hermine, O., Pujol, A., Peterson, P., Mogensen, T.H., Rowen, L., Mond, J., Debette, S., de Lamballerie, X., Duval, X., Mentre, F., Zins, M., Soler-Palacin, P., Colobran, R.,

Gorochov, G., Solanich, X., Susen, S., Martinez-Picado, J., Raoult, D., Vasse, M., Gregersen, P.K., Piemonti, L., Rodriguez-Gallego, C., Notarangelo, L.D., Su, H.C., Kisand, K., Okada, S., Puel, A., Jouanguy, E., Rice, C.M., Tiberghien, P., Zhang, Q., Cobat, A., Abel, L., and Casanova, J.L. 2021. Autoantibodies neutralizing type I IFNs are present in ~4% of uninfected individuals over 70 years old and account for ~20% of COVID-19 deaths. Sci Immunol 6 (62). doi: 10.1126/sciimmunol.abl4340.

Bastard, P., Rosen, L.B., Zhang, Q., Michailidis, E., Hoffmann, H.H., Zhang, Y., Dorgham, K., Philippot, Q., Rosain, J., Beziat, V., Manry, J., Shaw, E., Haljasmagi, L., Peterson, P., Lorenzo, L., Bizien, L., Trouillet-Assant, S., Dobbs, K., de Jesus, A.A., Belot, A., Kallaste, A., Catherinot, E., Tandjaoui-Lambiotte, Y., Le Pen, J., Kerner, G., Bigio, B., Seeleuthner, Y., Yang, R., Bolze, A., Spaan, A.N., Delmonte, O.M., Abers, M.S., Aiuti, A., Casari, G., Lampasona, V., Piemonti, L., Ciceri, F., Bilguvar, K., Lifton, R.P., Vasse, M., Smadja, D.M., Migaud, M., Hadjadj, J., Terrier, B., Duffy, D., Quintana-Murci, L., van de Beek, D., Roussel, L., Vinh, D.C., Tangye, S.G., Haerynck, F., Dalmau, D., Martinez-Picado, J., Brodin, P., Nussenzweig, M.C., Boisson-Dupuis, S., Rodriguez-Gallego, C., Vogt, G., Mogensen, T.H., Oler, A.J., Gu, J., Burbelo, P.D., Cohen, J.I., Biondi, A., Bettini, L.R., D'Angio, M., Bonfanti, P., Rossignol, P., Mayaux, J., Rieux-Laucat, F., Husebye, E.S., Fusco, F., Ursini, M.V., Imberti, L., Sottini, A., Paghera, S., Quiros-Roldan, E., Rossi, C., Castagnoli, R., Montagna, D., Licari, A., Marseglia, G.L., Duval, X., Ghosn, J., Lab, H., Group, N.-U.I.R.t.C., Clinicians, C., Clinicians, C.-S., Imagine, C.G., French, C.C.S.G., Milieu Interieur, C., Co, V.C.C., Amsterdam, U.M.C.C.-B., Effort, C.H.G., Tsang, J.S., Goldbach-Mansky, R., Kisand, K., Lionakis, M.S., Puel, A., Zhang, S.Y., Holland, S.M., Gorochov, G., Jouanguy, E., Rice, C.M., Cobat, A., Notarangelo, L.D., Abel, L., Su, H.C., and Casanova, J.L. 2020. Autoantibodies against type I IFNs in patients with life-threatening COVID-19. Science 370 (6515). doi: 10.1126/science.abd4585.

Bhalla, N., Gardner, C.L., Downs, S.N., Dunn, M., Sun, C., and Klimstra, W.B. 2019. Macromolecular Synthesis Shutoff Resistance by Myeloid Cells Is Critical to IRF7-Dependent Systemic Interferon Alpha/Beta Induction after Alphavirus Infection. J Virol 93 (24). doi: 10.1128/JVI.00872-19.

Bhalla, N., Sun, C., Metthew Lam, L.K., Gardner, C.L., Ryman, K.D., and Klimstra, W.B. 2016. Host translation shutoff mediated by non-structural protein 2 is a critical factor in the antiviral state resistance of Venezuelan equine encephalitis virus. Virology 496: 147-165. doi: 10.1016/j.virol.2016.06.005.

Blanco-Melo, D., Nilsson-Payant, B.E., Liu, W.C., Uhl, S., Hoagland, D., Moller, R., Jordan, T.X., Oishi, K., Panis, M., Sachs, D., Wang, T.T., Schwartz, R.E., Lim, J.K., Albrecht, R.A., and tenOever, B.R. 2020. Imbalanced Host Response to SARS-CoV-2 Drives Development of COVID-19. Cell 181 (5): 1036-1045 e9. doi: 10.1016/j.cell.2020.04.026.

Bogdan, C., and Schleicher, U. 2006. Production of interferon-gamma by myeloid cells--fact or fancy? Trends Immunol 27 (6): 282-90. doi: 10.1016/j.it.2006.04.004.

Bolen, C.R., Ding, S., Robek, M.D., and Kleinstein, S.H. 2014. Dynamic expression profiling of type I and type III interferon-stimulated hepatocytes reveals a stable hierarchy of gene expression. Hepatology 59 (4): 1262-72. doi: 10.1002/hep.26657.

Breakwell, L., Dosenovic, P., Karlsson Hedestam, G.B., D'Amato, M., Liljestrom, P., Fazakerley, J., and McInerney, G.M. 2007. Semliki Forest virus nonstructural protein 2 is involved in suppression of the type I interferon response. J Virol 81 (16): 8677-84. doi: 10.1128/JVI.02411-06.

Brisse, M., and Ly, H. 2019. Comparative Structure and Function Analysis of the RIG-I-Like Receptors: RIG-I and MDA5. Front Immunol 10: 1586. doi: 10.3389/fimmu.2019.01586.

Brustolin, M., Pujhari, S., Henderson, C.A., and Rasgon, J.L. 2018. Anopheles mosquitoes may drive invasion and transmission of Mayaro virus across geographically diverse regions. PLoS Negl Trop Dis 12 (11): e0006895. doi: 10.1371/journal.pntd.0006895.

Buitrago-Garcia, D., Egli-Gany, D., Counotte, M.J., Hossmann, S., Imeri, H., Ipekci, A.M., Salanti, G., and Low, N. 2020. Occurrence and transmission potential of asymptomatic and presymptomatic SARS-CoV-2 infections: A living systematic review and meta-analysis. PLoS Med 17 (9): e1003346. doi: 10.1371/journal.pmed.1003346.

Burke, C.W., Gardner, C.L., Steffan, J.J., Ryman, K.D., and Klimstra, W.B. 2009. Characteristics of alpha/beta interferon induction after infection of murine fibroblasts with wild-type and mutant alphaviruses. Virology 395 (1): 121-32. doi: 10.1016/j.virol.2009.08.039.

Cameron, M.J., Bermejo-Martin, J.F., Danesh, A., Muller, M.P., and Kelvin, D.J. 2008. Human immunopathogenesis of severe acute respiratory syndrome (SARS). Virus Res 133 (1): 13-9. doi: 10.1016/j.virusres.2007.02.014.

Cameron, M.J., Ran, L., Xu, L., Danesh, A., Bermejo-Martin, J.F., Cameron, C.M., Muller, M.P., Gold, W.L., Richardson, S.E., Poutanen, S.M., Willey, B.M., DeVries, M.E., Fang, Y., Seneviratne, C., Bosinger, S.E., Persad, D., Wilkinson, P., Greller, L.D., Somogyi, R., Humar, A., Keshavjee, S., Louie, M., Loeb, M.B., Brunton, J., McGeer, A.J., Canadian, S.R.N., and Kelvin, D.J. 2007. Interferon-mediated immunopathological events are associated with atypical innate and adaptive immune responses in patients with severe acute respiratory syndrome. J Virol 81 (16): 8692-706. doi: 10.1128/JVI.00527-07.

Campos, D., Navarro, S., Llamas-Gonzalez, Y.Y., Sugasti, M., and Gonzalez-Santamaria, J. 2020. Broad Antiviral Activity of Ginkgolic Acid against Chikungunya, Mayaro, Una, and Zika Viruses. Viruses 12 (4). doi: 10.3390/v12040449.

Cao-Lormeau, V.M., and Musso, D. 2014. Emerging arboviruses in the Pacific. Lancet 384 (9954): 1571-2. doi: 10.1016/S0140-6736(14)61977-2.

Carfi, A., Bernabei, R., Landi, F., and Gemelli Against, C.-P.-A.C.S.G. 2020. Persistent Symptoms in Patients After Acute COVID-19. JAMA 324 (6): 603-605. doi: 10.1001/jama.2020.12603.

Carrasco, L., Sanz, M.A., and Gonzalez-Almela, E. 2018. The Regulation of Translation in Alphavirus-Infected Cells. Viruses 10 (2). doi: 10.3390/v10020070.

Carrasco-Hernandez, R., Jacome, R., Lopez Vidal, Y., and Ponce de Leon, S. 2017. Are RNA Viruses Candidate Agents for the Next Global Pandemic? A Review. ILAR J 58 (3): 343-358. doi: 10.1093/ilar/ilx026.

Carvalho, C.A.M., Silva, J.L., Oliveira, A.C., and Gomes, A.M.O. 2017. On the entry of an emerging arbovirus into host cells: Mayaro virus takes the highway to the cytoplasm through fusion with early endosomes and caveolae-derived vesicles. PeerJ 5: e3245. doi: 10.7717/peerj.3245.

Casadevall, A., Weiss, S.R., and Imperiale, M.J. 2021. Can Science Help Resolve the Controversy on the Origins of the SARS-CoV-2 Pandemic? mBio 12 (4): e0194821. doi: 10.1128/mBio.01948-21.

Casals, J., and Whitman, L. 1957. Mayaro virus: a new human disease agent. I. Relationship to other arbor viruses. Am J Trop Med Hyg 6 (6): 1004-11.

Chakrabarti, A., Jha, B.K., and Silverman, R.H. 2011. New insights into the role of RNase L in innate immunity. J Interferon Cytokine Res 31 (1): 49-57. doi: 10.1089/jir.2010.0120.

Channappanavar, R., Fehr, A.R., Vijay, R., Mack, M., Zhao, J., Meyerholz, D.K., and Perlman, S. 2016. Dysregulated Type I Interferon and Inflammatory Monocyte-Macrophage Responses Cause Lethal Pneumonia in SARS-CoV-Infected Mice. Cell Host Microbe 19 (2): 181-93. doi: 10.1016/j.chom.2016.01.007.

Chen, F., Knutson, T.P., Rossow, S., Saif, L.J., and Marthaler, D.G. 2019. Decline of transmissible gastroenteritis virus and its complex evolutionary relationship with porcine respiratory coronavirus in the United States. Sci Rep 9 (1): 3953. doi: 10.1038/s41598-019-40564-z.

Couderc, T., Chretien, F., Schilte, C., Disson, O., Brigitte, M., Guivel-Benhassine, F., Touret, Y., Barau, G., Cayet, N., Schuffenecker, I., Despres, P., Arenzana-Seisdedos, F., Michault, A., Albert, M.L., and Lecuit, M. 2008. A mouse model for Chikungunya: young age and inefficient type-I interferon signaling are risk factors for severe disease. PLoS Pathog 4 (2): e29. doi: 10.1371/journal.ppat.0040029.

Daffis, S., Szretter, K.J., Schriewer, J., Li, J., Youn, S., Errett, J., Lin, T.Y., Schneller, S., Zust, R., Dong, H., Thiel, V., Sen, G.C., Fensterl, V., Klimstra, W.B., Pierson, T.C., Buller, R.M., Gale, M., Jr., Shi, P.Y., and Diamond, M.S. 2010. 2'-O methylation of the viral mRNA cap evades host restriction by IFIT family members. Nature 468 (7322): 452-6. doi: 10.1038/nature09489.

Dar, A.C., Dever, T.E., and Sicheri, F. 2005. Higher-order substrate recognition of eIF2alpha by the RNA-dependent protein kinase PKR. Cell 122 (6): 887-900. doi: 10.1016/j.cell.2005.06.044.

Davoudi-Monfared, E., Rahmani, H., Khalili, H., Hajiabdolbaghi, M., Salehi, M., Abbasian, L., Kazemzadeh, H., and Yekaninejad, M.S. 2020. A Randomized Clinical Trial of the Efficacy and Safety of Interferon beta-1a in Treatment of Severe COVID-19. Antimicrob Agents Chemother 64 (9). doi: 10.1128/AAC.01061-20.

de Groot, R.J., Hardy, W.R., Shirako, Y., and Strauss, J.H. 1990. Cleavage-site preferences of Sindbis virus polyproteins containing the non-structural proteinase. Evidence for temporal regulation of polyprotein processing in vivo. EMBO J 9 (8): 2631-8.

de Weerd, N.A., and Nguyen, T. 2012. The interferons and their receptors--distribution and regulation. Immunol Cell Biol 90 (5): 483-91. doi: 10.1038/icb.2012.9.

Decker, T., Lew, D.J., Mirkovitch, J., and Darnell, J.E., Jr. 1991. Cytoplasmic activation of GAF, an IFN-gamma-regulated DNA-binding factor. EMBO J 10 (4): 927-32.

Denison, M.R., and Perlman, S. 1986. Translation and processing of mouse hepatitis virus virion RNA in a cell-free system. J Virol 60 (1): 12-8. doi: 10.1128/JVI.60.1.12-18.1986.

Diagne, C.T., Bengue, M., Choumet, V., Hamel, R., Pompon, J., and Misse, D. 2020. Mayaro Virus Pathogenesis and Transmission Mechanisms. Pathogens 9 (9). doi: 10.3390/pathogens9090738.

Dighe, A., Jombart, T., Van Kerkhove, M.D., and Ferguson, N. 2019. A systematic review of MERS-CoV seroprevalence and RNA prevalence in dromedary camels: Implications for animal vaccination. Epidemics 29: 100350. doi: 10.1016/j.epidem.2019.100350.

Dixit, E., Boulant, S., Zhang, Y., Lee, A.S., Odendall, C., Shum, B., Hacohen, N., Chen, Z.J., Whelan, S.P., Fransen, M., Nibert, M.L., Superti-Furga, G., and Kagan, J.C. 2010. Peroxisomes are signaling platforms for antiviral innate immunity. Cell 141 (4): 668-81. doi: 10.1016/j.cell.2010.04.018.

Dorobantu, C.M., Albulescu, L., Harak, C., Feng, Q., van Kampen, M., Strating, J.R., Gorbalenya, A.E., Lohmann, V., van der Schaar, H.M., and van Kuppeveld, F.J. 2015. Modulation of the Host Lipid Landscape to Promote RNA Virus Replication: The Picornavirus Encephalomyocarditis Virus Converges on the Pathway Used by Hepatitis C Virus. PLoS Pathog 11 (9): e1005185. doi: 10.1371/journal.ppat.1005185.

Duffy, S., Shackelton, L.A., and Holmes, E.C. 2008. Rates of evolutionary change in viruses: patterns and determinants. Nat Rev Genet 9 (4): 267-76. doi: 10.1038/nrg2323.

Eckerle, L.D., Lu, X., Sperry, S.M., Choi, L., and Denison, M.R. 2007. High fidelity of murine hepatitis virus replication is decreased in nsp14 exoribonuclease mutants. J Virol 81 (22): 12135-44. doi: 10.1128/JVI.01296-07.

Elco, C.P., Guenther, J.M., Williams, B.R., and Sen, G.C. 2005. Analysis of genes induced by Sendai virus infection of mutant cell lines reveals essential roles of interferon regulatory factor 3, NF-kappaB, and interferon but not toll-like receptor 3. J Virol 79 (7): 3920-9. doi: 10.1128/JVI.79.7.3920-3929.2005.

Felgenhauer, U., Schoen, A., Gad, H.H., Hartmann, R., Schaubmar, A.R., Failing, K., Drosten, C., and Weber, F. 2020. Inhibition of SARS-CoV-2 by type I and type III interferons. J Biol Chem. doi: 10.1074/jbc.AC120.013788.

Fensterl, V.C., S.; Sen G. C. 2015. No Love Lost Between Viruses and Interferons. Annu Rev Virol 2 (2015): 549-572. doi: 10.1146/annurev-virology-100114-055249.

Figueiredo, C.M., Neris, R., Gavino-Leopoldino, D., da Silva, M.O.L., Almeida, J.S., Dos-Santos, J.S., Figueiredo, C.P., Bellio, M., Bozza, M.T., and Assuncao-Miranda, I. 2019. Mayaro Virus Replication Restriction and Induction of Muscular Inflammation in Mice Are Dependent on Age, Type-I Interferon Response, and Adaptive Immunity. Front Microbiol 10: 2246. doi: 10.3389/fmicb.2019.02246.

Finkel, Y., Mizrahi, O., Nachshon, A., Weingarten-Gabbay, S., Morgenstern, D., Yahalom-Ronen, Y., Tamir, H., Achdout, H., Stein, D., Israeli, O., Beth-Din, A., Melamed, S., Weiss, S., Israely, T., Paran, N., Schwartz, M., and Stern-Ginossar, N. 2021. The coding capacity of SARS-CoV-2. Nature 589 (7840): 125-130. doi: 10.1038/s41586-020-2739-1.

Floyd-Smith, G., Slattery, E., and Lengyel, P. 1981. Interferon action: RNA cleavage pattern of a (2'-5')oligoadenylate--dependent endonuclease. Science 212 (4498): 1030-2. doi: 10.1126/science.6165080.

Fong, S.W., Kini, R.M., and Ng, L.F.P. 2018. Mosquito Saliva Reshapes Alphavirus Infection and Immunopathogenesis. J Virol 92 (12). doi: 10.1128/JVI.01004-17.

Forni, D., Cagliani, R., Clerici, M., and Sironi, M. 2017. Molecular Evolution of Human Coronavirus Genomes. Trends Microbiol 25 (1): 35-48. doi: 10.1016/j.tim.2016.09.001.

Forrester, N.L., Palacios, G., Tesh, R.B., Savji, N., Guzman, H., Sherman, M., Weaver, S.C., and Lipkin, W.I. 2012. Genome-scale phylogeny of the alphavirus genus suggests a marine origin. J Virol 86 (5): 2729-38. doi: 10.1128/JVI.05591-11.

Frolova, E.I., Fayzulin, R.Z., Cook, S.H., Griffin, D.E., Rice, C.M., and Frolov, I. 2002. Roles of nonstructural protein nsP2 and Alpha/Beta interferons in determining the outcome of Sindbis virus infection. J Virol 76 (22): 11254-64. doi: 10.1128/jvi.76.22.11254-11264.2002.

Fros, J.J., Liu, W.J., Prow, N.A., Geertsema, C., Ligtenberg, M., Vanlandingham, D.L., Schnettler, E., Vlak, J.M., Suhrbier, A., Khromykh, A.A., and Pijlman, G.P. 2010. Chikungunya virus nonstructural protein 2 inhibits type I/II interferon-stimulated JAK-STAT signaling. J Virol 84 (20): 10877-87. doi: 10.1128/JVI.00949-10.

Fros, J.J., van der Maten, E., Vlak, J.M., and Pijlman, G.P. 2013. The C-terminal domain of chikungunya virus nsP2 independently governs viral RNA replication, cytopathicity, and inhibition of interferon signaling. J Virol 87 (18): 10394-400. doi: 10.1128/JVI.00884-13.

Fu, X.Y., Kessler, D.S., Veals, S.A., Levy, D.E., and Darnell, J.E., Jr. 1990. ISGF3, the transcriptional activator induced by interferon alpha, consists of multiple interacting

polypeptide chains. Proc Natl Acad Sci U S A 87 (21): 8555-9. doi: 10.1073/pnas.87.21.8555.

Gack, M.U., Albrecht, R.A., Urano, T., Inn, K.S., Huang, I.C., Carnero, E., Farzan, M., Inoue, S., Jung, J.U., and Garcia-Sastre, A. 2009. Influenza A virus NS1 targets the ubiquitin ligase TRIM25 to evade recognition by the host viral RNA sensor RIG-I. Cell Host Microbe 5 (5): 439-49. doi: 10.1016/j.chom.2009.04.006.

Gack, M.U., Shin, Y.C., Joo, C.H., Urano, T., Liang, C., Sun, L., Takeuchi, O., Akira, S., Chen, Z., Inoue, S., and Jung, J.U. 2007. TRIM25 RING-finger E3 ubiquitin ligase is essential for RIG-I-mediated antiviral activity. Nature 446 (7138): 916-920. doi: 10.1038/nature05732.

Ganjian, N., and Riviere-Cinnamond, A. 2020. Mayaro virus in Latin America and the Caribbean. Rev Panam Salud Publica 44: e14. doi: 10.26633/RPSP.2020.14.

Garaigorta, U., and Chisari, F.V. 2009. Hepatitis C virus blocks interferon effector function by inducing protein kinase R phosphorylation. Cell Host Microbe 6 (6): 513-22. doi: 10.1016/j.chom.2009.11.004.

Garcia-Sastre, A. 2017. Ten Strategies of Interferon Evasion by Viruses. Cell Host Microbe 22 (2): 176-184. doi: 10.1016/j.chom.2017.07.012.

Gardner, J., Anraku, I., Le, T.T., Larcher, T., Major, L., Roques, P., Schroder, W.A., Higgs, S., and Suhrbier, A. 2010. Chikungunya virus arthritis in adult wild-type mice. J Virol 84 (16): 8021-32. doi: 10.1128/JVI.02603-09.

Goertz, G.P., McNally, K.L., Robertson, S.J., Best, S.M., Pijlman, G.P., and Fros, J.J. 2018. The Methyltransferase-Like Domain of Chikungunya Virus nsP2 Inhibits the Interferon Response by Promoting the Nuclear Export of STAT1. J Virol 92 (17). doi: 10.1128/JVI.01008-18.

Gomez de Cedron, M., Ehsani, N., Mikkola, M.L., Garcia, J.A., and Kaariainen, L. 1999. RNA helicase activity of Semliki Forest virus replicase protein NSP2. FEBS Lett 448 (1): 19-22. doi: 10.1016/s0014-5793(99)00321-x.

Gomez, G.N., Abrar, F., Dodhia, M.P., Gonzalez, F.G., and Nag, A. 2019. SARS coronavirus protein nsp1 disrupts localization of Nup93 from the nuclear pore complex. Biochem Cell Biol 97 (6): 758-766. doi: 10.1139/bcb-2018-0394.

Goodfellow, I. 2011. The genome-linked protein VPg of vertebrate viruses - a multifaceted protein. Curr Opin Virol 1 (5): 355-62. doi: 10.1016/j.coviro.2011.09.003.

Gorchakov, R., Frolova, E., and Frolov, I. 2005. Inhibition of transcription and translation in Sindbis virus-infected cells. J Virol 79 (15): 9397-409. doi: 10.1128/JVI.79.15.9397-9409.2005.

Gori Savellini, G., Anichini, G., Gandolfo, C., and Cusi, M.G. 2021. SARS-CoV-2 N Protein Targets TRIM25-Mediated RIG-I Activation to Suppress Innate Immunity. Viruses 13 (8). doi: 10.3390/v13081439.

Habjan, M., Andersson, I., Klingstrom, J., Schumann, M., Martin, A., Zimmermann, P., Wagner, V., Pichlmair, A., Schneider, U., Muhlberger, E., Mirazimi, A., and Weber, F. 2008. Processing of genome 5' termini as a strategy of negative-strand RNA viruses to avoid RIG-I-dependent interferon induction. PLoS One 3 (4): e2032. doi: 10.1371/journal.pone.0002032.

Hadjadj, J., Yatim, N., Barnabei, L., Corneau, A., Boussier, J., Smith, N., Pere, H., Charbit, B., Bondet, V., Chenevier-Gobeaux, C., Breillat, P., Carlier, N., Gauzit, R., Morbieu, C., Pene, F., Marin, N., Roche, N., Szwebel, T.A., Merkling, S.H., Treluyer, J.M., Veyer, D., Mouthon, L., Blanc, C., Tharaux, P.L., Rozenberg, F., Fischer, A., Duffy, D., Rieux-Laucat, F., Kerneis, S., and Terrier, B. 2020. Impaired type I interferon activity and inflammatory responses in severe COVID-19 patients. Science 369 (6504): 718-724. doi: 10.1126/science.abc6027.

Hahn, C.S., Strauss, E.G., and Strauss, J.H. 1985. Sequence analysis of three Sindbis virus mutants temperature-sensitive in the capsid protein autoprotease. Proc Natl Acad Sci U S A 82 (14): 4648-52. doi: 10.1073/pnas.82.14.4648.

Halsey, E.S., Siles, C., Guevara, C., Vilcarromero, S., Jhonston, E.J., Ramal, C., Aguilar, P.V., and Ampuero, J.S. 2013. Mayaro virus infection, Amazon Basin region, Peru, 2010-2013. Emerg Infect Dis 19 (11): 1839-42. doi: 10.3201/eid1911.130777.

Heim, M.H., Kerr, I.M., Stark, G.R., and Darnell, J.E., Jr. 1995. Contribution of STAT SH2 groups to specific interferon signaling by the Jak-STAT pathway. Science 267 (5202): 1347-9. doi: 10.1126/science.7871432.

Herrel, M., Hoefs, N., Staeheli, P., and Schneider, U. 2012. Tick-borne Nyamanini virus replicates in the nucleus and exhibits unusual genome and matrix protein properties. J Virol 86 (19): 10739-47. doi: 10.1128/JVI.00571-12.

Hoarau, J.J., Jaffar Bandjee, M.C., Krejbich Trotot, P., Das, T., Li-Pat-Yuen, G., Dassa, B., Denizot, M., Guichard, E., Ribera, A., Henni, T., Tallet, F., Moiton, M.P., Gauzere, B.A., Bruniquet, S., Jaffar Bandjee, Z., Morbidelli, P., Martigny, G., Jolivet, M., Gay, F., Grandadam, M., Tolou, H., Vieillard, V., Debre, P., Autran, B., and Gasque, P. 2010. Persistent chronic inflammation and infection by Chikungunya arthritogenic alphavirus in spite of a robust host immune response. J Immunol 184 (10): 5914-27. doi: 10.4049/jimmunol.0900255.

Hoffmann, M., Kleine-Weber, H., Schroeder, S., Kruger, N., Herrler, T., Erichsen, S., Schiergens, T.S., Herrler, G., Wu, N.H., Nitsche, A., Muller, M.A., Drosten, C., and Pohlmann, S. 2020. SARS-CoV-2 Cell Entry Depends on ACE2 and TMPRSS2 and Is Blocked by a Clinically Proven Protease Inhibitor. Cell 181 (2): 271-280 e8. doi: 10.1016/j.cell.2020.02.052.

Holmes, E.C. 2009. The Evolutionary Genetics of Emerging Viruses. Annu Rev Ecol Evol Syst 40: 353-372.

Honda, K., Takaoka, A., and Taniguchi, T. 2006. Type I interferon [corrected] gene induction by the interferon regulatory factor family of transcription factors. Immunity 25 (3): 349-60. doi: 10.1016/j.immuni.2006.08.009.

Honda, K., Yanai, H., Negishi, H., Asagiri, M., Sato, M., Mizutani, T., Shimada, N., Ohba, Y., Takaoka, A., Yoshida, N., and Taniguchi, T. 2005. IRF-7 is the master regulator of type-I interferon-dependent immune responses. Nature 434 (7034): 772-7. doi: 10.1038/nature03464.

Hoque, H., Islam, R., Ghosh, S., Rahaman, M.M., Jewel, N.A., and Miah, M.A. 2021. Implementation of in silico methods to predict common epitopes for vaccine development against Chikungunya and Mayaro viruses. Heliyon 7 (3): e06396. doi: 10.1016/j.heliyon.2021.e06396.

Hornung, V., Ellegast, J., Kim, S., Brzozka, K., Jung, A., Kato, H., Poeck, H., Akira, S., Conzelmann, K.K., Schlee, M., Endres, S., and Hartmann, G. 2006. 5'-Triphosphate RNA is the ligand for RIG-I. Science 314 (5801): 994-7. doi: 10.1126/science.1132505.

Hosseini Rad Sm, A., and McLellan, A.D. 2020. Implications of SARS-CoV-2 Mutations for Genomic RNA Structure and Host microRNA Targeting. Int J Mol Sci 21 (13). doi: 10.3390/ijms21134807.

Hotez, P.J., and Murray, K.O. 2017. Dengue, West Nile virus, chikungunya, Zika-and now Mayaro? PLoS Negl Trop Dis 11 (8): e0005462. doi: 10.1371/journal.pntd.0005462.

Hu, Y., Li, W., Gao, T., Cui, Y., Jin, Y., Li, P., Ma, Q., Liu, X., and Cao, C. 2017. The Severe Acute Respiratory Syndrome Coronavirus Nucleocapsid Inhibits Type I Interferon Production by Interfering with TRIM25-Mediated RIG-I Ubiquitination. J Virol 91 (8). doi: 10.1128/JVI.02143-16.

Huang, C., Lokugamage, K.G., Rozovics, J.M., Narayanan, K., Semler, B.L., and Makino, S. 2011. SARS coronavirus nsp1 protein induces template-dependent endonucleolytic cleavage of mRNAs: viral mRNAs are resistant to nsp1-induced RNA cleavage. PLoS Pathog 7 (12): e1002433. doi: 10.1371/journal.ppat.1002433.

Huang, C., Wang, Y., Li, X., Ren, L., Zhao, J., Hu, Y., Zhang, L., Fan, G., Xu, J., Gu, X., Cheng, Z., Yu, T., Xia, J., Wei, Y., Wu, W., Xie, X., Yin, W., Li, H., Liu, M., Xiao, Y., Gao, H., Guo, L., Xie, J., Wang, G., Jiang, R., Gao, Z., Jin, Q., Wang, J., and Cao, B. 2020. Clinical features of patients infected with 2019 novel coronavirus in Wuhan, China. Lancet 395 (10223): 497-506. doi: 10.1016/S0140-6736(20)30183-5.

Ishida, R., Cole, J., Lopez-Orozco, J., Fayad, N., Felix-Lopez, A., Elaish, M., Luo, S.Y., Julien, O., Kumar, A., and Hobman, T.C. 2021. Mayaro Virus Non-Structural Protein 2 Circumvents the Induction of Interferon in Part by Depleting Host Transcription Initiation Factor IIE Subunit 2. Cells 10 (12). doi: doi.org/10.3390/cells10123510.

Israelow, B., Song, E., Mao, T., Lu, P., Meir, A., Liu, F., Alfajaro, M.M., Wei, J., Dong, H., Homer, R.J., Ring, A., Wilen, C.B., and Iwasaki, A. 2020. Mouse Model of SARS-CoV-2 Reveals Inflammatory Role of Type I Interferon Signaling. SSRN: 3628297. doi: 10.2139/ssrn.3628297.

Jauregui, A.R., Savalia, D., Lowry, V.K., Farrell, C.M., and Wathelet, M.G. 2013. Identification of residues of SARS-CoV nsp1 that differentially affect inhibition of gene expression and antiviral signaling. PLoS One 8 (4): e62416. doi: 10.1371/journal.pone.0062416.

Jiang, H.W., Zhang, H.N., Meng, Q.F., Xie, J., Li, Y., Chen, H., Zheng, Y.X., Wang, X.N., Qi, H., Zhang, J., Wang, P.H., Han, Z.G., and Tao, S.C. 2020. SARS-CoV-2 Orf9b suppresses type I interferon responses by targeting TOM70. Cell Mol Immunol 17 (9): 998-1000. doi: 10.1038/s41423-020-0514-8.

Johansson, M.A., Quandelacy, T.M., Kada, S., Prasad, P.V., Steele, M., Brooks, J.T., Slayton, R.B., Biggerstaff, M., and Butler, J.C. 2021. SARS-CoV-2 Transmission From People Without COVID-19 Symptoms. JAMA Netw Open 4 (1): e2035057. doi: 10.1001/jamanetworkopen.2020.35057.

Jose, J., Snyder, J.E., and Kuhn, R.J. 2009. A structural and functional perspective of alphavirus replication and assembly. Future Microbiol 4 (7): 837-56. doi: 10.2217/fmb.09.59.

Kak, G., Raza, M., and Tiwari, B.K. 2018. Interferon-gamma (IFN-gamma): Exploring its implications in infectious diseases. Biomol Concepts 9 (1): 64-79. doi: 10.1515/bmc-2018-0007.

Kamitani, W., Huang, C., Narayanan, K., Lokugamage, K.G., and Makino, S. 2009. A two-pronged strategy to suppress host protein synthesis by SARS coronavirus Nsp1 protein. Nat Struct Mol Biol 16 (11): 1134-40. doi: 10.1038/nsmb.1680.

Kamitani, W., Narayanan, K., Huang, C., Lokugamage, K., Ikegami, T., Ito, N., Kubo, H., and Makino, S. 2006. Severe acute respiratory syndrome coronavirus nsp1 protein suppresses host gene expression by promoting host mRNA degradation. Proc Natl Acad Sci U S A 103 (34): 12885-90. doi: 10.1073/pnas.0603144103.

Kato, H., Takeuchi, O., Mikamo-Satoh, E., Hirai, R., Kawai, T., Matsushita, K., Hiiragi, A., Dermody, T.S., Fujita, T., and Akira, S. 2008. Length-dependent recognition of double-stranded ribonucleic acids by retinoic acid-inducible gene-I and melanoma differentiation-associated gene 5. J Exp Med 205 (7): 1601-10. doi: 10.1084/jem.20080091.

Kawai, T., and Akira, S. 2009. The roles of TLRs, RLRs and NLRs in pathogen recognition. Int Immunol 21 (4): 317-37. doi: 10.1093/intimm/dxp017.

Kawasaki, T., and Kawai, T. 2014. Toll-like receptor signaling pathways. Front Immunol 5: 461. doi: 10.3389/fimmu.2014.00461.

Khateeb, J., Li, Y., and Zhang, H. 2021. Emerging SARS-CoV-2 variants of concern and potential intervention approaches. Crit Care 25 (1): 244. doi: 10.1186/s13054-021-03662-x.

Kindler, E., Thiel, V., and Weber, F. 2016. Interaction of SARS and MERS Coronaviruses with the Antiviral Interferon Response. Adv Virus Res 96: 219-243. doi: 10.1016/bs.aivir.2016.08.006.

Klein, S., Cortese, M., Winter, S.L., Wachsmuth-Melm, M., Neufeldt, C.J., Cerikan, B., Stanifer, M.L., Boulant, S., Bartenschlager, R., and Chlanda, P. 2020. SARS-CoV-2 structure and replication characterized by in situ cryo-electron tomography. Nat Commun 11 (1): 5885. doi: 10.1038/s41467-020-19619-7.

Knoops, K., Kikkert, M., Worm, S.H., Zevenhoven-Dobbe, J.C., van der Meer, Y., Koster, A.J., Mommaas, A.M., and Snijder, E.J. 2008. SARS-coronavirus replication is supported by a reticulovesicular network of modified endoplasmic reticulum. PLoS Biol 6 (9): e226. doi: 10.1371/journal.pbio.0060226.

Konno, Y., Kimura, I., Uriu, K., Fukushi, M., Irie, T., Koyanagi, Y., Sauter, D., Gifford, R.J., Consortium, U.-C., Nakagawa, S., and Sato, K. 2020. SARS-CoV-2 ORF3b Is a Potent Interferon Antagonist Whose Activity Is Increased by a Naturally Occurring Elongation Variant. Cell Rep 32 (12): 108185. doi: 10.1016/j.celrep.2020.108185.

Krause, P.R., Fleming, T.R., Longini, I.M., Peto, R., Briand, S., Heymann, D.L., Beral, V., Snape, M.D., Rees, H., Ropero, A., Balicer, R.D., Cramer, J.P., Muñoz-Fontela, C., Gruber, M., Gaspar, R., Singh, J.A., Subbarao, K., Van Kerkhove, M.D., Swaminathan, S., Ryan, M.J., and Henao-Restrepo, A. 2021. SARS-CoV-2 Variants and Vaccines. N Engl J Med 385 (2): 179. doi: 10.1056/NEJMsr2105280.

Krebs, D.L., and Hilton, D.J. 2001. SOCS proteins: negative regulators of cytokine signaling. Stem Cells 19 (5): 378-87. doi: 10.1634/stemcells.19-5-378.

Kumar, A., Hou, S., Airo, A.M., Limonta, D., Mancinelli, V., Branton, W., Power, C., and Hobman, T.C. 2016. Zika virus inhibits type-I interferon production and downstream signaling. EMBO Rep 17 (12): 1766-1775. doi: 10.15252/embr.201642627.

Kumar, A., Ishida, R., Strilets, T., Cole, J., Lopez-Orozco, J., Fayad, N., Felix-Lopez, A., Elaish, M., Evseev, D., Magor, K.E., Mahal, L.K., Nagata, L.P., Evans, D.H., and Hobman, T.C. 2021. SARS-CoV-2 Nonstructural Protein 1 Inhibits the Interferon Response by Causing Depletion of Key Host Signaling Factors. J Virol 95 (13): e0026621. doi: 10.1128/JVI.00266-21.

Kumar, V., Singh, J., Hasnain, S.E., and Sundar, D. 2021. Possible Link between Higher Transmissibility of Alpha, Kappa and Delta Variants of SARS-CoV-2 and Increased Structural Stability of Its Spike Protein and hACE2 Affinity. Int J Mol Sci 22 (17). doi: 10.3390/ijms22179131.

Kundu, P., Raychaudhuri, S., Tsai, W., and Dasgupta, A. 2005. Shutoff of RNA polymerase II transcription by poliovirus involves 3C protease-mediated cleavage of the TATA-binding protein at an alternative site: incomplete shutoff of transcription interferes with efficient viral replication. J Virol 79 (15): 9702-13. doi: 10.1128/JVI.79.15.9702-9713.2005.

Lan, J., Ge, J., Yu, J., Shan, S., Zhou, H., Fan, S., Zhang, Q., Shi, X., Wang, Q., Zhang, L., and Wang, X. 2020. Structure of the SARS-CoV-2 spike receptor-binding domain bound to the ACE2 receptor. Nature 581 (7807): 215-220. doi: 10.1038/s41586-020-2180-5.

Lane, W.C., Dunn, M.D., Gardner, C.L., Lam, L.K.M., Watson, A.M., Hartman, A.L., Ryman, K.D., and Klimstra, W.B. 2018. The Efficacy of the Interferon Alpha/Beta Response versus Arboviruses Is Temperature Dependent. mBio 9 (2). doi: 10.1128/mBio.00535-18.

Langendries, L., Abdelnabi, R., Neyts, J., and Delang, L. 2021. Repurposing Drugs for Mayaro Virus: Identification of EIDD-1931, Favipiravir and Suramin as Mayaro Virus Inhibitors. Microorganisms 9 (4). doi: 10.3390/microorganisms9040734.

Larner, A.C., Chaudhuri, A., and Darnell, J.E., Jr. 1986. Transcriptional induction by interferon. New protein(s) determine the extent and length of the induction. J Biol Chem 261 (1): 453-9.

Laurent-Rolle, M., Morrison, J., Rajsbaum, R., Macleod, J.M.L., Pisanelli, G., Pham, A., Ayllon, J., Miorin, L., Martinez, C., tenOever, B.R., and Garcia-Sastre, A. 2014. The interferon signaling antagonist function of yellow fever virus NS5 protein is activated by type I interferon. Cell Host Microbe 16 (3): 314-327. doi: 10.1016/j.chom.2014.07.015.

Lavergne, A., de Thoisy, B., Lacoste, V., Pascalis, H., Pouliquen, J.F., Mercier, V., Tolou, H., Dussart, P., Morvan, J., Talarmin, A., and Kazanji, M. 2006. Mayaro virus: complete nucleotide sequence and phylogenetic relationships with other alphaviruses. Virus Res 117 (2): 283-90. doi: 10.1016/j.virusres.2005.11.006.

Leal Filho, W., Bönecke, J., Spielmann, H., Azeiteiro, U.M., Alves, F., Lopez de Carvalho, M., and Nagy, G.J. 2017. Climate change and health: An analysis of causal relations on the spread of vector-borne diseases in Brazil. J. Clean. Prod. 177: 589-596. doi: 10.1016/j.jclepro.2017.12.144.

Lee, A.J., and Ashkar, A.A. 2018. The Dual Nature of Type I and Type II Interferons. Front Immunol 9: 2061. doi: 10.3389/fimmu.2018.02061.

Lei, X., Dong, X., Ma, R., Wang, W., Xiao, X., Tian, Z., Wang, C., Wang, Y., Li, L., Ren, L., Guo, F., Zhao, Z., Zhou, Z., Xiang, Z., and Wang, J. 2020. Activation and evasion of type I interferon responses by SARS-CoV-2. Nat Commun 11 (1): 3810. doi: 10.1038/s41467-020-17665-9.

Lemm, J.A., Rumenapf, T., Strauss, E.G., Strauss, J.H., and Rice, C.M. 1994. Polypeptide requirements for assembly of functional Sindbis virus replication complexes: a model for the temporal regulation of minus- and plus-strand RNA synthesis. EMBO J 13 (12): 2925-34.

Letko, M., Marzi, A., and Munster, V. 2020. Functional assessment of cell entry and receptor usage for SARS-CoV-2 and other lineage B betacoronaviruses. Nat Microbiol 5 (4): 562-569. doi: 10.1038/s41564-020-0688-y.

Levy, D.E., Kessler, D.S., Pine, R., Reich, N., and Darnell, J.E., Jr. 1988. Interferon-induced nuclear factors that bind a shared promoter element correlate with positive and negative transcriptional control. Genes Dev 2 (4): 383-93. doi: 10.1101/gad.2.4.383.

Li, J.Y., Liao, C.H., Wang, Q., Tan, Y.J., Luo, R., Qiu, Y., and Ge, X.Y. 2020. The ORF6, ORF8 and nucleocapsid proteins of SARS-CoV-2 inhibit type I interferon signaling pathway. Virus Res 286: 198074. doi: 10.1016/j.virusres.2020.198074.

Li, K., Markosyan, R.M., Zheng, Y.M., Golfetto, O., Bungart, B., Li, M., Ding, S., He, Y., Liang, C., Lee, J.C., Gratton, E., Cohen, F.S., and Liu, S.L. 2013. IFITM proteins restrict viral membrane hemifusion. PLoS Pathog 9 (1): e1003124. doi: 10.1371/journal.ppat.1003124.

Li, W., Moore, M.J., Vasilieva, N., Sui, J., Wong, S.K., Berne, M.A., Somasundaran, M., Sullivan, J.L., Luzuriaga, K., Greenough, T.C., Choe, H., and Farzan, M. 2003. Angiotensin-converting enzyme 2 is a functional receptor for the SARS coronavirus. Nature 426 (6965): 450-4. doi: 10.1038/nature02145.

Lin, C.M., Saif, L.J., Marthaler, D., and Wang, Q. 2016. Evolution, antigenicity and pathogenicity of global porcine epidemic diarrhea virus strains. Virus Res 226: 20-39. doi: 10.1016/j.virusres.2016.05.023.

Liu, T., Zhang, L., Joo, D., and Sun, S.C. 2017. NF-kappaB signaling in inflammation. Signal Transduct Target Ther 2. doi: 10.1038/sigtrans.2017.23.

Liu, Y. 2020. A code within the genetic code: codon usage regulates co-translational protein folding. Cell Commun Signal 18 (1): 145. doi: 10.1186/s12964-020-00642-6.

Llagonne-Barets, M., Icard, V., Leparc-Goffart, I., Prat, C., Perpoint, T., Andre, P., and Ramiere, C. 2016. A case of Mayaro virus infection imported from French Guiana. J Clin Virol 77: 66-8. doi: 10.1016/j.jcv.2016.02.013.

Lokugamage, K.G., Hage, A., de Vries, M., Valero-Jimenez, A.M., Schindewolf, C., Dittmann, M., Rajsbaum, R., and Menachery, V.D. 2020. Type I Interferon Susceptibility Distinguishes SARS-CoV-2 from SARS-CoV. J Virol 94 (23). doi: 10.1128/JVI.01410-20.

Lokugamage, K.G., Narayanan, K., Nakagawa, K., Terasaki, K., Ramirez, S.I., Tseng, C.T., and Makino, S. 2015. Middle East Respiratory Syndrome Coronavirus nsp1 Inhibits Host Gene Expression by Selectively Targeting mRNAs Transcribed in the Nucleus while Sparing mRNAs of Cytoplasmic Origin. J Virol 89 (21): 10970-81. doi: 10.1128/JVI.01352-15.

Mahase, E. 2020. Covid-19: What do we know about "long covid"? BMJ 370: m2815. doi: 10.1136/bmj.m2815.

Malakhova, O.A., Kim, K.I., Luo, J.K., Zou, W., Kumar, K.G., Fuchs, S.Y., Shuai, K., and Zhang, D.E. 2006. UBP43 is a novel regulator of interferon signaling independent of its ISG15 isopeptidase activity. EMBO J 25 (11): 2358-67. doi: 10.1038/sj.emboj.7601149.

Mantlo, E., Bukreyeva, N., Maruyama, J., Paessler, S., and Huang, C. 2020. Antiviral activities of type I interferons to SARS-CoV-2 infection. Antiviral Res 179: 104811. doi: 10.1016/j.antiviral.2020.104811.

McNab, F., Mayer-Barber, K., Sher, A., Wack, A., and O'Garra, A. 2015. Type I interferons in infectious disease. Nat Rev Immunol 15 (2): 87-103. doi: 10.1038/nri3787.

Melancon, P., and Garoff, H. 1987. Processing of the Semliki Forest virus structural polyprotein: role of the capsid protease. J Virol 61 (5): 1301-9. doi: 10.1128/JVI.61.5.1301-1309.1987.

Menachery, V.D., Yount, B.L., Jr., Debbink, K., Agnihothram, S., Gralinski, L.E., Plante, J.A., Graham, R.L., Scobey, T., Ge, X.Y., Donaldson, E.F., Randell, S.H., Lanzavecchia, A., Marasco, W.A., Shi, Z.L., and Baric, R.S. 2015. A SARS-like cluster of circulating bat coronaviruses shows potential for human emergence. Nat Med 21 (12): 1508-13. doi: 10.1038/nm.3985.

Mesev, E.V., LeDesma, R.A., and Ploss, A. 2019. Decoding type I and III interferon signalling during viral infection. Nat Microbiol 4 (6): 914-924. doi: 10.1038/s41564-019-0421-x.

Miorin, L., Kehrer, T., Sanchez-Aparicio, M.T., Zhang, K., Cohen, P., Patel, R.S., Cupic, A., Makio, T., Mei, M., Moreno, E., Danziger, O., White, K.M., Rathnasinghe, R., Uccellini, M., Gao, S., Aydillo, T., Mena, I., Yin, X., Martin-Sancho, L., Krogan, N.J., Chanda, S.K., Schotsaert, M., Wozniak, R.W., Ren, Y., Rosenberg, B.R., Fontoura, B.M.A., and Garcia-Sastre, A. 2020. SARS-CoV-2 Orf6 hijacks Nup98 to block STAT nuclear import and antagonize interferon signaling. Proc Natl Acad Sci U S A 117 (45): 28344-28354. doi: 10.1073/pnas.2016650117.

Mir, T., Almas, T., Kaur, J., Faisaluddin, M., Song, D., Ullah, W., Mamtani, S., Rauf, H., Yadav, S., Latchana, S., Michaelson, N.M., Connerney, M., and Sattar, Y. 2021. Coronavirus disease 2019 (COVID-19): Multisystem review of pathophysiology. Ann Med Surg (Lond) 69: 102745. doi: 10.1016/j.amsu.2021.102745.

Monk, P.D., Marsden, R.J., Tear, V.J., Brookes, J., Batten, T.N., Mankowski, M., Gabbay, F.J., Davies, D.E., Holgate, S.T., Ho, L.P., Clark, T., Djukanovic, R., Wilkinson, T.M.A., and Inhaled Interferon Beta, C.-S.G. 2021. Safety and efficacy of inhaled nebulised interferon beta-1a (SNG001) for treatment of SARS-CoV-2 infection: a randomised, double-blind, placebo-controlled, phase 2 trial. Lancet Respir Med 9 (2): 196-206. doi: 10.1016/S2213-2600(20)30511-7.

Mu, J., Fang, Y., Yang, Q., Shu, T., Wang, A., Huang, M., Jin, L., Deng, F., Qiu, Y., and Zhou, X. 2020a. SARS-CoV-2 N protein antagonizes type I interferon signaling by suppressing phosphorylation and nuclear translocation of STAT1 and STAT2. Cell Discov 6 (1): 65. doi: 10.1038/s41421-020-00208-3.

Nakkhara, P., Chongsuvivatwong, V., and Thammapalo, S. 2013. Risk factors for symptomatic and asymptomatic chikungunya infection. Trans R Soc Trop Med Hyg 107 (12): 789-96. doi: 10.1093/trstmh/trt083.

Narayanan, K., Huang, C., Lokugamage, K., Kamitani, W., Ikegami, T., Tseng, C.T., and Makino, S. 2008. Severe acute respiratory syndrome coronavirus nsp1 suppresses host gene expression, including that of type I interferon, in infected cells. J Virol 82 (9): 4471-9. doi: 10.1128/JVI.02472-07.

Neufeldt, C.J., Cerikan, B., Cortese, M., Frankish, J., Lee, J., Plociennikowska, A., Heigwer, F., Joecks, S., Burkart, S.S., Zander, D.Y., Gendarme, M., El Debs, B., Halama, N., Merle, U., Boutros, M., Binder, M., and Bartenschlager, R. 2020. SARS-CoV-2 infection induces a pro-inflammatory cytokine response through cGAS-STING and NF-κB. bioRxiv. doi: https://doi.org/10.1101/2020.07.21.212639.

Ng, S.L., Friedman, B.A., Schmid, S., Gertz, J., Myers, R.M., Tenoever, B.R., and Maniatis, T. 2011. IkappaB kinase epsilon (IKK(epsilon)) regulates the balance between type I and type II interferon responses. Proc Natl Acad Sci U S A 108 (52): 21170-5. doi: 10.1073/pnas.1119137109.

O'Brien, T.R., Prokunina-Olsson, L., and Donnelly, R.P. 2014. IFN-lambda4: the paradoxical new member of the interferon lambda family. J Interferon Cytokine Res 34 (11): 829-38. doi: 10.1089/jir.2013.0136.

Oh, S.J., and Shin, O.S. 2021. SARS-CoV-2 Nucleocapsid Protein Targets RIG-I-Like Receptor Pathways to Inhibit the Induction of Interferon Response. Cells 10 (3). doi: 10.3390/cells10030530.

Okamoto, S., Watanabe, Y., Takakura, Y., and Hashida, M. 1998. Cationic liposome-mediated efficient induction of type I interferons by a low dose of poly I:poly C in mouse cell lines. J Biochem 124 (4): 697-701. doi: 10.1093/oxfordjournals.jbchem.a022168.

Ou, X., Liu, Y., Lei, X., Li, P., Mi, D., Ren, L., Guo, L., Guo, R., Chen, T., Hu, J., Xiang, Z., Mu, Z., Chen, X., Chen, J., Hu, K., Jin, Q., Wang, J., and Qian, Z. 2020. Characterization of spike glycoprotein of SARS-CoV-2 on virus entry and its immune cross-reactivity with SARS-CoV. Nat Commun 11 (1): 1620. doi: 10.1038/s41467-020-15562-9.

Paul, D., and Bartenschlager, R. 2015. Flaviviridae Replication Organelles: Oh, What a Tangled Web We Weave. Annu Rev Virol 2 (1): 289-310. doi: 10.1146/annurev-virology-100114-055007.

Pichlmair, A., Schulz, O., Tan, C.P., Naslund, T.I., Liljestrom, P., Weber, F., and Reis e Sousa, C. 2006. RIG-I-mediated antiviral responses to single-stranded RNA bearing 5'-phosphates. Science 314 (5801): 997-1001. doi: 10.1126/science.1132998.

Pietila, M.K., Hellstrom, K., and Ahola, T. 2017. Alphavirus polymerase and RNA replication. Virus Res 234: 44-57. doi: 10.1016/j.virusres.2017.01.007.

Powers, A.M., Brault, A.C., Shirako, Y., Strauss, E.G., Kang, W., Strauss, J.H., and Weaver, S.C. 2001. Evolutionary relationships and systematics of the alphaviruses. J Virol 75 (21): 10118-31. doi: 10.1128/JVI.75.21.10118-10131.2001.

Powers, J.M., Haese, N.N., Denton, M., Ando, T., Kreklywich, C., Bonin, K., Streblow, C.E., Kreklywich, N., Smith, P., Broeckel, R., DeFilippis, V., Morrison, T.E., Heise, M.T., and Streblow, D.N. 2021. Non-replicating adenovirus based Mayaro virus vaccine elicits protective immune responses and cross protects against other alphaviruses. PLoS Negl Trop Dis 15 (4): e0009308. doi: 10.1371/journal.pntd.0009308.

Prem, K., Liu, Y., Russell, T.W., Kucharski, A.J., Eggo, R.M., Davies, N., Centre for the Mathematical Modelling of Infectious Diseases, C.-W.G., Jit, M., and Klepac, P. 2020. The effect of control strategies to reduce social mixing on outcomes of the COVID-19 epidemic in Wuhan, China: a modelling study. Lancet Public Health 5 (5): e261-e270. doi: 10.1016/S2468-2667(20)30073-6.

Pythoud, C., Rodrigo, W.W., Pasqual, G., Rothenberger, S., Martinez-Sobrido, L., de la Torre, J.C., and Kunz, S. 2012. Arenavirus nucleoprotein targets interferon regulatory factor-activating kinase IKKepsilon. J Virol 86 (15): 7728-38. doi: 10.1128/JVI.00187-12.

Rafael, K.C., Preciado-Llanes, L., Azar, S.R., Kim, Y.C., Brandon, O., Lopez-Camacho, C., Reyes-Sandoval, A., and Rossi, S.L. 2020. Adenoviral-Vectored Mayaro and Chikungunya Virus Vaccine Candidates Afford Partial Cross-Protection From Lethal Challenge in A129 Mouse Model. Front Immunol 11: 591885. doi: 10.3389/fimmu.2020.591885.

Rashid, F., Suleman, M., Shah, A., Dzakah, E.E., Wang, H., Chen, S., and Tang, S. 2021. Mutations in SARS-CoV-2 ORF8 Altered the Bonding Network With Interferon Regulatory Factor 3 to Evade Host Immune System. Front Microbiol 12: 703145. doi: 10.3389/fmicb.2021.703145.

Reynaud, J.M., Kim, D.Y., Atasheva, S., Rasalouskaya, A., White, J.P., Diamond, M.S., Weaver, S.C., Frolova, E.I., and Frolov, I. 2015. IFIT1 Differentially Interferes with Translation and Replication of Alphavirus Genomes and Promotes Induction of Type I Interferon. PLoS Pathog 11 (4): e1004863. doi: 10.1371/journal.ppat.1004863.

Ribeiro-Filho, H.V., Coimbra, L.D., Cassago, A., Rocha, R.P.F., Guerra, J., de Felicio, R., Carnieli, C.M., Leme, L., Padilha, A.C., Paes Leme, A.F., Trivella, D.B.B., Portugal, R.V., Lopes-de-Oliveira, P.S., and Marques, R.E. 2021. Cryo-EM structure of the mature and infective Mayaro virus at 4.4 A resolution reveals features of arthritogenic alphaviruses. Nat Commun 12 (1): 3038. doi: 10.1038/s41467-021-23400-9.

Rogers, K.J., Jones-Burrage, S., Maury, W., and Mukhopadhyay, S. 2020. TF protein of Sindbis virus antagonizes host type I interferon responses in a palmitoylation-dependent manner. Virology 542: 63-70. doi: 10.1016/j.virol.2020.01.001.

Roundy, C.M., Azar, S.R., Rossi, S.L., Weaver, S.C., and Vasilakis, N. 2017. Insect-Specific Viruses: A Historical Overview and Recent Developments. Adv Virus Res 98: 119-146. doi: 10.1016/bs.aivir.2016.10.001.

Russo, A.T., White, M.A., and Watowich, S.J. 2006. The crystal structure of the Venezuelan equine encephalitis alphavirus nsP2 protease. Structure 14 (9): 1449-58. doi: 10.1016/j.str.2006.07.010.

Saisawang, C., Sillapee, P., Sinsirimongkol, K., Ubol, S., Smith, D.R., and Ketterman, A.J. 2015. Full length and protease domain activity of chikungunya virus nsP2 differ from other alphavirus nsP2 proteases in recognition of small peptide substrates. Biosci Rep 35 (3). doi: 10.1042/BSR20150086.

Sallard, E., Halloy, J., Casane, D., Decroly, E., and van Helden, J. 2021. Tracing the origins of SARS-COV-2 in coronavirus phylogenies: a review. Environ Chem Lett: 1-17. doi: 10.1007/s10311-020-01151-1.

Santiago, F.W., Halsey, E.S., Siles, C., Vilcarromero, S., Guevara, C., Silvas, J.A., Ramal, C., Ampuero, J.S., and Aguilar, P.V. 2015. Long-Term Arthralgia after Mayaro Virus Infection Correlates with Sustained Pro-inflammatory Cytokine Response. PLoS Negl Trop Dis 9 (10): e0004104. doi: 10.1371/journal.pntd.0004104.

Sanz, M.A., Garcia-Moreno, M., and Carrasco, L. 2015. Inhibition of host protein synthesis by Sindbis virus: correlation with viral RNA replication and release of nuclear proteins to the cytoplasm. Cell Microbiol 17 (4): 520-41. doi: 10.1111/cmi.12381.

Sauter, D., Specht, A., and Kirchhoff, F. 2010. Tetherin: holding on and letting go. Cell 141 (3): 392-8. doi: 10.1016/j.cell.2010.04.022.

Schilte, C., Couderc, T., Chretien, F., Sourisseau, M., Gangneux, N., Guivel-Benhassine, F., Kraxner, A., Tschopp, J., Higgs, S., Michault, A., Arenzana-Seisdedos, F., Colonna, M., Peduto, L., Schwartz, O., Lecuit, M., and Albert, M.L. 2010. Type I IFN controls chikungunya virus via its action on nonhematopoietic cells. J Exp Med 207 (2): 429-42. doi: 10.1084/jem.20090851.

Schlee, M., Roth, A., Hornung, V., Hagmann, C.A., Wimmenauer, V., Barchet, W., Coch, C., Janke, M., Mihailovic, A., Wardle, G., Juranek, S., Kato, H., Kawai, T., Poeck, H., Fitzgerald, K.A., Takeuchi, O., Akira, S., Tuschl, T., Latz, E., Ludwig, J., and Hartmann, G. 2009. Recognition of 5' triphosphate by RIG-I helicase requires short blunt double-stranded RNA as contained in panhandle of negative-strand virus. Immunity 31 (1): 25-34. doi: 10.1016/j.immuni.2009.05.008.

Schneider, W.M., Chevillotte, M.D., and Rice, C.M. 2014. Interferon-stimulated genes: a complex web of host defenses. Annu Rev Immunol 32: 513-45. doi: 10.1146/annurev-immunol-032713-120231.

Schoggins, J.W., and Rice, C.M. 2011. Interferon-stimulated genes and their antiviral effector functions. Curr Opin Virol 1 (6): 519-25. doi: 10.1016/j.coviro.2011.10.008.

Schubert, K., Karousis, E.D., Jomaa, A., Scaiola, A., Echeverria, B., Gurzeler, L.A., Leibundgut, M., Thiel, V., Muhlemann, O., and Ban, N. 2020. SARS-CoV-2 Nsp1 binds the ribosomal mRNA channel to inhibit translation. Nat Struct Mol Biol 27 (10): 959-966. doi: 10.1038/s41594-020-0511-8.

Seth, R.B., Sun, L., Ea, C.K., and Chen, Z.J. 2005. Identification and characterization of MAVS, a mitochondrial antiviral signaling protein that activates NF-kappaB and IRF 3. Cell 122 (5): 669-82. doi: 10.1016/j.cell.2005.08.012.

Shemesh, M., Aktepe, T.E., Deerain, J.M., McAuley, J.L., Audsley, M.D., David, C.T., Purcell, D.F.J., Urin, V., Hartmann, R., Moseley, G.W., Mackenzie, J.M., Schreiber, G., and Harari, D. 2021. SARS-CoV-2 suppresses IFNbeta production mediated by NSP1, 5, 6, 15, ORF6 and ORF7b but does not suppress the effects of added interferon. PLoS Pathog 17 (8): e1009800. doi: 10.1371/journal.ppat.1009800.

Shin, D., Mukherjee, R., Grewe, D., Bojkova, D., Baek, K., Bhattacharya, A., Schulz, L., Widera, M., Mehdipour, A.R., Tascher, G., Geurink, P.P., Wilhelm, A., van der Heden van Noort, G.J., Ovaa, H., Muller, S., Knobeloch, K.P., Rajalingam, K., Schulman, B.A., Cinatl, J., Hummer, G., Ciesek, S., and Dikic, I. 2020. Papain-like protease regulates SARS-CoV-2 viral spread and innate immunity. Nature. doi: 10.1038/s41586-020-2601-5.

Slegers, C.A., Keuter, M., Gunther, S., Schmidt-Chanasit, J., van der Ven, A.J., and de Mast, Q. 2014. Persisting arthralgia due to Mayaro virus infection in a traveler from Brazil: is there a risk for attendants to the 2014 FIFA World Cup? J Clin Virol 60 (3): 317-9. doi: 10.1016/j.jcv.2014.04.020.

Snijder, E.J., Limpens, R., de Wilde, A.H., de Jong, A.W.M., Zevenhoven-Dobbe, J.C., Maier, H.J., Faas, F., Koster, A.J., and Barcena, M. 2020. A unifying structural and functional model of the coronavirus replication organelle: Tracking down RNA synthesis. PLoS Biol 18 (6): e3000715. doi: 10.1371/journal.pbio.3000715.

Strauss, E.G., De Groot, R.J., Levinson, R., and Strauss, J.H. 1992. Identification of the active site residues in the nsP2 proteinase of Sindbis virus. Virology 191 (2): 932-40. doi: 10.1016/0042-6822(92)90268-t.

Strauss, E.G., Rice, C.M., and Strauss, J.H. 1983. Sequence coding for the alphavirus nonstructural proteins is interrupted by an opal termination codon. Proc Natl Acad Sci U S A 80 (17): 5271-5. doi: 10.1073/pnas.80.17.5271.

Suhrbier, A., Jaffar-Bandjee, M.C., and Gasque, P. 2012. Arthritogenic alphaviruses--an overview. Nat Rev Rheumatol 8 (7): 420-9. doi: 10.1038/nrrheum.2012.64.

Suhrbier, A., and Mahalingam, S. 2009. The immunobiology of viral arthritides. Pharmacol Ther 124 (3): 301-8. doi: 10.1016/j.pharmthera.2009.09.005.

Sun, J., He, W.T., Wang, L., Lai, A., Ji, X., Zhai, X., Li, G., Suchard, M.A., Tian, J., Zhou, J., Veit, M., and Su, S. 2020. COVID-19: Epidemiology, Evolution, and Cross-Disciplinary Perspectives. Trends Mol Med 26 (5): 483-495. doi: 10.1016/j.molmed.2020.02.008.

Sungnak, W., Huang, N., Becavin, C., Berg, M., Queen, R., Litvinukova, M., Talavera-Lopez, C., Maatz, H., Reichart, D., Sampaziotis, F., Worlock, K.B., Yoshida, M., Barnes, J.L., and Network, H.C.A.L.B. 2020. SARS-CoV-2 entry factors are highly expressed in nasal epithelial cells together with innate immune genes. Nat Med 26 (5): 681-687. doi: 10.1038/s41591-020-0868-6.

Tasso de Oliveira Mota, M., Rocha Ribeiro, M., Vedovello, D., and Lacerda Nogueira, M. 2015. Mayaro virus: a neglected arbovirus of the Americas. Future Virol 10 (9). doi: 10.2217/fvl.15.76.

Taylor, S.F., Patel, P.R., and Herold, T.J. 2005. Recurrent arthralgias in a patient with previous Mayaro fever infection. South Med J 98 (4): 484-5. doi: 10.1097/01.SMJ.0000145879.14102.F4.

Teijaro, J.R. 2016. Type I interferons in viral control and immune regulation. Curr Opin Virol 16: 31-40. doi: 10.1016/j.coviro.2016.01.001.

Theilacker, C., Held, J., Allering, L., Emmerich, P., Schmidt-Chanasit, J., Kern, W.V., and Panning, M. 2013. Prolonged polyarthralgia in a German traveller with Mayaro virus infection without inflammatory correlates. BMC Infect Dis 13: 369. doi: 10.1186/1471-2334-13-369.

Thoms, M., Buschauer, R., Ameismeier, M., Koepke, L., Denk, T., Hirschenberger, M., Kratzat, H., Hayn, M., Mackens-Kiani, T., Cheng, J., Straub, J.H., Sturzel, C.M., Frohlich, T., Berninghausen, O., Becker, T., Kirchhoff, F., Sparrer, K.M.J., and Beckmann, R. 2020. Structural basis for translational shutdown and immune evasion by the Nsp1 protein of SARS-CoV-2. Science 369 (6508): 1249-1255. doi: 10.1126/science.abc8665.

Torres, J.R., Russell, K.L., Vasquez, C., Barrera, R., Tesh, R.B., Salas, R., and Watts, D.M. 2004. Family cluster of Mayaro fever, Venezuela. Emerg Infect Dis 10 (7): 1304-6. doi: 10.3201/eid1007.030860.

Totura, A.L., and Baric, R.S. 2012. SARS coronavirus pathogenesis: host innate immune responses and viral antagonism of interferon. Curr Opin Virol 2 (3): 264-75. doi: 10.1016/j.coviro.2012.04.004.

Tsai, P.H., Lai, W.Y., Lin, Y.Y., Luo, Y.H., Lin, Y.T., Chen, H.K., Chen, Y.M., Lai, Y.C., Kuo, L.C., Chen, S.D., Chang, K.J., Liu, C.H., Chang, S.C., Wang, F.D., and Yang, Y.P. 2021.

Clinical manifestation and disease progression in COVID-19 infection. J Chin Med Assoc 84 (1): 3-8. doi: 10.1097/JCMA.0000000000000463.

Tsetsarkin, K.A., Vanlandingham, D.L., McGee, C.E., and Higgs, S. 2007. A single mutation in chikungunya virus affects vector specificity and epidemic potential. PLoS Pathog 3 (12): e201. doi: 10.1371/journal.ppat.0030201.

Uhrlaub, J.L., Pulko, V., DeFilippis, V.R., Broeckel, R., Streblow, D.N., Coleman, G.D., Park, B.S., Lindo, J.F., Vickers, I., Anzinger, J.J., and Nikolich-Zugich, J. 2016. Dysregulated TGF-beta Production Underlies the Age-Related Vulnerability to Chikungunya Virus. PLoS Pathog 12 (10): e1005891. doi: 10.1371/journal.ppat.1005891.

V'Kovski, P., Kratzel, A., Steiner, S., Stalder, H., and Thiel, V. 2021. Coronavirus biology and replication: implications for SARS-CoV-2. Nat Rev Microbiol 19 (3): 155-170. doi: 10.1038/s41579-020-00468-6.

van Hemert, M.J., van den Worm, S.H., Knoops, K., Mommaas, A.M., Gorbalenya, A.E., and Snijder, E.J. 2008. SARS-coronavirus replication/transcription complexes are membrane-protected and need a host factor for activity in vitro. PLoS Pathog 4 (5): e1000054. doi: 10.1371/journal.ppat.1000054.

Vanderheiden, A., Ralfs, P., Chirkova, T., Upadhyay, A.A., Zimmerman, M.G., Bedoya, S., Aoued, H., Tharp, G.M., Pellegrini, K.L., Manfredi, C., Sorscher, E., Mainou, B., Lobby, J.L., Kohlmeier, J.E., Lowen, A.C., Shi, P.Y., Menachery, V.D., Anderson, L.J., Grakoui, A., Bosinger, S.E., and Suthar, M.S. 2020a. Type I and Type III IFN Restrict SARS-CoV-2 Infection of Human Airway Epithelial Cultures. J Virol. doi: 10.1128/JVI.00985-20.

Vannini, A., and Cramer, P. 2012. Conservation between the RNA polymerase I, II, and III transcription initiation machineries. Mol Cell 45 (4): 439-46. doi: 10.1016/j.molcel.2012.01.023.

Vasiljeva, L., Merits, A., Auvinen, P., and Kaariainen, L. 2000. Identification of a novel function of the alphavirus capping apparatus. RNA 5'-triphosphatase activity of Nsp2. J Biol Chem 275 (23): 17281-7. doi: 10.1074/jbc.M910340199.

Walls, A.C., Park, Y.J., Tortorici, M.A., Wall, A., McGuire, A.T., and Veesler, D. 2020. Structure, Function, and Antigenicity of the SARS-CoV-2 Spike Glycoprotein. Cell 181 (2): 281-292 e6. doi: 10.1016/j.cell.2020.02.058.

Wang, D., Hu, B., Hu, C., Zhu, F., Liu, X., Zhang, J., Wang, B., Xiang, H., Cheng, Z., Xiong, Y., Zhao, Y., Li, Y., Wang, X., and Peng, Z. 2020. Clinical Characteristics of 138 Hospitalized Patients With 2019 Novel Coronavirus-Infected Pneumonia in Wuhan, China. JAMA. doi: 10.1001/jama.2020.1585.

Wang, W., Zhou, Z., Xiao, X., Tian, Z., Dong, X., Wang, C., Li, L., Ren, L., Lei, X., Xiang, Z., and Wang, J. 2021. SARS-CoV-2 nsp12 attenuates type I interferon production by

inhibiting IRF3 nuclear translocation. Cell Mol Immunol 18 (4): 945-953. doi: 10.1038/s41423-020-00619-y.

Wang, X., Hinson, E.R., and Cresswell, P. 2007. The interferon-inducible protein viperin inhibits influenza virus release by perturbing lipid rafts. Cell Host Microbe 2 (2): 96-105. doi: 10.1016/j.chom.2007.06.009.

Wathelet, M.G., Orr, M., Frieman, M.B., and Baric, R.S. 2007. Severe acute respiratory syndrome coronavirus evades antiviral signaling: role of nsp1 and rational design of an attenuated strain. J Virol 81 (21): 11620-33. doi: 10.1128/JVI.00702-07.

Webster, B., Werneke, S.W., Zafirova, B., This, S., Coleon, S., Decembre, E., Paidassi, H., Bouvier, I., Joubert, P.E., Duffy, D., Walzer, T., Albert, M.L., and Dreux, M. 2018. Plasmacytoid dendritic cells control dengue and Chikungunya virus infections via IRF7-regulated interferon responses. Elife 7. doi: 10.7554/eLife.34273.

Wiersinga, W.J., Rhodes, A., Cheng, A.C., Peacock, S.J., and Prescott, H.C. 2020. Pathophysiology, Transmission, Diagnosis, and Treatment of Coronavirus Disease 2019 (COVID-19): A Review. JAMA 324 (8): 782-793. doi: 10.1001/jama.2020.12839.

Wies, E., Wang, M.K., Maharaj, N.P., Chen, K., Zhou, S., Finberg, R.W., and Gack, M.U. 2013. Dephosphorylation of the RNA sensors RIG-I and MDA5 by the phosphatase PP1 is essential for innate immune signaling. Immunity 38 (3): 437-49. doi: 10.1016/j.immuni.2012.11.018.

Wiggins, K., Eastmond, B., and Alto, B.W. 2018. Transmission potential of Mayaro virus in Florida Aedes aegypti and Aedes albopictus mosquitoes. Med Vet Entomol 32 (4): 436-442. doi: 10.1111/mve.12322.

Witte, K., Witte, E., Sabat, R., and Wolk, K. 2010. IL-28A, IL-28B, and IL-29: promising cytokines with type I interferon-like properties. Cytokine Growth Factor Rev 21 (4): 237-51. doi: 10.1016/j.cytogfr.2010.04.002.

Wu, A., Peng, Y., Huang, B., Ding, X., Wang, X., Niu, P., Meng, J., Zhu, Z., Zhang, Z., Wang, J., Sheng, J., Quan, L., Xia, Z., Tan, W., Cheng, G., and Jiang, T. 2020. Genome Composition and Divergence of the Novel Coronavirus (2019-nCoV) Originating in China. Cell Host Microbe 27 (3): 325-328. doi: 10.1016/j.chom.2020.02.001.

Wu, Z., and McGoogan, J.M. 2020. Characteristics of and Important Lessons From the Coronavirus Disease 2019 (COVID-19) Outbreak in China: Summary of a Report of 72314 Cases From the Chinese Center for Disease Control and Prevention. JAMA 323 (13): 1239-1242. doi: 10.1001/jama.2020.2648.

Xia, H., Cao, Z., Xie, X., Zhang, X., Chen, J.Y., Wang, H., Menachery, V.D., Rajsbaum, R., and Shi, P.Y. 2020. Evasion of Type I Interferon by SARS-CoV-2. Cell Rep 33 (1): 108234. doi: 10.1016/j.celrep.2020.108234.

Yang, D., Chu, H., Hou, Y., Chai, Y., Shuai, H., Lee, A.C., Zhang, X., Wang, Y., Hu, B., Huang, X., Yuen, T.T., Cai, J.P., Zhou, J., Yuan, S., Zhang, A.J., Chan, J.F., and Yuen, K.Y. 2020. Attenuated Interferon and Proinflammatory Response in SARS-CoV-2-Infected Human Dendritic Cells Is Associated With Viral Antagonism of STAT1 Phosphorylation. J Infect Dis 222 (5): 734-745. doi: 10.1093/infdis/jiaa356.

Yuan, S., Peng, L., Park, J.J., Hu, Y., Devarkar, S.C., Dong, M.B., Shen, Q., Wu, S., Chen, S., Lomakin, I.B., and Xiong, Y. 2020. Nonstructural Protein 1 of SARS-CoV-2 Is a Potent Pathogenicity Factor Redirecting Host Protein Synthesis Machinery toward Viral RNA. Mol Cell 80 (6): 1055-1066 e6. doi: 10.1016/j.molcel.2020.10.034.

Yue, C., Teitz, S., Miyabashi, T., Boller, K., Lewis-Ximenez, L.L., Baylis, S.A., and Blumel, J. 2019. Inactivation and Removal of Chikungunya Virus and Mayaro Virus from Plasma-derived Medicinal Products. Viruses 11 (3). doi: 10.3390/v11030234.

Yuen, C.K., Lam, J.Y., Wong, W.M., Mak, L.F., Wang, X., Chu, H., Cai, J.P., Jin, D.Y., To, K.K., Chan, J.F., Yuen, K.Y., and Kok, K.H. 2020. SARS-CoV-2 nsp13, nsp14, nsp15 and orf6 function as potent interferon antagonists. Emerg Microbes Infect 9 (1): 1418-1428. doi: 10.1080/22221751.2020.1780953.

Zaki, A.M., van Boheemen, S., Bestebroer, T.M., Osterhaus, A.D., and Fouchier, R.A. 2012. Isolation of a novel coronavirus from a man with pneumonia in Saudi Arabia. N Engl J Med 367 (19): 1814-20. doi: 10.1056/NEJMoa1211721.

Zhang, K., Miorin, L., Makio, T., Dehghan, I., Gao, S., Xie, Y., Zhong, H., Esparza, M., Kehrer, T., Kumar, A., Hobman, T.C., Ptak, C., Gao, B., Minna, J.D., Chen, Z., Garcia-Sastre, A., Ren, Y., Wozniak, R.W., and Fontoura, B.M.A. 2021. Nsp1 protein of SARS-CoV-2 disrupts the mRNA export machinery to inhibit host gene expression. Sci Adv 7 (6). doi: 10.1126/sciadv.abe7386.

Zhang, Q., Bastard, P., Liu, Z., Le Pen, J., Moncada-Velez, M., Chen, J., Ogishi, M., Sabli, I.K.D., Hodeib, S., Korol, C., Rosain, J., Bilguvar, K., Ye, J., Bolze, A., Bigio, B., Yang, R., Arias, A.A., Zhou, Q., Zhang, Y., Onodi, F., Korniotis, S., Karpf, L., Philippot, Q., Chbihi, M., Bonnet-Madin, L., Dorgham, K., Smith, N., Schneider, W.M., Razooky, B.S., Hoffmann, H.H., Michailidis, E., Moens, L., Han, J.E., Lorenzo, L., Bizien, L., Meade, P., Neehus, A.L., Ugurbil, A.C., Corneau, A., Kerner, G., Zhang, P., Rapaport, F., Seeleuthner, Y., Manry, J., Masson, C., Schmitt, Y., Schluter, A., Le Voyer, T., Khan, T., Li, J., Fellay, J., Roussel, L., Shahrooei, M., Alosaimi, M.F., Mansouri, D., Al-Saud, H., Al-Mulla, F., Almourfi, F., Al-Muhsen, S.Z., Alsohime, F., Al Turki, S., Hasanato, R., van de Beek, D., Biondi, A., Bettini, L.R., D'Angio, M., Bonfanti, P., Imberti, L., Sottini, A., Paghera, S., Quiros-Roldan, E., Rossi, C., Oler, A.J., Tompkins, M.F., Alba, C., Vandernoot, I., Goffard, J.C., Smits, G., Migeotte, I., Haerynck, F., Soler-Palacin, P., Martin-Nalda, A., Colobran, R., Morange, P.E., Keles, S., Colkesen, F., Ozcelik, T., Yasar, K.K., Senoglu, S., Karabela, S.N., Rodriguez-Gallego, C., Novelli, G., Hraiech, S., Tandjaoui-Lambiotte, Y., Duval, X., Laouenan, C., Clinicians, C.-S., Clinicians, C., Imagine, C.G., French, C.C.S.G., Co, V.C.C., Amsterdam, U.M.C.C.-B., Effort, C.H.G., Group, N.-U.T.C.I., Snow, A.L., Dalgard, C.L., Milner, J.D., Vinh, D.C., Mogensen,

T.H., Marr, N., Spaan, A.N., Boisson, B., Boisson-Dupuis, S., Bustamante, J., Puel, A., Ciancanelli, M.J., Meyts, I., Maniatis, T., Soumelis, V., Amara, A., Nussenzweig, M., Garcia-Sastre, A., Krammer, F., Pujol, A., Duffy, D., Lifton, R.P., Zhang, S.Y., Gorochov, G., Beziat, V., Jouanguy, E., Sancho-Shimizu, V., Rice, C.M., Abel, L., Notarangelo, L.D., Cobat, A., Su, H.C., and Casanova, J.L. 2020. Inborn errors of type I IFN immunity in patients with life-threatening COVID-19. Science 370 (6515). doi: 10.1126/science.abd4570.

Zhang, R., Kim, A.S., Fox, J.M., Nair, S., Basore, K., Klimstra, W.B., Rimkunas, R., Fong, R.H., Lin, H., Poddar, S., Crowe, J.E., Jr., Doranz, B.J., Fremont, D.H., and Diamond, M.S. 2018. Mxra8 is a receptor for multiple arthritogenic alphaviruses. Nature 557 (7706): 570-574. doi: 10.1038/s41586-018-0121-3.

Zhao, Y., Sui, L., Wu, P., Wang, W., Wang, Z., Yu, Y., Hou, Z., Tan, G., Liu, Q., and Wang, G. 2021. A dual-role of SARS-CoV-2 nucleocapsid protein in regulating innate immune response. Signal Transduct Target Ther 6 (1): 331. doi: 10.1038/s41392-021-00742-w.

Zheng, Y., Zhuang, M.W., Han, L., Zhang, J., Nan, M.L., Zhan, P., Kang, D., Liu, X., Gao, C., and Wang, P.H. 2020. Severe acute respiratory syndrome coronavirus 2 (SARS-CoV-2) membrane (M) protein inhibits type I and III interferon production by targeting RIG-I/MDA-5 signaling. Signal Transduct Target Ther 5 (1): 299. doi: 10.1038/s41392-020-00438-7.

Zhong, N.S., Zheng, B.J., Li, Y.M., Poon, Xie, Z.H., Chan, K.H., Li, P.H., Tan, S.Y., Chang, Q., Xie, J.P., Liu, X.Q., Xu, J., Li, D.X., Yuen, K.Y., Peiris, and Guan, Y. 2003. Epidemiology and cause of severe acute respiratory syndrome (SARS) in Guangdong, People's Republic of China, in February, 2003. Lancet 362 (9393): 1353-8. doi: 10.1016/s0140-6736(03)14630-2.

Zhou, P., Fan, H., Lan, T., Yang, X.L., Shi, W.F., Zhang, W., Zhu, Y., Zhang, Y.W., Xie, Q.M., Mani, S., Zheng, X.S., Li, B., Li, J.M., Guo, H., Pei, G.Q., An, X.P., Chen, J.W., Zhou, L., Mai, K.J., Wu, Z.X., Li, D., Anderson, D.E., Zhang, L.B., Li, S.Y., Mi, Z.Q., He, T.T., Cong, F., Guo, P.J., Huang, R., Luo, Y., Liu, X.L., Chen, J., Huang, Y., Sun, Q., Zhang, X.L., Wang, Y.Y., Xing, S.Z., Chen, Y.S., Sun, Y., Li, J., Daszak, P., Wang, L.F., Shi, Z.L., Tong, Y.G., and Ma, J.Y. 2018. Fatal swine acute diarrhoea syndrome caused by an HKU2-related coronavirus of bat origin. Nature 556 (7700): 255-258. doi: 10.1038/s41586-018-0010-9.

Zhu, N., Zhang, D., Wang, W., Li, X., Yang, B., Song, J., Zhao, X., Huang, B., Shi, W., Lu, R., Niu, P., Zhan, F., Ma, X., Wang, D., Xu, W., Wu, G., Gao, G.F., Tan, W., China Novel Coronavirus, I., and Research, T. 2020. A Novel Coronavirus from Patients with Pneumonia in China, 2019. N Engl J Med 382 (8): 727-733. doi: 10.1056/NEJMoa2001017.

Zou, X., Chen, K., Zou, J., Han, P., Hao, J., and Han, Z. 2020. Single-cell RNA-seq data analysis on the receptor ACE2 expression reveals the potential risk of different human organs

vulnerable to 2019-nCoV infection. Front Med 14 (2): 185-192. doi: 10.1007/s11684-020-0754-0.